Potassium-ion batteries: from laboratorial research to practical application

Abstract:
The limited and uneven distribution of lithium resources provides a strong motivation for developing new rechargeable batteries that use alternative charge carriers. Potassium-ion batteries (PIBs) are at the top of the alternatives list; not only because of the abundance but also because of the small desolvation energy and the low standard electrode potential. However, several challenges hinder the development of the PIBs such as the low reversible capacity, poor rate performance and inferior cycle stability. Research on the electrodes materials is currently focused on developing electrodes that can sustain high energy density and operate at large voltage windows. In addition to the layered transition metal oxides, polyanion compounds and organic compounds have been tested as cathode materials and revealed more complicated reactions mechanisms in comparison to the Li systems. Anodes based on intercalation reactions, conversion reactions, and alloying with potassium are currently under development, with promising results been published. The purposes of this article is to review the research effort to-date on optimizing the electrodes materials for PIBs with a focus on understanding the electrochemical reactions mechanisms and provide a platform for further development in this battery system.

Keywords: potassium-ion batteries; cathode; anode; practical application

1. Introduction

Large-scale energy storage is expected to play a critical role in enhancing the stability, security, and reliability of tomorrow's electrical power grid, including the support of intermittent renewable resources. Electrochemical energy storage methods are strong candidate solutions due to their high energy density, flexibility, scalability, and pollution-free operation. Batteries represent an excellent energy storage technology particularly for the integration of renewable resources due to their compact size and their ability to distribute in location. Today, for example, sodium/sulfur (Na/S) battery technology is commercially available for grid applications, with some 300 installations worldwide, the largest of them was opened in Abu Dhabi in 2019 with a capacity of 108 MW. Lead acid batteries come next with total of 45 MW discharge capacity. However, there is still a long way for current battery technologies to meet the durability, high-power operation, round-trip energy efficiency, and/or cost requirements for large-scale energy storage. Lead-acid batteries have a short cycle life, even at a limited depth of discharge. Redox flow batteries, such as the $Na/NiCl_2$ 'Zebra' battery, and various modifications of the conventional lead-acid system cannot operate at sufficiently high rates. Sodium/sulfur cells are much too expensive, as are the metal hydride/nickel cells currently used in hybrid automobiles. In addition, batteries are probably the only available solution to empower portable and wearable electronics. The vast growing dependence on electric and hybrids vehicles add more pressure on the batteries market, with more requirements on the rate performance and safety.

Lithium ion batteries, the front-runner for applications in portable electronics devices and electric vehicles, have recently began to penetrate into the grid-scale stationary electric energy storage market.[13-15] In 2017, Tesla turned on the world largest lithium ion battery plant with a 100

MW/129 MWh capacity in South Australia. General Electric introduced 1 MW portable unit in 2019, which provides more options for remote renewable energy facilities. Lithium ion batteries have several features that made them the most popular battery such as the high voltage and energy density, low self-discharge, and excellent rate capabilities.[1-7] To meet demand for energy storage application, the production of lithium around the world increased from 27,000 tons in 2008 to 95,000 tons in 2018. The increase in the production is associated with a steep increase in the materials cost, with the price of Li_2CO_3 increased from $5,180 per ton in 2010 to $13,000 per ton in 2019. The USGS estimated that the USA alone would need 54,000 tons of lithium a year to meet the demand for lithium in rechargeable batteries by 2050. Therefore, there are concerns that if the dependence on LIBs continues to increase on the same level, it might deplete the Earth of lithium resource. [16, 17]

Compare to lithium, both sodium and potassium have more resources in the earth's crust as shown in figure 1 b. Early this year, it was estimated that the world resources of potassium is about 250 billion tons.[25-28] In addition, sodium and potassium resources are available around the world, in contrast with lithium resources, which are mainly concentrated in South America. The prices of metals, carbonates, or layered oxides of both sodium and potassium are all much cheaper than those of corresponding lithium compounds. Therefore, both Sodium-ion batteries (SIBs) and potassium-ion batteries (PIBs) are considered as suitable candidates for LIBs [25-28]. The working principle of the PIBs and SIBs is similar to that of LIBs system, which is "rocking chair model" based on the insertion of K and Na ions into the cathode and anode materials (Fig. 1c). By contrast with Na^+, K^+ has more negative standard electrode potential *vs* SHE (-2.93 V for K^+/K *vs* -2.71 V for Na^+/Na), which guarantees a higher operating voltage and higher energy density for the batteries.[29,16] In addition, the standard voltage of K^+/K redox couple in propylene carbonate is lower than both Li^+/Li and Na^+/Na[30], beneficial to achieve high energy density in full cells. Furthermore, potassium does not alloy with aluminum, making it possible to use the cheaper aluminum foil current collector instead of Cu foils that traditionally used with commercial LIBs, which could reduce both the weight and the cost of PIBs. Moreover, due to the weaker Lewis acidity, K^+ with the largest atomic radius (1.38 Å) shows the smallest Stokes' radius in organic solvent among the three alkali metal ions (K^+(3.6 Å) < Na^+(4.6 Å) < Li^+ (4.8 Å)). Thus, K^+ has the highest ionic conductivity (~10 mS cm^{-1} in 1 M PC) amongst all the alkali ions in propylene carbonate (PC) solvents [32, 33]. In term of the solvation structure, both Na^+ and K^+ have disordered and flexible structures in EC, unlike Li+, which shows well-defined shell with a tetrahedral arrangement of the carbonyl oxygen atoms of the EC molecule. The less ordered solvation structure is reflected on the lowest desolvation of K^+ in EC (4.12 eV compared with 4.72 eV for Na^+ and 5.85 eV for Li^+), implying a faster diffusion for K^+ and hence higher charge/discharge rate. It should be mentioned that despite the higher atomic mass of K, the formula weight ratios of alkali metal ions in the respective metal oxide cathode materials, for example the layered cobalt oxides ($LiCoO_2$, P2-type $Na_{2/3}CoO_2$, and P2-type $K_{2/3}CoO_2$), only increase slightly from Li^+ to K^+ ions. Considering the aforementioned advantages, it is not a surprise that the scientific community is trying hard to develop PIBs that can meet the requirements of the future stationary and portable energy storage applications. The increasing number of published papers since 2015 (Fig. 1d) is an indicator of the believe in PIBs as future large scale energy storage system (Fig. 2).

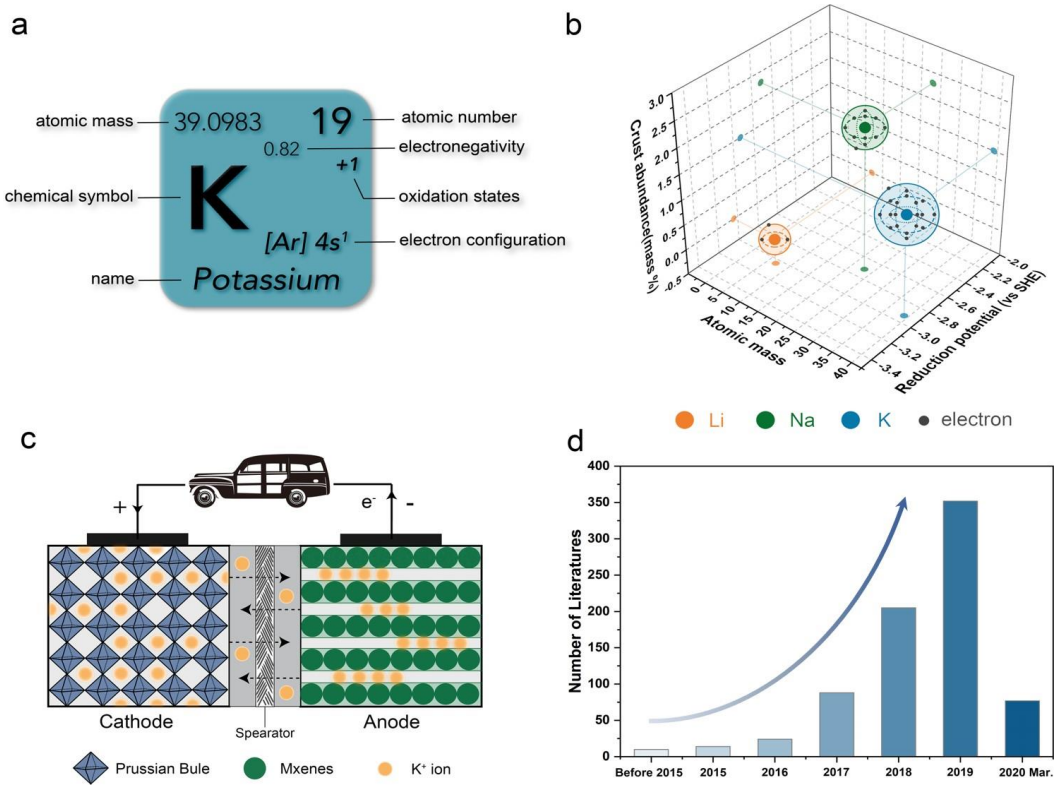

Fig. 1. The advantages and publications of PIBs in recent years. (a) The introduction of K elements; (b) The comparison among the lithium, sodium, and potassium ions; (c) The schematic illustration of the "rocking chair" model of PIBs for power battery; (d) Number of literatures on PIBs according to Web of Science (as of March 2020).

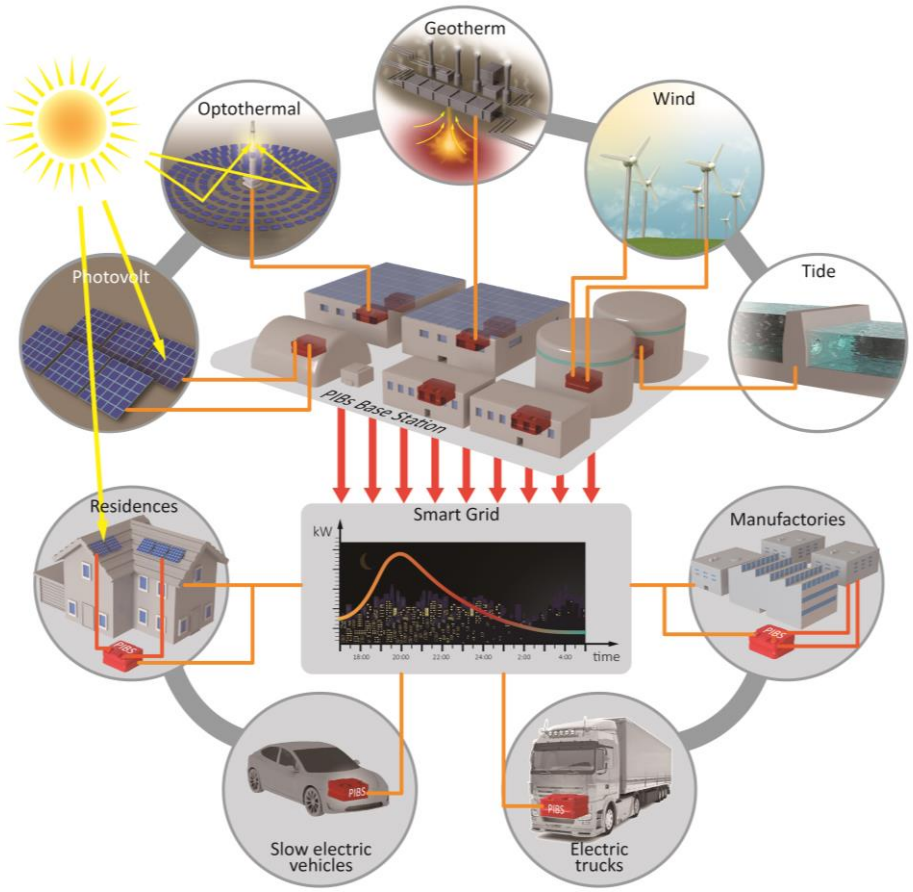

Fig. 2. The conception for the potential applications of PIBs to better support the future human life.

However, PIBs systems are still facing several challenges that make them come after LIBs and SIBs for practical commercial applications. First, the higher atomic weight of potassium means that the energy density of PIBs will always fall after that of LIBs and SIBs. Second, the larger potassium ion makes the volumetric changes during the charge/discharge process more significant for PIB than other alkali metal batteries, and hence causes structural instability of the electrodes. Also, the low diffusivity of K^+ in the solid electrodes materials constitutes limitation on rate performances. [34] Furthermore, the electrolyte in the PIBs suffers from decomposition and several parasitic reactions due to the high potential of K^+/K redox. For all these reasons, the development of PIBs is restricted by the discovery of new positive and negative electrodes materials. In this article, the detailed progress on the design and development of cathodes and anodes materials of PIBs were comprehensively reviwed as shown Fig. 3. We begin with the current overview of cathode materials, including potassium Prussian blue and its analogues, layered transition metal oxides, polyanion compounds, organic cathode materials, and all the attempts to improve their specific capacities (Fig. 4). Next, the recent strategies and advances on anode materials are explored in detail, which are mainly focus on the relationship between the material characteristics (i.e., composition, structure, morphology) and their electrochemical performance (such as cycling capacity and stability) of the intercalation anode materials, conversion anode materials, and alloying anode materials. Additionally, a brief introduction to the electrolyte, solvent, and separator, along with the formation of solid electrolyte interphase (SEI) layer, is also included in the whole context. Following these, we try to highlight the existent

challenges and possible perspectives for the low-cost and high-performance cathode and anode materials in various directions. Finally, we further suggest the solutions for the development of practical full-cell fabrication of PIBs system including the possible directions for electrolyte optimization, separators, electrodes fabrication, and highly safe structure design, which would provide a possible future development of next-generation PIBs and promote their evolution from experimental research to potential practical application in the near future.

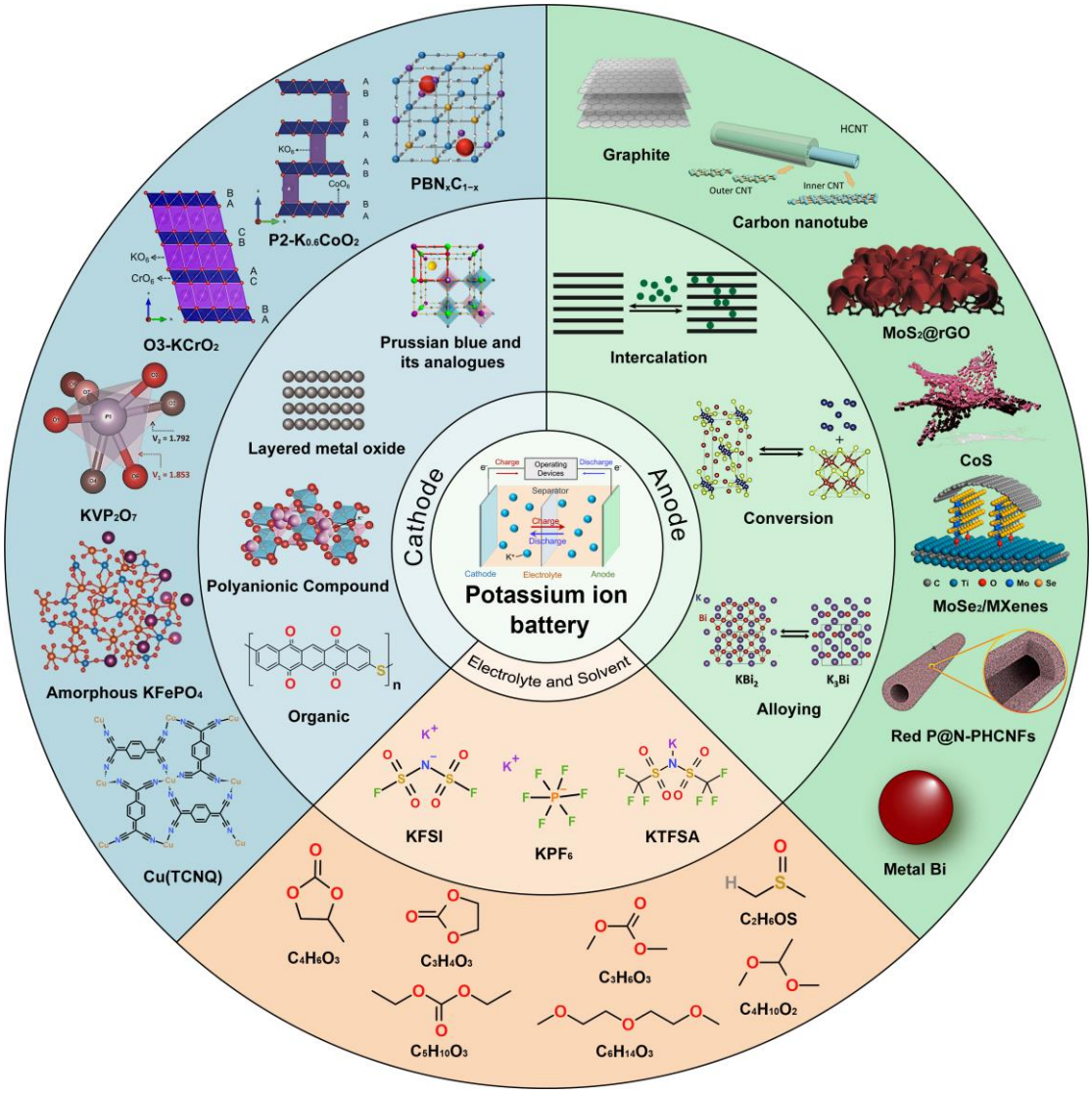

Fig. 3. Schematic diagram of the available cathodes, anodes, electrolytes, and solvents for PIBs system summarized from the recent literatures.

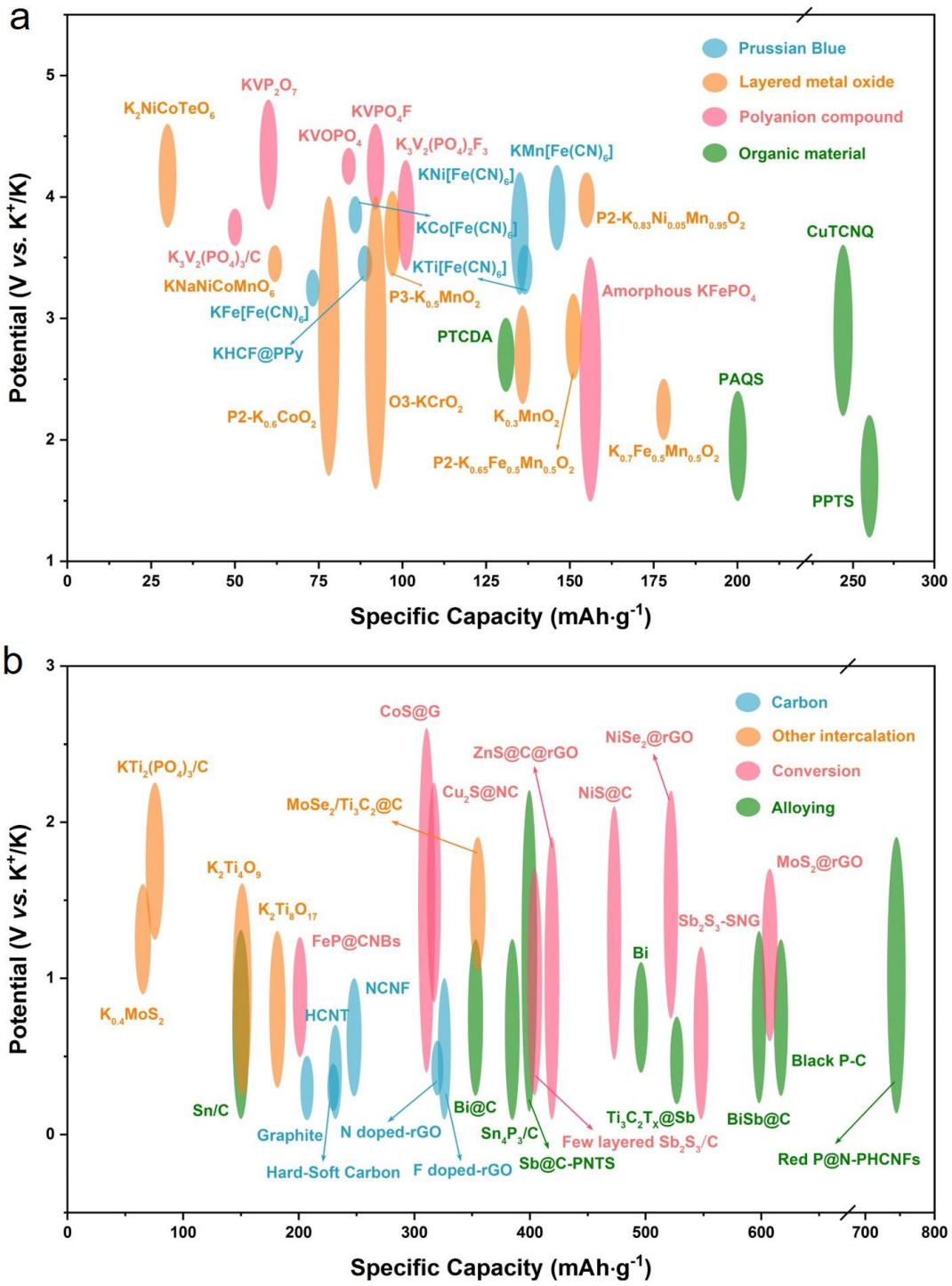

Fig. 4. The specific capacities and voltage window of recently reported cathode (a) and anode (b) materials in PIBs.

2. Cathode materials

2.1 Prussian blue and its analogues

One of the most competitive cathode materials for PIBs should be the potassium-containing Prussian blue (PB) and its analogues (PBAs), because of their advantages such as the open framework, structural controllability, excellent cycle stability, easy preparation, and low cost[35-37].

As early as 1936, the first face-centered cubic structure hypothesis of Prussian blue was proposed by Keggin and Miles[38]. Then, Melvin B. Robin[39] firstly reported the detailed structure and electronic configuration of dye Prussian blue with a face-centered cubic (FCC) structure in 1962. As shown in Fig. 5a, the chemical formula of the PBAs can be expressed as $A_xM[M'(CN)_6]_{1-y}\cdot nH_2O$ ($0 < x < 2$, $y < 1$), where A represents the alkali-metal ion (such as K, Na, or Li[20, 40, 41]) and M (or M') is the transition-metal ion, such as Ni, Fe, and Mn[42-44]. When A is replaced by K ions, a better reversible potassium storage capacity could be presented at a higher x value. The exchangeable transition-metal ions at M and M' are coordinated by nitrogen and carbon respectively, which are interconnected by a cyanide (CN) ligand. In each unit cell of PBAs, eight subunit cells with eight interstitial sites are obtained, which can accommodate not only neutral molecules but also transition ions[45]. After these ions are replaced, the charge balanced 3D network could still be maintained with abundant open channels and gap locations. The open frame could promote a rapid diffusion of various embedded ions in PBAs structure, which is beneficial to the rate performance. Furthermore, the water molecules can also enter into the interstitial sites of PBAs crystals (Fig. 5b) without any obvious structural changes, which also have great influence on their electrochemical performance[46].

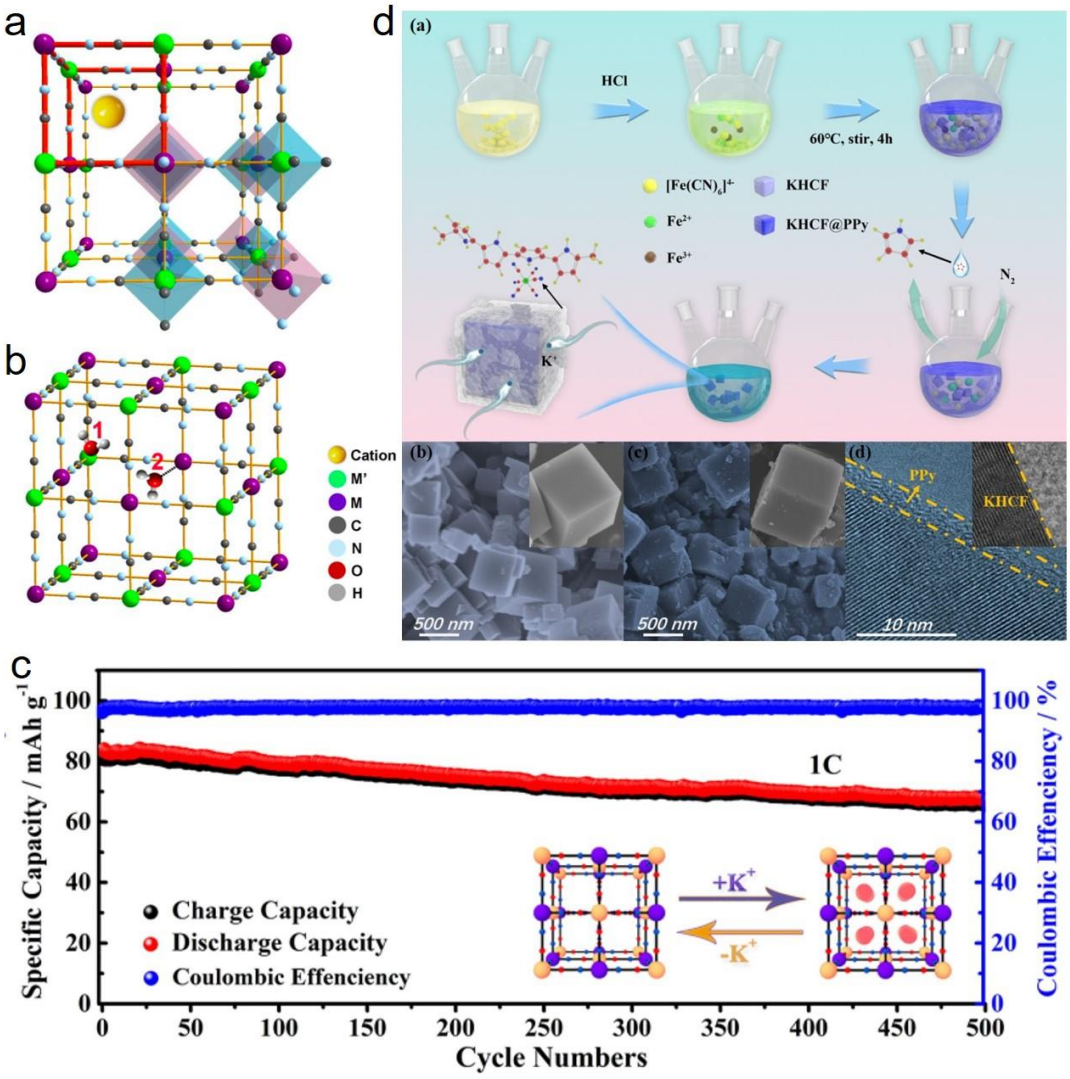

Fig. 5. a) Crystal structure of the PBAs; b) the similar structure with interstitial water.[47] c) The

long-term cyclic stability and electrochemical mechanism of $Fe_4^{III}[Fe^{II}(CN)_6]_3 \cdot 3.4H_2O$ (at 1C) in a three-electrode cell. d) The illustration scheme of the synthesis process of KHCF@PPy (a); SEM of pure KHCF (b) and KHCF@PPy (c); TEM of KHCF@PPy (d) and KHCF (insert of (d)). a polypyrrole (PPy)-coated K-rich iron hexacyanoferrate composite (KHCF@PPy)

In recent years, the study on the composition optimization of PBAs cathode materials by co-doping with Fe, Co, Ni, Zn and Mn ions has gradually increased[48, 49]. Huang et al.[50] explored a high-performance PBA material doped with nickel ions via a modified coprecipitation method, which could deliver a discharge capacity of up to 135 mAh g^{-1} in comparison with the 120 mAh g^{-1} for nondoped PB. The excellent cycling performance with 83.1% capacity retention after 300 cycles (0.1 A g^{-1}) was presented at the same time. In previous studies, actually, these PBAs electrodes are mainly confirmed to be efficient for water-based PIBs[51]. For example, Xia et al.[52] reported a commercial $Fe_4^{III}[Fe^{II}(CN)_6]_3 \cdot 3.4H_2O$ cathode performed well in aqueous K-ion batteries. As shown in Fig. 5c, the specific capacity could be about 80 mAh g^{-1} at 1C, along with 82.4% retention over 500 cycles. But until recently, PBAs also show good electrochemical properties in non-aqueous PIBs. Zhang et al.[47] synthesized the $K_{0.220}Fe[Fe(CN)_6]_{0.805} \cdot 4.01H_2O$ by precipitation method and applied it to potassium ion half-cell and whole battery to study its electrochemical performance, which further proved that the electrochemical reaction mechanism of Prussian blue by ectopic test: Prussian White ↔ Prussian Blue ↔ Prussian Yellow.

Although these PBAs electrodes have exhibited excellent cycling stability during the charge/discharge process, their low potassium content are always limits sound reversible specific capacity, which is only around 68.5 mAh g^{-1} at 100 mA g^{-1}. Therefore, it is also significant to improve the stoichiometry of K ions in the PBAs cathode materials. Luo et al.[53] synthesized a titanium-containing PBA electrode $K_{0.3}Ti_{0.75}Fe_{0.25}[Fe(CN)_6]0.95 \cdot 2.8H_2O$ by a coprecipitation method, which showed a high reversible specific capacity of 136.7mAh g^{-1} at 50 mA g^{-1} with the first cycle efficiency of 118%. Xue et al.[54] also synthesized a manganese-containing PBA electrode ($K_{1.89}Mn[Fe(CN)_6]_{0.92} \cdot 0.75H_2O$, KMHCF) by a precipitation method to increase the potassium content to 1.89, which is very close to its theoretical value of 2. The high-spin Mn^{III}/Mn^{II} and low-spinning Fe^{III}/Fe^{II} with similar energies resulted in two potential platforms centered at 3.6V. The KMHCF nanoparticles with a diameter of about 40 nm showed a higher charge specific capacity of 146.2 mAh g^{-1} at 0.2 C. Consistent with the ex-situ XRD results to track their structure during charging and discharging, the modified PBA also presented a good reversibility from 0.2 to 2 C. Huang et al.[55] prepared a ternary $K_2Ni_xCo_{1-x}Fe(CN)_6$ cathode by co-doping with Ni and Co ions connected to the N end. This novel ternary structure also exhibited much higher performance than the corresponding binary counterparts, which could provide a potential orientation for performance improvements of PIBs.

Additionally, surface modification of PBAs for use in PIBs has also been examined to enhance their cycling stability and rate capability. Chen et al.[56] proposed a polypyrrole-modified PB material (KHCF@PPy) via an in-situ polymerization coating method (Fig. 5b). The reported KHCF@PPy electrode with low defect concentration and high electronic conductivity could exhibit a discharge capacity of 88.9 mAh g^{-1} at 50 mA g^{-1}, which dropped slightly after 500 cycles. When the current density increased to 1000 mA g^{-1}, the initial discharge capacity could still keep 72.1 mAh g^{-1} with 85.7% capacity retention after 500 cycles. Furthermore, the composite electrode materials by combining electronically conducting matrix with ionic conductors were also proposed recently to mitigate the current issues associated with PBAs cathodes for PIBs.

Dryfe et al.[57] reported a carbon nanotube/PB nanocomposite as free-standing transparent thin films for the potential cathode of aqueous rechargeable PIBs. The fabricated coin-cell devices with the nanocomposite cathode and activated carbon anode presented a capacity of 47.6 mAh g^{-1} at 0.25 A g^{-1} with the energy density of 33.75 Wh kg^{-1}. Zarbin et al.[58] also synthesized a similar graphene/PB nanocomposite film with the capacity up to 141 mAh g^{-1} at 0.093 A g^{-1}. All these composition and structure optimization, surface modification, and composite method could represent promising strategies to promote the practical applications of PBAs cathodes in PIBs.

2.2 Layered transition metal oxide

In the commercial application of LIBs and SIBs, layered transition metal oxides have been widely used as cathode materials because of their high energy density, excellent stability, and low cost[59-62]. In the layered oxide structure, the transition metal and alkali ions segregate into alternating slabs with abundant two-dimensional open frameworks, which could also benefit the migration of large K^+ ions. The $K_{0.3}MnO_2$ is one of the earliest layered transition metal oxides for PIBs cathodes by using potassium permanganate as raw material.[63] The layered $K_{0.3}MnO_2$ has a two-layer orthorhombic unit-cell, the Mn atoms are octahedrally coordinated by oxygen anions while the K^+ ions are located between the transition metal layers with trigonal prismatic coordination. The as-prepared flake-like $K_{0.3}MnO_2$ cathodes delivered a reversible capacity of 125 mAh g^{-1}. However, two stable stages were exhibited at 3.7 V and 3.9 V corresponding to two different phase reactions, which caused irreversible expansion of the volume and further leaded to the decline of capacity. By reducing the upper limit voltage, the phase reactions were avoided, and the capacity were maintained about 57% after 685 cycles.

In order to solve this capacity attenuation caused by the phase change at high voltage, Choi et al.[64] designed the P2 type layered $K_{0.83}[Ni_{0.05}Mn_{0.95}]O_2$, which could retain the P2-type structure during charging to 4.3V (*vs.* K^+/K). By avoiding large volume expansion, this cathode shows excellent capacities of 155 mAh g^{-1} at a current density of 52 mA g^{-1} with capacity retention of 83% for 200 cycles and 120 mAh g^{-1} at a current density of 520 mA g^{-1} with capacity retention of 77% for 500 cycles. Kim et al.[65] reported a P3-type $K_{0.5}MnO_2$ compound, which obtained a reversible capacity of 110 mAh g^{-1} ranging in 1.5-3.9 V. Guo ZP et al.[66] introduced the cobalt ions to replace the manganese site in the K_xMnO_2 layered oxide electrode material (Fig. 6a-b), which shows that with only 5% Co, the reversible capacity of this material increases by 30% at 22 mA g^{-1} and by 92% at 440 mA g^{-1} (Fig. 6c-e). Myung et al.[67] also proposed a P3-$K_{0.54}[Co_{0.5}Mn_{0.5}]O_2$ cathode for PIBs with a high discharge capacity of 78 mAh g^{-1} at 500 mA g^{-1}. Du et al.[68] designed a new Ni/Mn-based P2-type $K_{0.44}Ni_{0.22}Mn_{0.78}O_2$ layered oxide with a high specific capacity of 125.5 mAh g^{-1} at 10 mA g^{-1} and good cycle stability with capacity retention of 67% over 500 cycles. After fabricating into a full cell using soft carbon as the counter electrode, the capacity retention could still reach about 90% over 500 cycles. Myung et al.[69] also designed a similar P2-$K_{0.75}[Ni_{1/3}Mn_{2/3}]O_2$ cathode material via electrochemical ion-exchange from P2-$Na_{0.75}[Ni_{1/3}Mn_{2/3}]O_2$, which exhibited an unexpectedly high reversible capacity of about 91 mAh g^{-1} (1400 mA g^{-1}) with excellent capacity retention of 83% over 500 cycles. Recently, other transition metal elements substituted layered manganese oxides, such as Fe-doped layered P3-type $K_{0.45}Mn_{1-x}Fe_xO_2$ ($x \leq 0.5$), were also developed as low-cost promising cathode materials for high-performance PIBs[70]. In addition, the introduction of alkali elements might also be an effective way to enhance their electrochemical K storage properties. Liu et al.[71] reported a layered

$K_{0.67-x}Na_xNi_{0.17}Co_{0.17}Mn_{0.66}O_2$ (x=0, 0.1, 0.2, 0.3, 0.4, 0.5), which found that the content of Na element could stabilize the layered structure, and improve its specific capacity and rate performance. The specific capacity of 62 mAh g^{-1} at 100 mA g^{-1} is much higher than that without Na (47.8 mAh·g^{-1}). Beyond these progresses, we recently proposed a novel anion doped $K_{0.6}CoO_{2-x}N_x$ porous nanoframe cathode for PIBs[72]. The partial substitution of O with N atoms effectively improved the electronic conductivity and enlarged the interlayer spacing, which could accommodate more K^+ intercalation and promote K^+ migration. In combination with its unique hollow structure for providing more electrochemical active sites, the $K_{0.6}CoO_{2-x}N_x$ nanoframe delivered an enhanced reversible capacity of 86 mAh g^{-1} at 50 mA g^{-1} with a capacity retention of about 77% over 400 cycles.

Moreover, other types of layered transition metal oxides were also successively proposed. For example, Hironaka et al.[73] confirmed that the P2-type K_xCoO_2 could deliver a high reversible capacity of 60 mAh g^{-1} between 2.0-3.9 V. Masese et al. reported a high voltage (4.3 V *vs.* K^+/K) honeycomb layered cathodes P2-type $K_2NiCoTeO_6$ for rechargeable PIBs due to the virtue of its moderately inductive TeO_6^{6-} framework[74], and also attributed to a honeycomb-layered $K_2Ni_2TeO_6$ cathode with a high average discharge voltage of 3.6 V versus K^+/K; and a reversible capacity of about 70 mAh g^{-1}. Various potassium vanadate compounds, including $K_2V_3O_8$ and $K_{0.486}V_2O_5$, were also reported as novel active materials for K storage with suitable reversible capacity[75, 76]. The development of novel layered transition metal oxides cathode materials is still imperative and important for the improvement of PIBs.

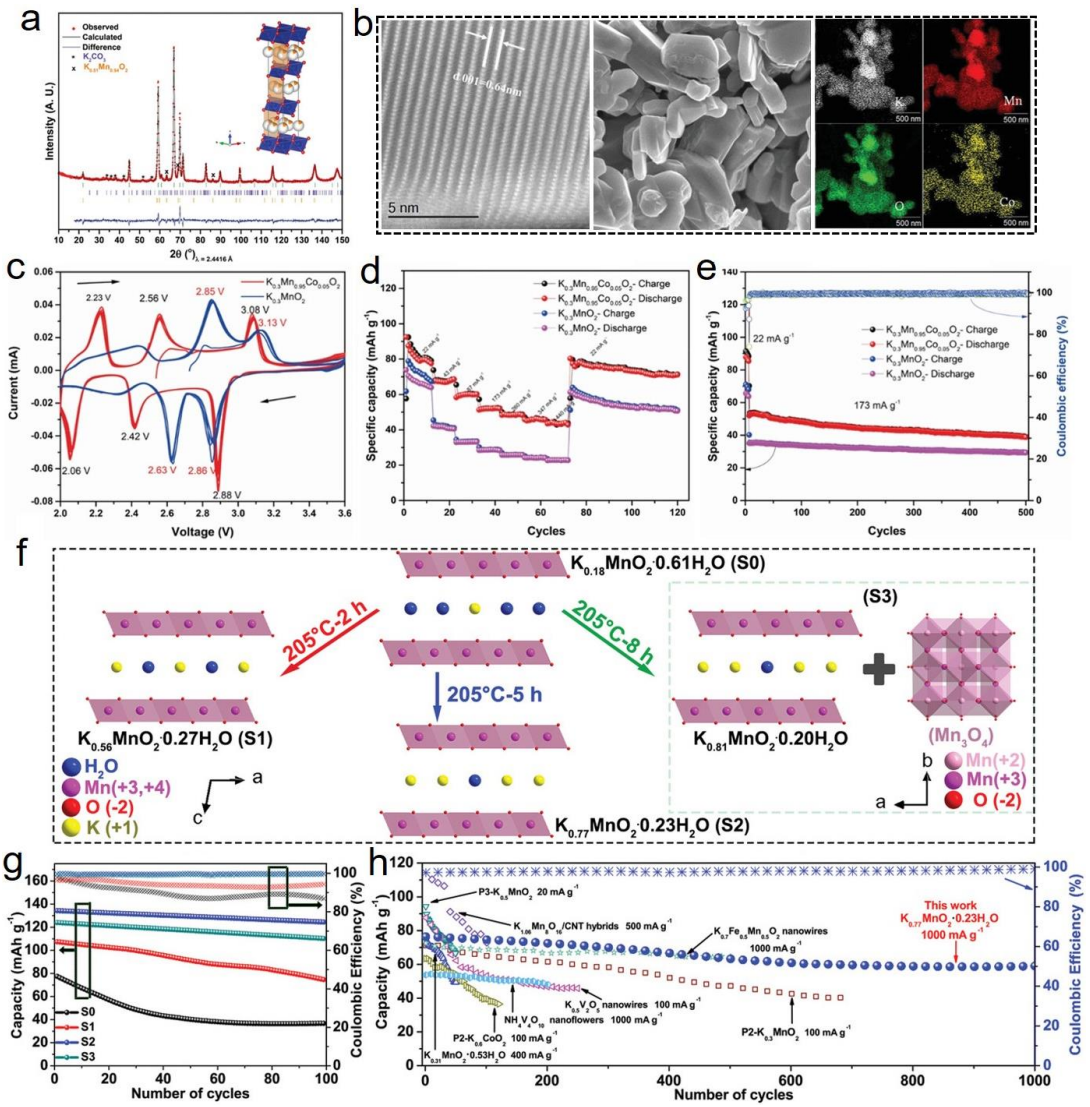

Fig. 6. (a) Rietveld refinement profiles using neutron powder diffraction data of the $K_{0.3}Mn_{0.95}Co_{0.05}O_2$, where the refined crystal structure of the main phase is shown inset with potassium in orange, manganese in blue, and oxygen in red. (b) The STEM dark field image, SEM image, and EDS elemental distribution of the $K_{0.3}Mn_{0.95}Co_{0.05}O_2$ particles. Cyclic voltammetry profiles (c), rate performance (d), long-term cyclability and coulombic efficiency (e) of the $K_{0.3}Mn_{0.95}Co_{0.05}O_2$ and $K_{0.3}MnO_2$ versus K in a half-cell. (f) Structural evolutions from S0 to S1, S2, and S3 during the "hydrothermal potassiation". (g) Cycle performances and Coulombic efficiencies of the electrodes S0, S1, S2, and S3 at a current density of 100 mA g^{-1}. (h) Long-term cycle performance of the $K_{0.77}MnO_2{\cdot}H_2O$ (S2) electrode compared with previously reported layered cathode materials.

Another major issues for the low specific capacity of these layered transition oxides is their deficient potassium content, which limits the amount of electrochemically active K ions in the PIBs system. To solve this problem, Kim et al.[77] reported a P2-type layered $K_{0.6}CoO_2$ with the specific capacity of about 60 mAh g^{-1}, which also pointed out that the layered structure would be destroyed when the ratio of K/M (transition metal) is closer to 1. According to the electronic configuration and density functional theory, they also found that the $KScO_2$ and $KCrO_2$ could be thermodynamically stable. After successfully synthesis of the O3-type $KCrO_2$ cathode material without K deficiency, the electrochemical performances obtained a reversible specific capacity of about 92 mAh g^{-1}.[78] To improve the continuous capacity fading of O3-type $KCrO_2$ during

subsequent cycles, Pyo et al.[79] proposed a slightly K-deficient compound P′3-type $K_{0.8}CrO_2$, which eventually exhibited a significant improvement in cyclic stability (99% retention after 300 cycles at 1 C).

Since 2018, K-Birnessite has been also synthesized as a promising cathode with a reversible capacity as high as 125 mAh g^{-1} at 0.2 C, in which an ion exchange approach is applied to improve the K content in K-Birnessite electrode[80]. Myung et al.[81] also confirmed that the $K_{0.28}MnO_2 \cdot 0.15H_2O$ could deliver a high reversible capacity of 150 mAh g^{-1} over 100 cycles at 15 mA g^{-1}. Xia et al.[82] further designed several birnessite nanosheet arrays with high K content ($K_{0.77}MnO_2 \cdot 0.23H_2O$) by a "hydrothermal potassiation" process (Fig. 6f), demonstrating an ultrahigh reversible specific capacity of 134 mAh g^{-1} at 100 mA g^{-1}, as well as superior rate capability and cycling stability (Fig. 6g-h).

Although the layered transition metal oxide cathode materials have shown excellent stability in commercial LIBs, the K ions with larger radius would seriously damage the layered structure during complicate potassiation/depotassiation process. The huge challenges for developing layered transition metal oxides, such as complicated phase transitions, the concomitant intercalation of various spices, low intercalation potentials, and steeper voltage curves with more voltage steps compared to those of LIBs and SIBs, still limit their commercial application. In future studies, the optimization, including chemical composition design and structural control to stabilize the layered structure and inhibit the volume change caused by K ions during intercalation and deintercalation, is urgently expected to improve their electrochemical performance for commercial application.

2.3 Polyanionic compound

Polyanionic compounds, including various compounds containing tetrahedral and octahedral anionic structural groups $(AO_m)^{n-}$ (A=P, S, Mo, W, etc.), which have attracted much attention as cathode materials for alkali-ion batteries[83-85]. In the field of LIBs, iron phosphate lithium ($LiFePO_4$)[86, 87] is the most widely studied polyanionic compound. These compounds usually own excellent advantages of low oxygen loss, high thermal stability, high operation potential, and long cycle stability, due to their strong covalent framework and inductive effect of the anionic group as well as the open channel structure with low diffusion energy for alkali metal ions. Therefore, the polyanionic compounds are also expected to be used as promising cathode materials for PIBs.

Unlike the commercialized $LiFePO_4$ material, the insertion/extraction of larger K ions in the olivine phase $FePO_4$ make it more difficult to maintain the crystallinity and structural stability, which would further lead to poor electrochemical properties. To solve these problems, Mathew et al.[88] reported an porous amorphous iron phosphate with a short-range-ordered structure for K ions storage. They found that the amorphous $FePO_4$ could gradually convert to crystalline phase during K ions intercalation, and then return to the amorphous state after the extraction process. The porous structure could also be conductive to the insertion/extraction of K ions, which could improve its cycle performances. When the current density is 5 mA g^{-1}, this $FePO_4$ compound obtained a specific capacity of 156 mAh g^{-1} with almost 70% of its theoretical capacities after 50 cycles. However, amorphous $FePO_4$ exhibits a lower operating potential (2.1- 2.4 V), which is not suitable for high-voltage PIBs.

Pyrophosphate and fluorophosphate have also been gradually developed as potential polyanionic compounds for the cathode materials for PIBs[89-91]. Most of these polyanion

compounds usually contain the iron vanadium elements with excellent electrochemical performance in secondary battery systems[92, 93]. Han et al.[94] reported a porous $K_3V_2(PO_4)_3$ with an attractive high working potential (the composite with carbon shows a high potential of 3.6-3.9 V). However, this electrode material presents a reversible specific capacity of about 50 mAh·g^{-1} at 20 mA g^{-1}. Chen et al.[95] also synthesized Rb-doped $K_{3-x}Rb_xV_2(PO_4)_3$/C (x = 0, 0.03, 0.05, 0.07) composites for high-voltage cathode via a facile sol-gel process. The Rb-doped composites delivered better electrochemical performance than the undoped $K_3V_2(PO_4)_3$/C, which could display a good initial discharge capacity of 55.7 mAh g^{-1} in the voltage range of 2.5- 4.6 V at 20 mA g^{-1}. And the discharge capacities of the $K_3V_2(PO_4)_3$/C and $K_{2.95}Rb_{0.05}V_2(PO_4)_3$/C decreased to 32.1 and 52.6 mAh g^{-1} after 50 cycles, respectively. Recently, Zhang et al.[96] reported a $K_3V_2(PO_4)_2F_3$ compound inheriting from the $Na_3V_2(PO_4)_2F_3$ analog as a robust cathode for PIBs. Through the characterization of in-situ XRD, they found that about two K ions could be provided in the electrode with the volume change of only 6.2% during the insertion/extraction process. As a result, the $K_3V_2(PO_4)_2F_3$ exhibited a capacity of over 100 mAh g^{-1} with a high average potential of ~3.7 V *vs.* K^+/K. Moreover, two similar vanadium-based cathode materials, $KVOPO_4$ and $KVPO_4F$, have also been extensively studied recently.[97-100] These compounds also contain open frame structure, which are composed of VO_6 octahedron and covalently bonded PO_4 tetrahedron. Chihara et al.[97] reported that the $KVOPO_4$ and $KVPO_4F$ could keep good performance stability with obvious charging and discharging platforms when the charging voltage rose to 5 V because of their minor volume changes during the discharge/charge cycles of only 3.3% and 5.8%, respectively. And the excellent rate performance was also confirmed at high current densities. Chen et al.[98] reported a new layered $KVOPO_4$ cathode with controllable morphologies via the hydrothermal method, which exhibited a high capacity of 115 mAh g^{-1} (0.2C, 1C = 120 mA h g^{-1}) with the cycling stability of 86.8% capacity retention after 100 cycles (0.5C) as well as the superior rate capability for PIBs. They further assemble a long lifespan K-ion full cell based on the $KVPO_4F/VPO_4$ with high operating voltage of 3.1 V, high capacity of 101 mAh g^{-1}, and considerable capacity retention of 86.8% over 2000 cycles[99].

Transition metal-based pyrophosphate compounds (KAP_2O_7, A=Ti, V, Mn, etc.) are also one type of common polyanionic compounds, which has been used as cathode materials for LIBs and SIBs. Park et al.[101] screened out seven pyrophosphates (such as KVP_2O_7, $KTiP_2O_7$, $KFeP_2O_7$, $KCrP_2O_7$, $KMoP_2O_7$, $KNiP_2O_7$, and $KCoP_2O_7$) as the cathode candidates for PIBs via the density functional theory calculation and inorganic crystal structure data. Among these compounds, the KVP_2O_7 material showed relatively pronounced redox peaks, which has a high discharge potential of about 4.2 V during the charge and discharge process. The reversible phase transition between monoclinic KVP_2O_7 and triclinic $K_{1-x}VP_2O_7$ (x≈0.6) also resulted in a stable specific capacity of about 60 mAh g^{-1}, which also corresponds to an energy density of 253 Wh kg^{-1} at 0.25 C. Kim et al.[102] introduced a novel high performance $K_4Fe_3(PO_4)_2(P_2O_7)$ cathode material for PIBs after first-principles theoretical prediction. In the $K_4Fe_3(PO_4)_2(P_2O_7)$ electrode, about ~3 mol of K^+ de/intercalation per formula unit was observed with a small volume change of ~4% during charge/discharge process, which leaded to a large specific discharge capacity of ~118 mAh g^{-1} at 6 mA g^{-1}. Because of the low activation barrier energy for K^+ diffusion in this material, almost ~70% of the theoretical specific capacity could still be retained after increasing the current density to 600 mA g^{-1}, and 82% of the initial capacity could be reserved after 500 cycles.

Recently, titanium-based cathode materials have also attracted more and more attention in the

K storage systems. Kim et al.[103] introduced a rhombohedral $KTi_2(PO_4)_3$ cathode material modified by electro-conducting carbon exhibiting a large capacity of 126 mAh g^{-1} (about 98.5% of its theoretical capacity) with a capacity retention rate of 89% after 500 cycles. Detail structural analyses indicated that the electrochemical reaction for the de/intercalation of K ions in the $KTi_2(PO_4)_3$ structure could be the $Ti^{4+/3+}$ biphasic redox process between the $KTi^{4+}{}_2(PO_4)_3$ and $K_3Ti^{3+}{}_2(PO_4)_3$ phases in the voltage range of 1-4 V (vs K^+/K). Fedotov et al.[104] firstly, reported on a record-breaking titanium-based cathode material, $KTiPO_4F$, with an electrode potential of 3.6 V in PIB system. A carbon-coated electrode material was further prepared and displayed no capacity fading after cycling at 5C rate for 100 cycles because of the extremely low energy barriers for K ion migration. These results confirmed that the titanium redox activity could be upshifted to near-4V electrode potentials, which provided the possibility to design sustainable and cost-effective titanium-based cathode materials with promising electrochemical performances for PIBs.

In addition, some other complex potassium compounds, like the sodium-containing sulfates and other compounds for SIBs[105, 106], have also been investigated as potential cathode materials in recent literatures. Cheng et al.[107] reported a fluoroxalate $KFeC_2O_4F$ cathode materials for PIBs (Fig. 7a, b), previously known as frustrated magnet, exhibiting an outstanding discharge capacity of ~112 mAh g^{-1} at 0.2 A g^{-1} with the 94% capacity retention after 2000 cycles (Fig. 7c). The detail analysis indicated that the unprecedented cycling stability is attributed to the rigid $[FeC_2O_4F]$ framework and open channels to minimize volume fluctuation during the intrinsic $Fe^{2+/3+}$ redox reaction (Fig. 7d-h). And the further fabricated potassium-ion full cell by pairing the $KFeC_2O_4F$ cathode with soft carbon anode also obtained impressive rate performance and 0.003% capacity decay within 200 cycles, as well as an excellent energy density of ~235 Wh kg^{-1} (Fig. 7i, j). The special structure features of $KFeC_2O_4F$ materials could help to develop novel promising PIB cathodes for practical large-scale energy storage applications. The potassium-based fluorsulfate, $KFeSO_4F$[83], was also synthesized as cathode to storage K^+ ions because of its spacious channels, being formed by the MO_4F_2 octahedra and SO_4 group. Feng et al.[108] reported a new high-performance hydroxysulfate cathode material, $K_2Fe_3(SO_4)_3(OH)_2(H_2O)_2$, for rechargeable alkali-ion (Li, Na, and K) batteries by a facile hydrothermal method. In the three alkali ion electrolytes, the $K_2Fe_3(SO_4)_3(OH)_2(H_2O)_2$ could exhibit good electrochemical activity, reversibility, stability, and rate performances, which also proposed a new design strategy for K-based polyanionic compounds as cathode materials of PIBs systems.

The stable frame structure of polyanionic compounds and the replaceability of anions make them considerable for high voltage and high energy PIBs. However, the K-based polyanionic compounds are always low density which would result in the low volumetric energy density. Moreover, the common electrolytes will decompose at high voltage, which will also cause the unideal Coulombic efficiency. After optimization of the electrolytes and developing suitable structure for potassium insertion/ extraction, the polyanionic compounds are still believed as promising cathode materials for PIBs.

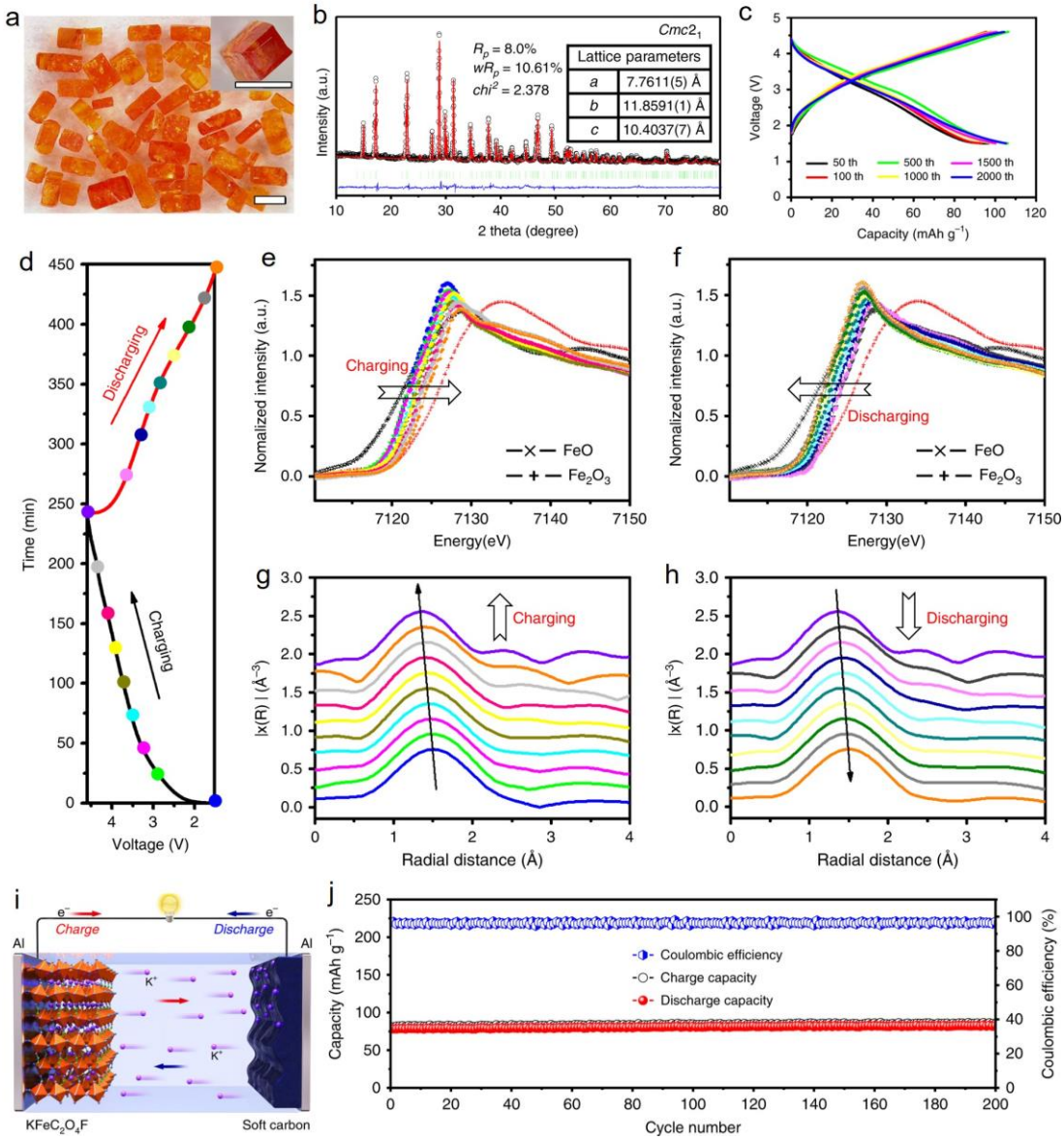

Fig. 7. (a) Optical images of as-synthesized $KFeC_2O_4F$ crystallites with the inset of a tetra-prismatic single crystal (scale bar = 1 mm). (b) Rietveld fitness of powder XRD on a pristine $KFeC_2O_4F$ sample. The inset shows the result of the fitness. (c) The charge-discharge curves of diverse cycles for $KFeC_2O_4F$ in K half-cells at a current density of 0.2 A g^{-1}. (d-h) The structural evolution and charge compensation mechanism of the $KFeC_2O_4F$ cathode. (d) The typical galvanometric charging-discharging curve of a stabilized half-cell at 0.1 A g^{-1} and corresponding synchrotron Fe K-edge XANES during charging (e) and discharging (f), and Fe EXAFS during charging (g) and discharging (h). (i) Working mechanism of full K ion cell in 1.7-4.4 V. (j) Cycling performance of the full cell at 0.1 A g^{-1}.

2.4 Organic materials

Unlike the traditional rigid inorganic materials, organic materials own more merits, such as versatile chemical structures, flexible structures, abundant, lower cost, and environmentally friendly, which have been considered as promising cathodes for advanced flexible secondary batteries. Because of their weak intermolecular interactions, the large K^+ ions could also easily

de/intercalate into these organic frameworks, achieving good specific capacity and rate performance as PIBs. The functional groups that leads to the electrochemically active oxidation/reduction have been investigated carefully in recent studies. Herein, we will give an introduction on the latest developments of their structures and properties.

Non-metal-containing organic materials were firstly used as cathodes for PIBs due to their abundant structural diversity. Chen et al.[109] reported a 3,4,9,10-per-tetracarboxylic acid-dianhydride (PTCDA) cathode material for PIBs, which is composed of a large number of one-dimensional rods with high degree of crystallinity. The electrode material formed a K_{11}PTCDA compound with K ions at a low discharge potential of 0.01 V and presented a specific capacity of ~753 mAh g^{-1}. K_2PTCDA and K_4PTCDA are formed at the potential of 1.5-3.5 V, resulting in a considerable specific capacity of 131 mAh g^{-1} at a current density of 10 mA g^{-1}. The discharge/charge platforms of the PTCDA were obvious, but the specific capacity dropped rapidly to about 60% after only 35 cycle. Xing et al.[110] also introduced the PTCDA material with a similar electrochemical performance. In addition, Jian et al.[111] synthesized a polyanthraquinone sulfide (PAQS) electrode, exhibiting a reversible specific capacity of ~200 mAh g^{-1} at current density of 20 mA·g^{-1}. Compared with the above-mentioned PTCDA, the PAQS obtained a better cycle stability, of which the specific capacity dropped to ~150mAh g^{-1} after 50 cycles. The polytriphenylamine (PTPAn) cathode material reported by Fan et al.[112] showed a greatly improved the cycle stability. The capacity retention rate can reach 75.5% after 500 cycles, but the reversible specific capacity was only 60 mAh g^{-1} at 50 mA g^{-1}. Wang et al.[113] investigated a high-performance cathode polypentenone sulfide (PPTS) for PIBs, which exhibited a high specific capacity of approximately 260 mAh g^{-1} at a current density of 0.1 A g^{-1}. After 3000 cycles at 5 A g^{-1}, the capacity is still maintained at 190 mAh g^{-1}, and the impressive rate performance showed that the specific capacity of the electrode is still as high as 163 mAh g^{-1} at a high current density of 10 A g^{-1}. Fan et al.[114] reported the perylene-3,4,9,10-tetracarboxylic diimide (PTCDI) as a new organic cathode for PIBs, delivering stable capacity of ~120 mAh g^{-1} after 600 cycles at 4 A g^{-1} in half cells. When fabricating into full cells, the PTCDI cathode displayed an average capacity of ~127 mA h g^{-1} at 50 mA g^{-1} over 30 cycles. Then, Fan and his group further developed an insoluble [N, N′-bis(2-anthraquinone)]-perylene-3,4,9,10-tetracarboxydiimide (PTCDI-DAQ) organic cathode (Fig. 8a), which could improve the specific capacity to 211 mAh g^{-1} and maintain the capacity 133 mAh g^{-1} at 20 A g^{-1} (Fig. 8b,c), using 1 m KPF6 in dimethoxyethane (DME) as electrolyte[115]. After fabricating with the reduced potassium terephthalate (K4TP) anode (Fig. 8d), the resulted full PIBs could achieve a superlong stable lifespan with the discharge capacity of 62 mAh g^{-1} after 10 000 cycles at 3 A g^{-1} (Fig. 8f). The energy density and power density could be as high as 295 Wh $kg^{-1}_{cathode}$ (213 mAh $g^{-1}_{cathode}$ × 1.38 V) and 13800 W $Kg^{-1}_{cathode}$ (94 mAh g^{-1} × 1.38 V @ 10 A g^{-1}) during the working voltage of 0.2-3.2 V (Fig. 8e), respectively. A novel high-energy and high-power-density PIB, in Troshin et al.'s work[116], was designed by using the high-voltage poly(N-phenyl-5,10-dihydrophenazine) (p-DPPZ) as active cathode material. The p-DPPZ electrode presented an impressive specific capacity of 162 mA h g^{-1} at 200 mA g^{-1}, operated efficiently at high current densities of 10 A g^{-1}, and delivered an excellent capacity retention of 96 and 79% after 100 and 1000 charge/discharge cycles, respectively.

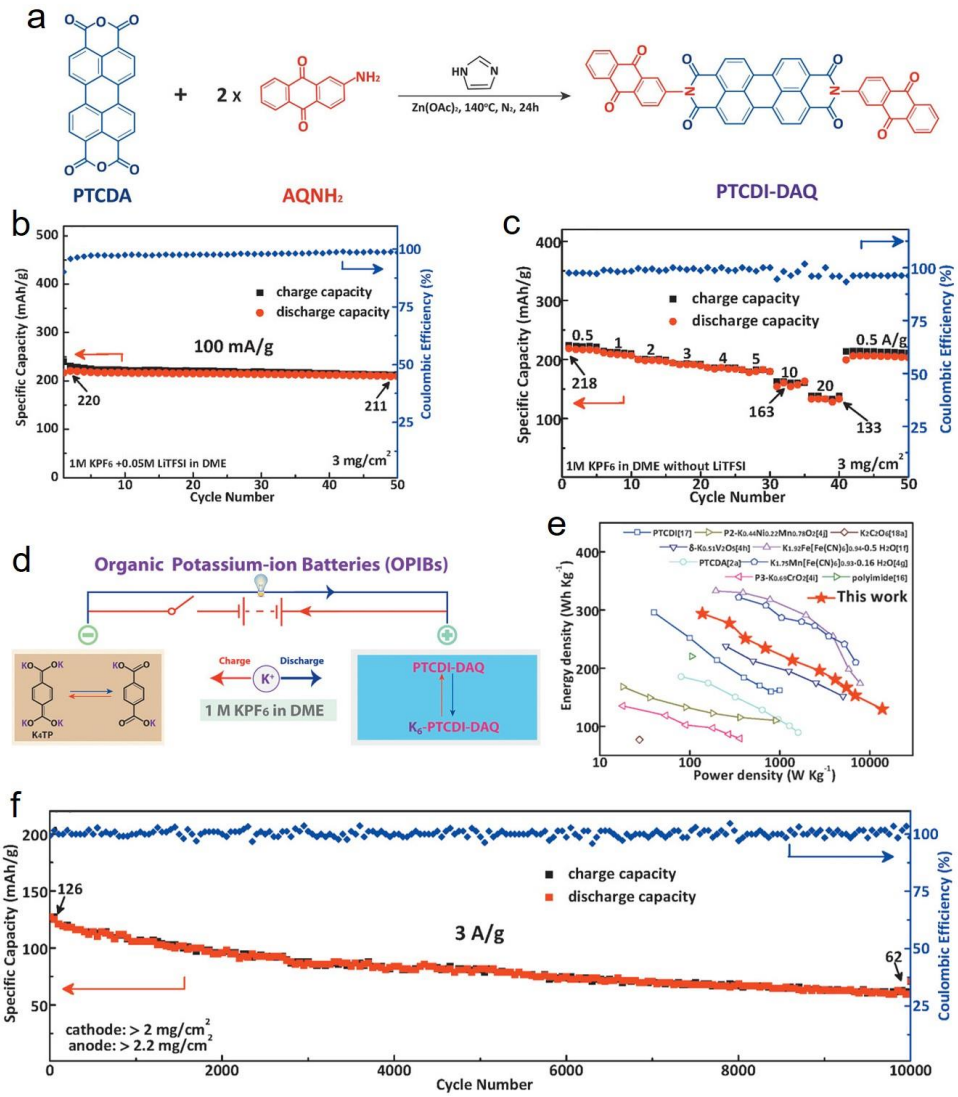

Fig. 8. a) The synthetic route of the PTCDI-DAQ; b) The cycle performance of the PTCDI-DAQ cathode at 100 mA g^{-1}; c) The rate performance of the PTCDI-DAQ compound; d) The configuration of the K_4TP||PTCDI-DAQ full cells; (e) The comparison of energy density and power density of the full cells in this work and other PIB full cells; f) The long-cycle stability of the K_4TP||PTCDI-DAQ full cell at 3 A g^{-1}.

Meanwhile, Lee et al.[117] introduced a simple polymerization processing to optimize the electronic structures, redox kinetics, and interfaces of the 3,4,9,10-perylene-tetracarboxylic acid-dianhydride (PTCDA) cathode and electrolyte, which achieved an impressive cycling stability with negligible capacity degradation after 1000 cycle at 7.35 C. When the current density increased to 147 C, the energy density could still maintain at 113 Wh kg^{-1}, which means that a fully discharge would be well accomplished within 10 s. The full battery using the dipotassium terephthalate anode also obtained a superior energy density and cycling stability in comparison with other the reported all-organic full PIBs. Ning et al.[118] synthesized carbonyl-based organic polymers with different microstructure as cathodes for PIBs, such as one-dimensional (1D) polyimide (PI), 1D polyquinoneimide (PQI), and 2D conjugated microporous polymer (PI-CMP). Among these electrode materials, PQI showed the highest initial capacity because of its highest carbonyl groups but faded rapidly due to the dense potassiated carbonyl groups. Although the

PI-CMP showed a moderate specific capacity, it possessed the best cycling stability and rate performances because of its extended π-conjugation structure. These studies could provide practical pathways to develop novel high-performance organic cathode materials and pave the way to promote PIBs for large-scale applications.

In addition, metal-containing organic compounds, including transition metal ions and alkali ions, are more attractive for practical application, which could be effect with the familiar graphite anodes. Copper tetracyanocyanodimethane (CuTCNQ) is firstly reported as excellent cathode for SIBs[119], in which both of the Cu^+ and $TCNQ^-$ exhibited electrochemical activity with a high reversible specific capacity of 255 mAh g^{-1}. Then, Li et al.[120] used this material as a cathode material for PIBs, confirming an electrochemical activity in the high voltage range of 2-4.1 V. At a current density of 50 mA g^{-1}, the first specific capacity could reach 244 mAh g^{-1}, maintain 170 mAh g^{-1} after 50 cycles, and exhibit a rate performance of 125 mAh g^{-1} at 1 A g^{-1}. Wang et al.[121] introduced an azobenzene-4,4′-dicarboxylic acid potassium salts (ADAPTS) with an azo group as the redox center for PIBs. The extended π-conjugated structure and stable surface reactions between ADAPTS and K ions could enable the reversible charge/discharge process at higher temperatures. When operated at 50 °C, the electrode delivered a capacity of 109 mAh g^{-1} at 1C after 400 cycles. And it showed a high capacity of 113 mAh g^{-1} with 81% capacity retention at 2C after 80 cycles at 60 °C. Chen et al.[122] reported a series of expanded oxocarbon salts $M_2(CO)_n$ (M=Li, Na, K; n=4, 5, 6) for PIBs, preparing via a one-pot proton exchange reaction method. Although most of these $M_2(CO)_n$ salts are soluble in commonly used organic electrolytes, the $K_2C_5O_5$ and $K_2C_6O_6$ obtained high reversible specific capacities, which were also confirmed by the in-situ Raman spectroscopy. Polyanionic sodium anthraquinone-2,6-disulfonate ($Na_2AQ26DS$) was discovered as a new cathode material for PIB full cells by Fan et al.[123], using the K-intercalated reduced-state graphite as anode material. This compound delivered an average capacity of 105 mAh g^{-1} after 250 cycles at the current density of 100 mA g^{-1} and kept 64 mAh g^{-1} for 2500 cycles at 500 mA g^{-1}. Zhao et al.[124] also prepared a para-disodium-2,5-dihydroxy-1,4-benzoquinone (p-$Na_2C_6H_2O_6$) compound for both the SIBs and PIBs, which confirmed that the reversible capacity could reach to 190.6 mAh g^{-1} at 0.1 C for PIBs.

Moreover, the insufficient cycle life, resulting from the dissolution of organic active material and mismatch of electrodes and electrolytes, still hindered their practical applications in PIBs. Zhou et al.[125] improved the cycle life of insoluble anthraquinone-1,5-disulfonic acid sodium salt (AQDS) cathode to 1000 cycles with the capacity retention of 80% at 3 C through a SEI regulation strategy in ether-based electrolytes. The authors confirmed that the excellent performances were attributed to the fast reaction kinetics, dense and stable ether-electrolyte-derived SEI films, which were also protected by an inorganic-rich inner layer. All these delivered a constant and small transfer resistance for K ions in the SEI films, which give critical suggestions for the regulation of electrolytes and SEI to enhance the cycling stability of common organic cathodes.

Organic compounds have been considered as promising cathodes for the practical application of PIBs because of their high theoretical capacities. However, the low operation voltages are still limited for the high energy densities of PIBs. The poor capacity retention should be improved by addressing their dissolution in conventional organic electrolytes, and the initial cycle coulombic efficiencies also needed to be enhanced simultaneously. The metal-containing organic cathodes, especially the K-containing organic compounds, should be further investigations because of their

alterable the electrostatic repulsion and van der Waals interaction forces, thus the commercial graphite anode could be considered to promote the practical applications of PIBs.

2.5 Structural design to improve the electrochemical performances

Since the potassium-containing Prussian blue analogues are usually prepared synthetically in a solution system, the existence of interstitial water is unavoidable. But the interstitial water further leads to a higher quality of the cathode materials, which would have a great impact on the actual specific capacity. With reference to the application of Prussian blue analogs for SIBs, slowing down the crystal growth rate in the synthesis and subsequent heat treatment process can effectively reduce the content of interstitial water, thereby improving the electrochemical performances[40, 46]. In addition, by increasing the proportions and changing the types of coordination ions in Prussian blue analogs, the active sites of such materials in the electrochemical process increase, and their structure can be fine-tuned. Huang et al.[55] synthesized a multivariate Prussian blue analog containing Ni, Co, and Fe by controlled the content of Co and Fe through the synthesis conditions, which confirms that its electrochemical performance is better than the single transition metal Prussian blue analog. The as-prepared Prussian blue samples are in dense spherical packing morphology, and the nickel and cobalt elements are evenly distributed in the particles. Since the $PBN_{0.4}C_{0.6}$ sample has a smaller particle size, the best electrochemical performances, including of the actual specific capacity, cycle performance, rate performance, and alternating-current impedance, are obtained when compared with the PBN and PBC samples.

The intercalation and de-intercalation of K ions in the layered structure are the main way to achieve its electrochemical process. Due to the large radius of K ions, the layered structure always possesses irreversible structural damage during charging and discharging, which leads to a rapid decline in battery capacity. Therefore, stabilizing the layered structure of the electrode material is an urgent problem to be solved. At present, weaving such a metal oxide with a layered structure into a stable skeleton form is an effective method to increase its structural stability. Mai et al.[126] synthesized novel earth-abundant $K_{0.7}Fe_{0.5}Mn_{0.5}O_2$ interconnected nanowires with three-dimensional (3D) network structure (Fig. 9a-d), which can promote the rapid diffusion of K ions and result in high rate performance. The relative stable framework can also reduce the delamination of cathodes caused by K ion intercalation, which is conductive to good cycling stability. And the carbon framework improves the electronic conductivity of the interconnected nanowires by forming a 3D electron transport network. Consequently, the interconnected $K_{0.7}Fe_{0.5}Mn_{0.5}O_2$ nanowires exhibit both high discharge capacity and excellent cycling stability. When used as a cathode material for K-ion full batteries, the capacity retention could keep 76% over 250 cycles (Fig. 9e, f). The novel design will push the development of potential layered cathodes for practical PIBs energy storage systems.

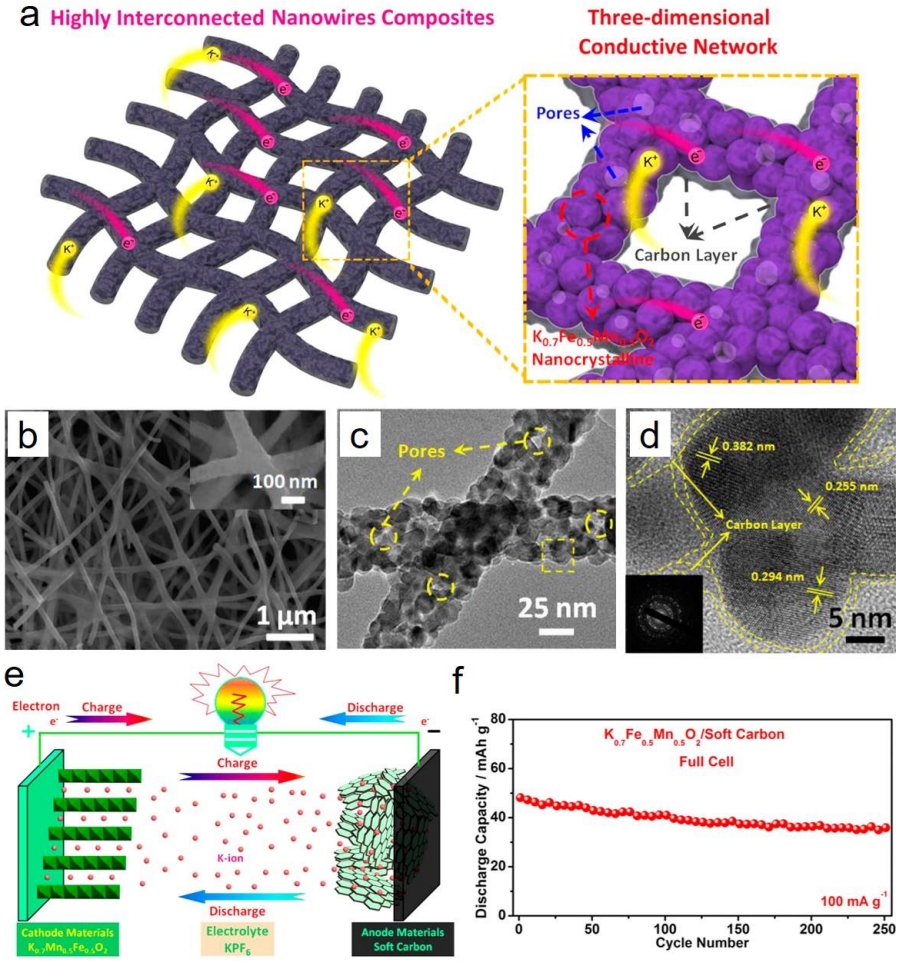

Fig. 9. (a) The design of the 3D interconnected $K_{0.7}Fe_{0.5}Mn_{0.5}O_2$ nanowires. (b-c) SEM image (b), TEM images (c) and high-resolution TEM image (d) of as-prepared nanowire. (e) Schematic illustration of the K-ion full battery based on the interconnected $K_{0.7}Fe_{0.5}Mn_{0.5}O_2$ nanowires/soft carbon. (f) Cycling performance of the K-ion full battery at 100 mA g^{-1}.

Furthermore, Deng et al.[127] prepared P2-type layered $K_{0.65}Fe_{0.5}Mn_{0.5}O_2$ (P2-sKFMO) microspheres by an improved solvothermal method. Based on Rietveld refinement, it shows a typical P2-type layered MO_2 (M = Fe, Mn) structure, where the K ions are located at the prismatic centers of two adjacent MO_2 sheets. Thanks to the stable unique microsphere, the intercalation/de-intercalation kinetics of K ions in P2-KFMO are also enhanced. Compared with microspheres synthesized by high-temperature solid state methods (P2-cKFMO), the P2-sKFMO exhibits better cycling stability and rate performance, and it can still maintain a relatively high specific capacity after charging and discharging at large current densities. The capacity retention rate after 350 cycles is 78% at the current density of 100 mA·g^{-1}. This strategy by constructing microspheres to withstand volume expansion has also been applied to P3 type layered $K_{0.5}Mn_{0.72}Ni_{0.15}Co_{0.13}O_2$,[128] which could improve the capacity retention rate by 28% after 300 cycles at 200 mA g^{-1} as compared to the bulk-like samples.

Recently, there are few studies on polyanionic compounds as cathodes for PIBs system, according to their application in LIBs and SIBs[129]. Because of their low electronic conductivity, the polyanionic compounds have serious impact on the migration of electrons, making the rate performance decay rapidly with the increase of current density. Theoretically, the incorporation of

conductive carbon and the construction of a porous structure can promote electron migration. However, the low specific capacity and poor rate performance still limit the practical application of the currently prepared polyanionic compound and carbon composite electrode materials.

The main problem of the cathode of organic materials is the small molecular compounds generated are easily decomposed during the electrochemical reaction, leading to a significant decrease in specific capacity with the increasing cycle number. Therefore, it is possible to avoid dissolution of small molecules through anchoring, polymerization, salt formation, and electrolyte solidification, thereby triumphing over the shortcomings of poor cycle performance, which has been well proven in the field of SIBs[130, 131].

3. Anode materials

Due to the violent reactivity of K metals, they can hardly be used as an anode material for commercial PIBs because of the potential safety issues, which are quite different from that as a counter electrode for half-cell studies in lab. Thus, the high-performance K storage anode materials are also urgently required to break through the bottleneck of cell potential and capacity. Recently, the investigation on the anode materials for PIBs has been sparked and increased rapidly. In this section, we will detail the recent research on anode materials for PIBs as shown in Table 1, such as graphite, non-graphite carbon, metals/alloys, metal oxides, metal sulfides/selenides, and various composite materials. According to the possible K storage mechanisms of anode materials, this section is divided into three categories: intercalation anodes, conversion anodes, and alloying anodes.

Table 1 Specific capacity and voltage window of anode materials for potassium-ion batteries reported currently 表格内需要列出参考文献吗

Materials	Reaction	Capacity ($mAh\ g^{-1}$)	Rate performance ($mAh\ g^{-1}$)	First CE (%)	Capacity retention	Voltage window(V)
Graphite	Insertion	207 at 5 $mA\ g^{-1}$	141 at 0.2 $A\ g^{-1}$	74.3	-	0-2
Pencil Graphite	Insertion	~230 at 0.2 $A\ g^{-1}$	-	-	~75% after 350 cycles (0.4 $A\ g^{-1}$)	0-2
Reduced graphene oxide	Insertion	222 at 5 $mA\ g^{-1}$	~50 at 0.1 $A\ g^{-1}$	~50	-	0-2
Expanded graphite	Insertion	263 at 10 $mA\ g^{-1}$	175 at 0.2 $A\ g^{-1}$	81.56	~97% after 500 cycles (0.2 $A\ g^{-1}$)	0-3
F-doped graphene	Insertion	326 at 50 $mA\ g^{-1}$	212.6 at 0.5 $A\ g^{-1}$	41.2	~50% after 200 cycles (0.5 $A\ g^{-1}$)	0-3
N-doped graphene (CVD)	Insertion	270 at 0.1 $A\ g^{-1}$	-	80	~96.5% after 50 cycles (0.1 $A\ g^{-1}$)	0-1.5
N-doped graphene	Insertion	320 at 50 $mA\ g^{-1}$	170 at 0.5 $A\ g^{-1}$	37.29	~88% after 500 cycles (0.5 $A\ g^{-1}$)	0-3
Activated carbon	Insertion	209 at 0.1 $A\ g^{-1}$	30 at 1 $A\ g^{-1}$	~62	62% after 100 cycles (0.2 $A\ g^{-1}$)	0-2
amorphous ordered mesoporous carbon	Insertion	286.4 at 0.05 $A\ g^{-1}$	144.2 at 1 $A\ g^{-1}$	63.6	~70% after 1000 cycles (1 $A\ g^{-1}$)	0.01-2.5
Hard Carbon Microspheres	Insertion	262 at 1 C	136 at 5 C	~62	~83% after 100 cycles (0.1 C)	0.01-1.5
N-doped Hard Carbon Microspheres	Insertion	250 at 0.12 C	154 at 7.2 C	75	~75% after 4000 cycles (1.8 C)	0-3
N/O-doped Hard Carbon	Insertion	365 at 25 $mA\ g^{-1}$	118 at 3 $A\ g^{-1}$	45.4	69.5% after 1100 cycles (1.05 $A\ g^{-1}$)	0-3
S/N/O-dope Hard Carbon	Insertion	423 at 0.05 $A\ g^{-1}$	251 at 1 $A\ g^{-1}$	-	~89% after 300 cycles (0.5 $A\ g^{-1}$)	0.01-3
S/O-doped Hard Carbon Microspheres	Insertion	226.6 at 50 $mA\ g^{-1}$	158 at 1 $A\ g^{-1}$	61.7	~68% after 2000 cycles (1 $A\ g^{-1}$)	0.01-2.5
S/N-dope carbon	Insertion	437 at 0.1 $A\ g^{-1}$	72 at 10 Ag^{-1}	45	75% after 3000 cycles (2 $A\ g^{-1}$)	0.01-3
Hard-soft Composite Carbon	Insertion	230 at 0.5 C	45 at 10 C	67	93% after 200 cycles (1 C)	0.1-2

HCNT	Insertion	232 at 0.1 A g^{-1}	162 at 1.6 A g^{-1}	15	90% after 500 cycles (0.1 A g^{-1})	0-2.5
NCNT	Insertion	248 at 25 mA g^{-1}	101 at 20 A g^{-1}	49	~95% after 4000 cycles (2 A g^{-1})	0-3
$KTi_2(PO_4)_3$/C	Insertion	75.6 at 0.5 C	~69 at 5 C	~79	~118% after 100 cycles (0.5 C)	1.2-2.8
$K_2Ti_8O_{17}$	Insertion	181.5 at 20 mA g^{-1}	44.2 at 0.5 A g^{-1}	65.4	~61% after 50 cycles (20 mA g^{-1})	0.01-3
$K_2Ti_4O_9$	Insertion	97 at 30 mA g^{-1}	20 at 2 A g^{-1}	20	-	0.01-2.5
$K_2Ti_4O_9$	Insertion	151 at 50 mA g^{-1}	88 at 0.3 A g^{-1}	26	51% after 900 cycles (0.2 A g^{-1})	0.01-3
$K_{0.4}MoS_2$	Insertion	65.4 at 20 mA g^{-1}	-	74.4	97.5% after 200 cycles (20 mA g^{-1})	0.5-2
ReS_2/N-CNF	Insertion	253 at 50 mA g^{-1}	-	67.3	~71% after 100 cycles (50 mA g^{-1})	0.01-3
Ti_3CNTz	Insertion	202 at 20 mA g^{-1}	32 at 0.5A g^{-1}	28.4	27% after 100 cycles (20 mA g^{-1})	0.01-3
Ti_3C_2	Insertion	136 at 0.2 A g^{-1}		27	-	0.01-3
TiO_xN_y/C	Insertion	150 at 0.2 A g^{-1}	75 at 1.6 A g^{-1}	~26	~23% after 1200 cycles (0.2 A g^{-1})	0.01-3
$MoSe_2/Ti_3C_2$@C	Insertion	355 at 0.2 A g^{-1}	183 at 10 A g^{-1}	54.2	99.2% after 100 cycles (0.2 A g^{-1})	0.01-3
MOFs-NCNTs	Insertion	254.7 at 50 mA g^{-1}	102 at 2 A g^{-1}	24.45	77.86% after 500 cycles (2 A g^{-1})	0-3
Co_3O_4-F_2O_3/C	Conversion	420 at 50 mA g^{-1}	278 at 1 A g^{-1}	54	60% after 100 cycles (50 mA g^{-1})	0.01-3
MoS_2@RGO	Conversion/Insertion	679 at 0.1 A g^{-1}	178 at 0.5 A g^{-1}	~30	~108% after 100 cycles (0.1 A g^{-1})	0.01-3
MoS_2@RGO	Conversion/Insertion	607.4 at 0.1 A g^{-1}	196.8 at 2 A g^{-1}	~72	116.9 after 1000 cycles (0.5 A g^{-1})	0.01-3
SnS_2-rGO	Conversion/Alloying	355 at 25 mA g^{-1}	120 at 2 A g^{-1}	56	-	0.01-2
Sb_2S_3-SNG	Conversion	548 at 20 mA g^{-1}	~340 at 1 A g^{-1}	69.7	89.4% after 100 cycles (50 mA g^{-1})	0.1-3
Few layered Sb_2S_3/C	Conversion	404 at 0.5 A g^{-1}	-	-	-	0.01-2
G@Y–S FeS_2@C	Conversion	521 at 0.15 A g^{-1}	203 at 10 A g^{-1}	36	~50% after 1000 cycle (1 A g^{-1})	0.05-2.8
FeP@CNBs	Conversion	201 at 0.1 A g^{-1}	37 at 2 A g^{-1}	47	~78 after 300 cycles (0.1 A g^{-1})	0.01-2.5
FeP@FGCS	Conversion	411 at 0.05 A g^{-1}	164 at 5 A g^{-1}	58.8	88.3% after 800 cycles (2 A g^{-1})	0.01-3
NiS@C	Conversion	473 at 0.1 A g^{-1}	143 at 1.6 A g^{-1}	-	-	0.01-3
$NiSe_2$@rGO	Conversion	522 at 20 mA g^{-1}	272 at 1 A g^{-1}	37.9	~95% after 1200 cycles (1 A g^{-1})	0.01-2.5
Cu_2S@NC	Conversion	317 at 1 A g^{-1}	257 at 6 A g^{-1}	57.4	83.2% after 800 cycles (0.5 A g^{-1})	0.01-2.6
CuSe	Conversion	340 at 0.1 A g^{-1}	280 at 5 A g^{-1}	92.4	92.6% after 340 cycles (2 A g^{-1})	0.01-3
ZnS@C@rGO	Conversion	419 at 20 mA g^{-1}	162 at 0.5 A g^{-1}	63.6	-	0.01-2.5
ZnSe/C	Conversion	318 at 50 mA g^{-1}	205 at 0.5 A g^{-1}	47.78	~92% after 1000 cycles (0.5 A g^{-1})	0.01-2.5
CoS@G	Conversion/Insertion	310.8 at 0.5 A g^{-1}	~225 at 4 C	64.4	70.2% after 100 cycles (0.5 C)	0.01-2.9
Sn	Alloying	66 at 50 mA g^{-1}	-	-	-	3-5
Sn/C	Alloying	150 at 25 mA g^{-1}	-	51.4	~81% after 30 cycles (25 mA g^{-1})	0.01-2
Sn_4P_3/C	Alloying	384.8 at 50 mA g^{-1}	221.9 at 1 A g^{-1}	~60	80% after 50 cycles (50 mA g^{-1})	0.01-2
Black Phosphorus-C	Alloying	617 at 50 mA g^{-1}	120 at 0.5 A g^{-1}	67	-	0.01-2
Red P@N-PHCNFs	Alloying	745 at 0.1 A g^{-1}	565 at 5 A g^{-1}	-	52% after 800 cycles (5 A g^{-1})	0.01-2
SnS_2@C@rGO	Alloying	499.4 at 0.05 A g^{-1}	287.8 at 0.5 A g^{-1}	53	59% after 500 cycles (0.5 A g^{-1})	0.01-3
Sb/C	Alloying	250 at 35 mA g^{-1}	-	~67	97% after 55 cycles (70 mA g^{-1})	0.05-2
Sb@PC	Alloying	250 at 0.1 A g^{-1}	70 at 2 A g^{-1}	46.2	~53% after 200 cycles (0.5 A g^{-1})	0.01-2.5
Sb@rGO	Alloying	300 at 0.2 A g^{-1}	222 at 1 A g^{-1}	-	96.7% after 60 cycles (0.1 A g^{-1})	0.01-2.5
Sb@C PNFs	Alloying	399.7 at 0.1 A g^{-1}	208.1 at 5 A g^{-1}	-	~85% after 500 cycles (2 A g^{-1})	0.01-3
Bi	Alloying	496 at 0.2 A g^{-1}	321.9 at 3 C	80.2	86.9% after 300 cycles (2 C)	0-1.5

Bi microparticles	Alloying	404 at 0.4 A g^{-1}	276 at 1.6 A g^{-1}	83	97% after 100 cycles (0.4 A g^{-1})	0.1-1.5
hollow Bi@C nanorods	Alloying	353 at 0.05 A g^{-1}	186.1 at 1.5 A g^{-1}	59.7	80.3% after 300 cycles (0.5 A g^{-1})	0.01-1.6
MXene@Sb	Alloying	516.8 at 50 mA g^{-1}	270 at 0.5 A g^{-1}	57.29	~79% after 500 cycles (0.5 A g^{-1})	0.01-1.2
BiSb@C	Alloying	598 at 0.1 A g^{-1}	152 at 2 A g^{-1}	70.2	97.5% after 600 cycles (0.5 A g^{-1})	-

3.1 Intercalation anodes

3.1.1 Graphite carbon materials

Graphite carbon materials have shown great potential as anode materials for rechargeable metal -ion (Li, K, Al) Batteries, because of their excellent electronic conductivity, thermal conductivity, and stable chemical structure for reversible insertion/extraction of guest metal ions between carbon layers [132-134]. It is known that the lithium and graphite react and form various intermediate compounds during the intercalation process, and finally transform into LiC_6. [135, 136] In a similar way, the K-graphite intercalation compounds are also formed in the process of electrochemical intercalation of K ions into graphite[137-140]. Both the ex-situ XRD and in-situ XRD results for the phase transitions in the first K-insertion confirmed that the KC_{36} is firstly formed ranging from 0.3 to 0.2 V, then transformed into KC_{24} between 0.2 to 0.1 V, and finally changed to KC_8 at 0.01 V. During the K-extraction, KC_8 is directly converted to KC_{36} compound at about 0.3 V, and subsequently replaced by the graphite with low crystallinity when then voltage is above 0.5 V. Some studies also reported the process of K ions embedded in graphite is $C \rightarrow KC_{24} \rightarrow KC_{16} \rightarrow KC_8$,[141] which is slightly different but similar. The DFT calculation was also used to investigate the complex K-insertion/extraction in graphite materials, which confirms that the K^+ ions can insert into the graphite layer more easily due to the lower formation enthalpy of KC_8 (-27.5 kJ/mol) than that of the LiC_6 (-16.5 kJ/mol)[142]. And the diffusion coefficient of KC_8 (2.0×10^{-10} m^2/s) is also much larger than that of LiC_6 (1.5×10^{-15} m^2/s), manifesting the advantages of K ions intercalation process in graphite[143]. As a result, the theoretical specific capacity of graphite carbon materials for PIBs could achieve 279 mAh g^{-1}.

Jian et al.[137] studied the electrochemical performances of potassium ions intercalation into the graphite in non-aqueous electrolytes, showing a specific capacity up to 475 mAh g^{-1} after initial potassiation process, while the first depotassiation process has a specific capacity of 273 mAh g^{-1}, which is very close to the theoretical specific capacity. The low initial Coulomb efficiency was only 57.4% because of the SEI film formed on the graphite surface, which is remarkably similar to the lithiation/delithiation behavior in graphite materials for LIBs. The research also exhibits a poor rate capability with the specific capacities of 263, 234, 172, and 80 mAh g^{-1} at 0.1, 0.2, 0.5, and 1 C (1 C= 279 mA g^{-1}). Moreover, the specific capacity also decreases rapidly from 197 mAh·g^{-1} to 100 mAh·g^{-1} after 50 cycles at 0.5 C. The structural damage of graphite materials in the whole potassiation/depotassiation might lead to a lower crystallinity and further affect the cycling performance.

In order to improve the rate capability and the cycle performance of graphite materials for PIBs, many efficient strategies have been performed, including the stable morphology control, the increase of interlayer distance, and the introduction of disorder region. Song et al.[144] reported a highly graphitized carbon hollow nanocage with an average diameter of 50 nm and a thickness of 5 nm as a PIBs anode. The interconnected hollow nanocage architecture could not only promote the electron transfer, but also reduce the ion diffusion distance and accommodate the interlayer expansion. The as-prepared sample finally obtained an excellent an excellent rate capability of 175

mAh g^{-1} at an unbelievable rate of 35 C, which is about 79% of that at 0.1 C. After 100 cycles at 0.2 C, the nanocage electrode could maintain a reversible capacity of 195 mAh g^{-1} with the capacity retention of 92%. The potassium storage mechanism is analyzed to be redox reactions (intercalation/deintercalation) and double-layer capacitance (surface adsorption/desorption), which presents new insights for the structural design of graphite carbon materials in PIBs. It is also interesting that Tai et al.[145] studied an ultra-flexible graphite anode via coating the filter paper by commercial 8B pencil. The rate performance of this electrode in PIBs is even better than that in LIBs from 0.1 A g^{-1} to 0.5 A g^{-1} (the retention rate of PIBs is 66%, while that of LIBs is 22%). After 350 cycles at 0.4 A g^{-1}, the capacity retention rate can keep 75%. Choi et al.[146] demonstrated the porous carbon microspheres with highly graphitized structure for potassium-ion storage, which exhibit a stable specific capacity of 292.0 mAh g^{-1} after 100 cycles. The high crystallinity and porous structure are critical to the desirable performances, which could alleviate the stress caused by the large volume expansion during the K-insertion/extraction. Zhang et al.[147] reported a nitrogen-doped and defect-rich graphitic nanocarbon (GNCs) as the PIB anode, which shows better electrochemical performance than other thin-walled graphitic carbon materials including carbon nanocages and nanotubes. For example, the capacity is 280 mAh g^{-1} at 50 mA g^{-1}, and when the current density increases to 200 mA g^{-1}, the capacity can still maintain at 189 mAh g^{-1} after 200 cycles. The chemical vapor deposition method was served to deposit graphitic nanodomains into the nanoporous graphenic carbon, which resulted in a unique short-range ordered and long-range disordered structure[148]. When the disordered structure is selected as an anode material for PIBs, it could obtain a capacity retention of 50% after 240 cycles. Activated carbon materials were used to develop graphite carbon because of its large interplanar spacing via high temperature annealing[149]. The resulted special structure, anchoring nanosized carbon sheets on the graphite particles, could rapidly intercalate/deintercalate the K ions with a larger diffusion coefficient than the pristine graphite carbon, which accounts for the enhanced rate performance during the discharge/charge process. In addition, expanded graphite can also intercalate/deintercalate K ions into the enlarged carbon layers with a similar potassium storage mechanism. An et al.[150] reported a large-sized expanded graphite that can be used commercially as an anode material for PIBs. The as-prepared expanded graphite electrodes provide a specific capacity of 263 mAh g^{-1} at a current density of 10 mA g^{-1}, which keeps almost unchanged after 500 cycles. At 200 mA g^{-1}, the specific capacity is still about 174 mAh g^{-1} with the Coulomb efficiency of almost 100%. The specific capacity of the expanded graphite is comparable to the commercial graphite materials, but the rate and cycling performance are much better. After performance optimization by these methods, the capacity and rate capability of the graphite anode materials have been enhanced. However, the initial Coulomb efficiency and cycling stability still limit their practical application in PIBs, which should be devoted in future studies.

In recent years, graphene materials, as a member of graphite carbon materials, have attracted more and more attentions because of their excellent chemical, physical, mechanical, electrical, thermal, and optical properties. For example, the theoretical specific surface area is 2630 m^2 g^{-1}, and the theoretical Young's modulus is 1.0 TPa[151], the carrier mobility up to 200,000 cm^2 $(V\ s)^{-1}$ at room temperature[152], and the thermal conductivity is 5300 W m^{-1} K^{-1}.[153] However, the electrochemical properties of the graphene is still imperfect. The commonly optimized principle for the graphene-based materials for PIBs are introducing more point defects, heteroatom, edges, grain boundaries, and structural design, which could adjust the surface wettability, improve the

electronic conductivity, shorten the ion transportation pathways and enhance the electrochemical performance of the graphene electrodes.

Since fluorine element is the most electronegative element, the induced hybridization of carbon atoms could be changed from sp^2 to sp^3 after doping with fluorine, possibly enhancing the electrochemical performance of graphene. Ju et al.[154] synthesized a few-layered F-doped graphene foam anode via a high-temperature solid-state method using PVDF as raw material. The reversible specific capacities are 326.1, 271.9, 250.7, and 212.6 mAh g^{-1} at the current densities of 50, 100, 200, and 500 mA g^{-1}, respectively. After 200 cycles at 500 mA g^{-1}, the F-doped graphene anode still maintain the capacity of 165.9 mAh g^{-1}. The authors reveal that the excellent rate capability and cycling stability are attributed to the synergistic effects of F in graphene, including the high specific surface area, fast ions and electrons transportation, and abundant active sites for K ions storage. Zhao et al.[155] reported a facile hydrofluoric acid solution immersion method to purify the low-grade microcrystalline graphite ore. The purity of modified graphite could be as high as 98.59 wt% with the effective F-corporation of the content about 1.02%, which could enlarge the interlayer distance and further lead to a fast K-ion diffusion and weak volume change. The F-doping-induced graphite electrode exhibits a prominent capacity of 320 mAh g^{-1}, an enhanced rate performance, and a stable cycling property with a capacity retention of 74.6% after 100 cycles. This study could pave the way of graphite ore as anode material for commercial PIBs. Chen et al.[156] proposed an unconventional microwave-based shock exfoliation strategy to decompose the graphite fluoride into few-layer fluorinated graphene, which also exhibits high capacity retention (220.3 mAh g^{-1}) after 50 cycles and excellent rate capacity as an anode for PIBs. Lu et al.[157] designed an oxygen/fluorine dual-doped porous carbon nanopolyhedra anode material, exhibiting a superior capacity (481 mAh g^{-1}) at 50 mA g^{-1} and excellent cycling performance of 218 mAh g^{-1} after 2000 cycles at 1 A g^{-1}. Even when the current density increase to 10 A g^{-1}, the reversible capacity is still maintained at 111 mAh g^{-1} after 5000 cycles. The potassium storage mechanism is explained to be the combined effect of diffusion and capacitance processes. And the O/F dual-doped in the carbon nanopolyhedra can promote the adsorption of K ions without obvious structural distortion, resulting in the outstanding specific capacity, rate capability, and cycling stability for commercial PIBs.

Nitrogen-doped carbon materials are the mostly studied strategies among the heteroatom-doped graphene materials in PIBs, which could generate abundant extrinsic defects and enhance the electronic conductivity and reaction activity. Pint et al.[158] firstly reported a few-layer N-doped graphene for the anode material of PIBs. The K ions storage capacity could be as high as about 350 mAh g^{-1} at the rate of 50 mA g^{-1}, which is very close to the theoretical capacity of the graphite anode in LIBs. Further studies on the cycling performance at 100 mA g^{-1} also indicate a stable and high capacity, which initially starts at 270 mAh g^{-1} and remains about 210 mAh g^{-1} after 100 cycles. Ju et al.[159] also prepared a similar N-doped graphene material via a bottom-up synthesis method. The enhanced conductivity, originating from the rich content of N-doping (14.68 at%), could account for the high specific capacity, superior rate performance, and long-term cycling capability of the graphene electrode in PIBs. Qiu et al.[160] reported the N-doped soft carbon frameworks by MgO template method, exhibiting rapid K^+ ions diffusion and electron transfer. The interconnected hierarchically porous structure delivers a large capacity of 293 mAh g^{-1} at 0.05 A g^{-1} and retains nearly 85.5% capacity after 500 cycles at 1 A g^{-1}. Li et al.[161] prepared a honeycomb-like N-doped carbon (N-C) nanosheet anode material for PIBs via a complex method

by growing MOFs on LDHs nanosheets followed with the pyrolysis and acid-etching processes. The as-prepared N-C material obtains high specific surface area, enlarged interlayer distance, and uniform micro/meso/macro-pores, delivering excellent cycling performance at 1 A g^{-1} after 2000 cycles (143 mAh g^{-1}) and stable rate capability up to 10 A g^{-1}. Yu et al.[162] fabricated an interconnected N-doped hierarchical porous carbon material, which shows superior reversible capacity (292 mAh g^{-1} at 0.1 A g^{-1}), excellent rate capability (94 mAh g^{-1} at 10.0 A g^{-1}), and outstanding cycle stability (157 mA g^{-1} after 12000 cycles at 2.0 A g^{-1}). The 3D hierarchical porous structure and N-doping mostly account for the excellent K storage performances. Guo et al.[163] also report a series of pyrrolic/pyridinic-N-doped necklace-like hollow carbon materials as free-standing anodes for enhancing PIBs. Because of their high specific surface area, ultra-high pyrrolic/pyridinic-N doping content, and abundant hierarchical micro/meso/macro-pores, the N-doped necklace-like hollow carbon materials deliver various advantages, such as promoting the intercalation/deintercalation of K ions, reducing the volume expansion, and finally improving the property stability of PIBs. The reversible specific capacity is obtained to be 293.5 mAh g^{-1} at 100 mA g^{-1}, and the rate performance could reach as high as 204.8 mAh g^{-1} at 2 A g^{-1} with an unbelievable cycling performance (161.3 mAh g^{-1} at 1 A g^{-1} after 1600 cycles). Tang et al.[164] also synthesized a N-doped carbon nanosheet anode material with an ultrahigh nitrogen content (22.7 at%) for PIBs, delivering similarly high-performance electrochemical performances. An et al.[165] designed a graphene-like N-doped porous carbon array on a 3D Cu substrate as a self-standing and binder-free anode for PIBs, which exhibits eminent potassium storage performances including reversible capacity, rate performance, and stability. Furthermore, the nitrogen and oxygen dual-doped carbon materials were also proposed recently as high-performance anodes for PIBs. Yu et al.[166] designed a nitrogen/oxygen co-doped carbon coated graphene foam films, which delivers a higher reversible capacity (319 mAh g^{-1} at 0.1 A g^{-1}) and a better long cycling stability (281 mAh $g^{-1}$with a capacity retention of 98.1% after 5500 cycles at 1 A g^{-1}) than others. Tai et al.[167] also reported a facile renewable method to synthesize the nitrogen/oxygen co-doped graphene-like carbon nanocages with impressive reversible both the lithiation and potassium storage capacities.

Like the doping of heteroatoms F and N, the sulfur or phosphorus elements are also used to enhance the electrochemical properties of the carbon anodes. Due to their large anion radii and additional potassium active sites, these S or P atoms can not only expand the distance of carbon layer and promote the insertion/deinsertion of K ions, but also increase the potassium storage amount, finally improving the potassium storage performances of PIBs. Mai et al.[168] reported a simple freeze-drying and subsequent thermal treatment method in sulfur steam to successfully prepare the sulfur-doped reduced graphene oxide sponges as free-standing anodes for PIBs. The as-prepared S-doped graphene sponges electrodes deliver a high capacity of 361 mAh g^{-1} at 50 mA g^{-1} after 50 cycles, which could also exhibit a highly stable capacity of 229 mAh g^{-1} at 1 A g^{-1} over 500 cycles. These K-ion storage performances outperforms most previously reported carbon-based anode materials for PIBs. After the reaction mechanism investigation via ex situ XPS, the role of the unique conductive structure and the resulted additional reversible reactions (such as K_2S) by S-doping together contribute to such a preeminent performance. Miltin et al.[169] created a sulfur-grafted hollow carbon sphere (SHCS) anode material for PIBs, which shows several advantages including the nanoscale diffusion distances (≈40 nm) and the special C-S chemical bonds. The SHCS electrode displays a extremely high reversible capacity of 581 mAh

g^{-1} at the current density of 25 mA g^{-1}, an excellent rate capability of 110 mAh g^{-1} at 5 A g^{-1}, and a stable capacity retention of 93% from the 5^{th} to 1000^{th} cycle at 5 A g^{-1}. Xing et al.[170] introduced a functional P and O dual-doped graphene (PODG) material as superior anode for PIBs, preparing by a thermal annealing method. This electrode delivers an ultra-high specific capacity and cycling stability, which could retain the capacity of 160 mA h g^{-1} after 600 cycles at 2 A g^{-1}. The co-doping of P and O atoms enlarges the interlayer spacing, facilitates the insertion and extraction of K ions, and further results in the superior electrochemical performances. These two different heteroatoms dual-doping strategies have also attracted much attentions in recent two years to further improve the potassium storage properties, combining advantages of each doping site. For example, Guo et al.[171] reported a 3D carbon framework assembled by the N and S dual-doped graphene nanosheets (CFM-SNG, Fig. 10a) with enlarged interlayer spacing (0.448 nm) and additional edge defects (Fig. 10b, c). As a result, the reversible capacity could be enhanced to 348.2 mAh g^{-1} at 50 mA g^{-1} and the rate capability is also prominently enhanced (Fig. 10d, e). When cycling at 2 A g^{-1} for 2000 cycles, the capacity can still maintain at 188.8 mAh g^{-1}. Further DFT calculations indicate that the pyrrolic N and S sites are more effective to enlarge the graphene interlayer spacing and promote the adsorption of K ions (Fig. 10f-k), delivering a high-performance as PIBs anodes. Other similar results, such as the N/S co-doped carbon micro-boxes[172], low-surface area S and N-rich carbon materials[173], N/S-containing 3D flower-like carbon architectures[174], and 3D S and N co-doped carbon nanofiber aerogels[175], were also obtained with enhanced electrochemical potassium storage performances. Moreover, the N and P co-doped graphene materials have also been prepared and used as stable anodes for PIBs recently. Qiu et al.[176] anchored the N and P dual-doped vertical graphene nanosheets on the carbon cloth (N, P-VG@CC), which was used as a binder-free anode for flexible PIBs. Thanks to the enhanced active sites, large specific surface area, expanded interlayer spacing, and highly robust and conductive network structure, this as-prepared anode displays a high capacity (344.3 mAh g^{-1} at 25 mA g^{-1}), excellent rate capability (the capacity retention of 46.5% at 2 A g^{-1}), and stable long-term cycling property (the capacity retention of 82% after 1000 cycles at 25 mA g^{-1}). Furthermore, the N, P-VG@CC material are fabricated into a full PIB, using the potassium Prussian blue as the cathode material. The energy density is calculated to be 232.5 Wh kg^{-1} along with prominent cycle stability.

For the structural design strategy of graphene carbon materials, Simon et al.[177] reported a 3D reduced graphene oxide (rGO) aerogel for the PIB anode. Because of the high apparent diffusion coefficient of K ions in the open porous structure, the as-prepared rGO aerogel delivers a high capacity of 267 mA h g^{-1} at 93 mA g^{-1} with a capacity retention of 78% over 100 cycles. Yang et al.[178] also obtained a flowable sulfur template method to synthesize the graphene-built porous carbons with controllable pore size and shape. The advantages including fast ion transport and large ion storage are also presented for this electrode, which further results in an ultrahigh volumetric potassium storage with an ultralong cycling performance over 500 cycles. A special graphene-based composite microsphere armored with a crystal carbon shell is also prepared, by Lu et al., to improve the structural stability of graphene materials[179]. As a PIB anode, this composite material displays an initial capacity of 297.89 mAh g^{-1} (CE≈99%) and outstanding cyclic stability nearly without any capacity loss after 1250 cycles at 100 mA g^{-1}. Lu et al.[180] introduced the carbon dots on the surface of rGO to obtain a freestanding and flexible 3D hybrid architecture defined as CDs@rGO paper anode for PIBs. Benefitting from the abundant defects,

oxygen-containing functional groups, and enhanced reaction kinetics because of the efficient ion and electron transfer channels, this electrode presents an obviously improved electrochemical performance, e.g. the high reversible capacity (310 mAh g^{-1} at 100 mA g^{-1}), excellent rate performance (185 mAh g^{-1} at 500 mA g^{-1}), and ultra-stable long cycle life (244 mAh g^{-1} after 840 cycles at 200 mA g^{-1}). However, as for the graphene carbon anode materials, the optimization on Coulomb efficiency, potential plateau, and voltage hysteresis are still needed in future to push the development of the advanced graphene anode materials in PIBs.

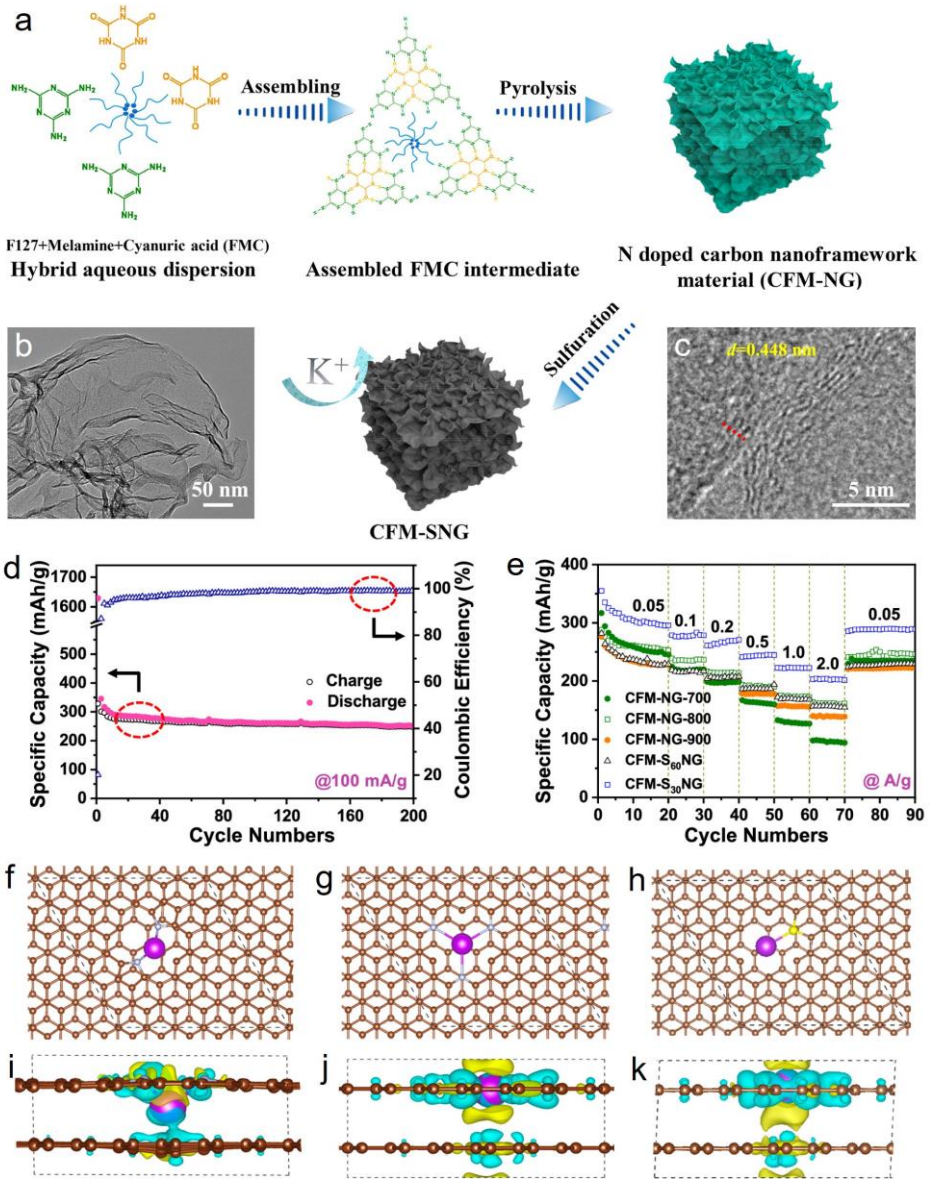

Fig. 10. (a) The synthesis of the CFM-SNG materials; (b) TEM images and (c) HRTEM images of the CFM-S30NG sample; (d) The discharge and charge capacity and CE of the CFM-S30NG electrode at 100 mA g^{-1}; (e) The rate performance of the CFM-SNG materials at different current densities, including 50, 100, 200, 500, 1000, and 2000 mA g^{-1}; (f-h) The adsorption of K ion on the (f) N5, (g) N6 and (h) S6 doped graphene structures; (i-k) The differences of the electron density of K absorbed on the (i) N5, (j) N6, and (k) S6 doped graphene structures. The C, N, S, and K atoms are presented in brown, blue, yellow, and purple colors, respectively. The yellow and blue areas in images (i-k) represent the increased electron density and decreased electron density, respectively.

3.1.2 Non-graphite carbon materials

Due to the advantages in ion diffusion and electron transportation from the disordered structure or partially disordered structure with randomly located graphitized microdomains or graphene nanosheets, the non-graphite carbon materials have also been well investigated as anode materials for PIBs. These materials usually include various amorphous carbons, such as hard carbon, soft carbon, and heteroatom-doping non-graphite carbon. In this section, we will focus on the preparation of these materials and their performance optimization as anodes for K storage. The previously reported hard carbon materials mainly contain biomass-derived carbon materials, metal-organic frameworks (MOFs)-derived carbon materials, and other porous hard carbon materials.

The biomass materials are mainly composed of C, H, and O elementals, such as sugars, pectins, cellulose, hemicelluloses, lignins, and proteins, which could transfer to the carbon materials after a simple pyrolysis process. We synthesized the amorphous ordered mesoporous carbon (OMC) as an anode for PIBs, using SBA-15 as a template and sucrose as carbon source[181]. Unlike the well-crystallized graphite, in which the K ions are squeezed into the restricted interlayer spacing, the amorphous OMC material possesses larger interlayer spacing in short range and fewer carbon atoms in one carbon-layers cluster. The special structure can intercalate more K ions into the carbon layer, accommodate the increase of the interlayer spacing, and tolerate the volume expansion during the intercalation/deintercalation of K ions. And the calculation results indicate that the OMC layer spacing changes by only 7% during the potassiation/depotassiation process. At the current density of 50 mA g^{-1}, the K storage capacity can remain 257.4 mAh g^{-1} over 100 cycles. When the current density increases to 1.0 A·g^{-1}, a highly reversible storage capacity of 146.5 mAh g^{-1} is still obtained over 1000 cycles with a Coulombic efficiency of nearly 100%. Komaba et al.[182] reported a high-capacity hard carbon for both the SIBs and PIBs, preparing by heat-treating the macro-porous phenolic resin. As the heat-treatment temperature increases from 1100 to 1500 °C, the distance of the carbon layer decrease and the void size of the pores increases, delivering an increasing reversible capacity with the increasing temperatures.

Most plants including trees, crops, and vegetables are also appropriate carbon sources for electrochemical energy storage, due to their abundance and environmental friendliness. Liu et al.[183] prepared a hierarchical porous hard carbon by using the low-cost and abundant soybeans as raw material. Benefiting from the medium surface area, low degree of graphitization, and large interplanar spacing, the obtained hard carbon electrode exhibits a high discharge capacity of 225 mAh g^{-1} at 40 mA g^{-1} and impressive cycling stability of 900 cycles. The adsorption-dominated mechanism is found to be responsible for the superior performance of the soybeans-derived hard carbon anode. Moreover, a thin Al_2O_3 film (about 2 nm) is further coated on the surface of hard carbon materials as an artificial SEI film, achieving the enhancement of Coulombic efficiency from 99.0% to 99.6%. Jiang et al.[184] constructed a N/O dual-doped hard carbon from the renewable sorghum stalks as the anode material for PIBs. Similarly, the as-prepared sample presents impressive electrochemical performances, including high reversible capacity (304.6 mAh g^{-1} after 100 cycles at 100 mA g^{-1}) and superior long cycling stability (189.5 mAh g^{-1} after 5000 cycles at 1 A g^{-1}). Furthermore, the loofah[185], corn husk[186], potato[187], Ganoderma lucidum spore[188], sycamore fruit[189], lotus root[190], cotton[191], cocoon silk[192], rice husk[193], waste orange peel[194], and mango seed shuck[195] are also used prepare various biomorphic carbon recently. When they are

used as the anode materials for PIBs, all the as-prepared carbon electrodes could exhibit high capacity and long cycling stability due to the capacitance and diffusion K^+ storage mechanisms, which might impel the development of low-cost and sustainable hard carbon-based anode materials for commercial PIBs.

Interestingly, Yan et al.[196] reported an onion-like carbon anode material from the facile combustion soot as the candle burnt. When assembled into a half cell for K^+ storage, the electrode exhibits a high reversible capacity (245 mAh g^{-1} at 50 mA g^{-1}), good rate performance (78 mAh g^{-1} at 10 A g^{-1}), and cycling stability (111 mAh g^{-1} at 2 A g^{-1} over 1000 cycles). After further fabricating into a K^+ ion hybrid capacitor using the onion-like carbon and activated carbon as the battery-type anode and capacitor-type cathode, the device could exhibit a high energy density of 142 W h kg^{-1} with a long cycling stability of 83% capacity retention after 6000 cycles, showing great potential for the high-power and high-energy K^+ ions storage systems.

Nanjundan et at.[197] reported an amorphous hard carbon material for high-performance PIBs, prepared via a simple pyrolysis method from the commercial cellulose. The high capacity (~294 mA h g^{-1} at 50 mA g^{-1}), good rate capability, and long cycling performance (~60 mA h g^{-1} after 1000 cycles at 1 A g^{-1}) are obtained, which could be credited to the low volume expansion and the enlarged interlayer spacing alongside the electronegative oxygen functional groups on the carbon material. Chitin, with intrinsic fibrous structure and nitrogen functional groups, has also shown much superiority as hard carbon anodes for PIBs. Guo et al.[198] reported the N-doped carbon nanofibers by direct carbonization of biowaste chitin, which could obtain a specific capacity of 200 mA h g^{-1} after 100 cycles at the current density of 55.8 mA g^{-1}. Zhang et al.[199] firstly reported a hierarchically porous N-doped carbon microsphere (NCS) anode for PIBs, using the plentiful discarded seafood waste as biomass raw material. The porous microstructure and N-doping could promote the electron/ion transport and offer more defects, enhancing the adsorption capability of K ions. Based on the surface-driven K storage mechanism, the porous N-doped carbon microsphere anode displays an ultralong cycling stability (180 mA h g^{-1} at 1.8 C) without obvious capacity decay over 4000 cycles and outstanding rate capability of 154 mA h g^{-1} at 72 C. Recently, the active sites enriched hard carbon porous nanobelts were also fabricated for K^+ storage by Zhang et al.[200], constructing via a self-template assisted pyrolysis strategy from the mineralized shrimp shells (Fig. 11a,b). Similarly, the hard carbon nanobelts possess the many advantages for the PIB anode, such as pyrrolic/pyridinic-N and O dual-doping (Fig. 11c), expanded interlayer spacing (Fig. 11e), and hierarchical micro/meso/macro-porous structure (Fig. 11d). As a result, the reversible capacity could achieve the amazing value of 468 mAh g^{-1} at 50 mA g^{-1} and a long cycling life at the high current density of 1 A g^{-1} (277 mAh g^{-1} over 1600 cycles) is also obtained in Fig. 11f. The capacitive-adsorbed K^+ storage mechanism is found by DFT and kinetics studies, which is further enhanced by the rich active sites in the N and O co-doped hard carbon nanobelts. After fabricating into a coin-type potassium dual-ion battery with the commercial expanded graphite cathode, they also exhibit a stable charge/discharge capacity of 89/84 mAh g^{-1} at 100 mA g^{-1} (Fig. 11g-i). All these studies could provide novel strategy for high-performance porous biomass-derived hard carbon anodes for excellent K^+ storage.

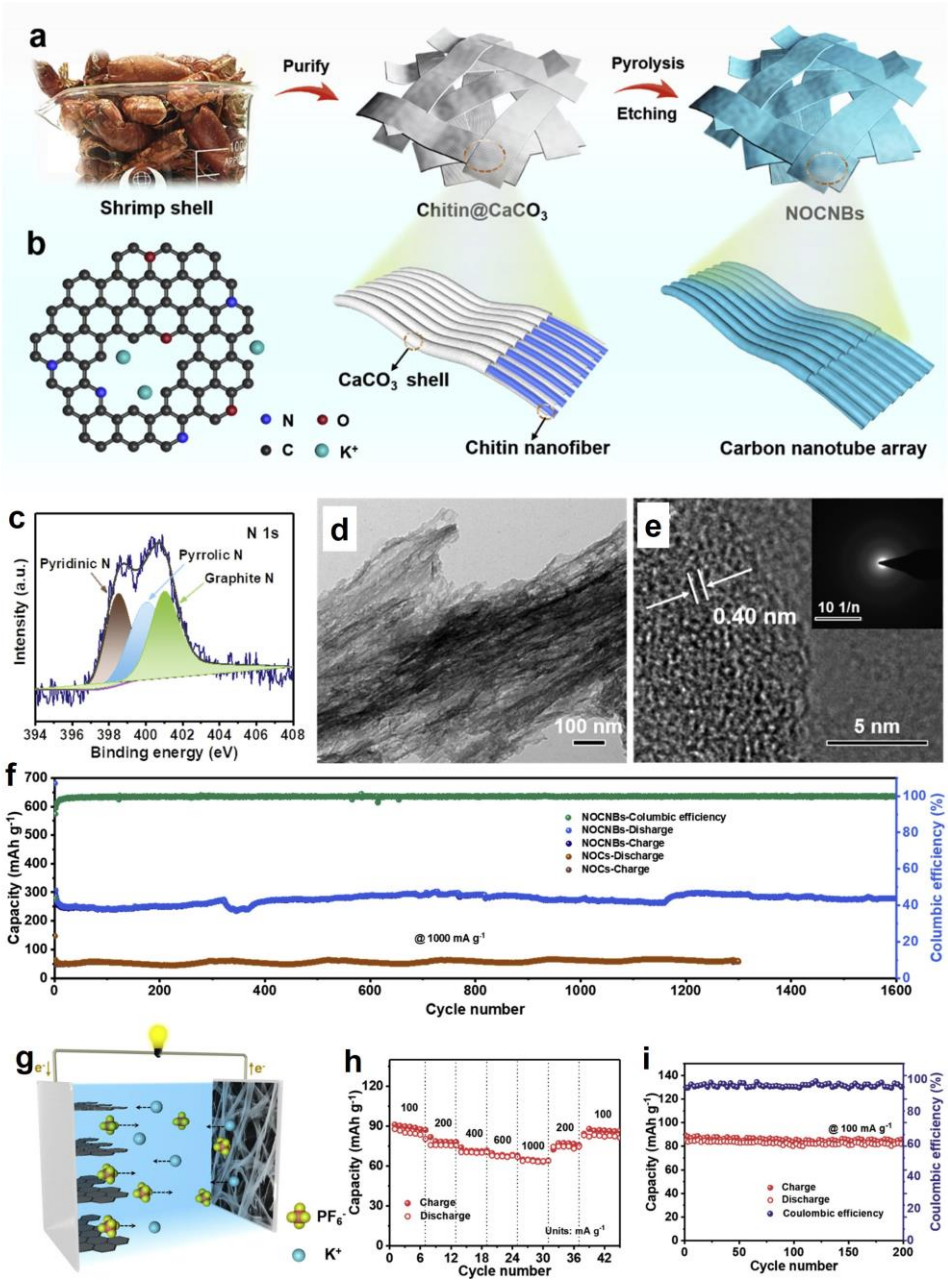

Fig. 11. (a) Schematic illustration for the preparation of N/O co-doped porous hard carbon nanobelts (NOCNBs); (b) The adsorption of K^+ on the NOCNBs anode; (c) The high-resolution XPS peak for N 1s, (d) TEM image, (f) HRTEM image and SAED pattern of NOCNBs; (f) Long cycling stability of the NOCNBs electrodes in PIBs; (g) The schematic diagram, (h) rate capability, and (i) cycling performance of NOCNBs//expanded graphite potassium dual-ion battery.

The porous MOFs, consisting of the organic linkers aggregated by numerous molecules and the inorganic metal clusters or transition metal ions, have been developed as the precursors for various carbon-based materials via a simple calcination process. However, the different composition in MOFs and different synthesis conditions always lead to MOFs-derived carbon materials with different morphologies and compositions, which further affect the electrochemical performances. Among the reported MOFs, the zeolitic imidazolate frameworks (ZIF) could be prepared in mild synthetic routes, making them more attractive in electrochemical energy storage. Hu et al.[201] reported a hollow carbon nanobubble material with the nanosized diameter and

thickness of around 70 and 10nm, respectively, by pyrolyzing from the Zn-containing MOF (ZIF-8) nanocrystals. The special structure could shorten the diffusion pathway and increase the active surface for K^+ ions, exhibiting a good specific capacity of 100 mAh g^{-1} at the high current density of 2 A g^{-1}. The Co-containing ZIF materials (ZIF-67) were also developed for N-doped carbon anodes for PIBs by Xu et al.[202] Different from the morphology of ZIF-8-dereived carbon nanobubbles, the ZIF-67 prefer to convert into the graphitic carbon nanotubes because of the catalysis effects of Co. As a result, the initial specific capacity could be about 102 mAh g^{-1} at 2 A g^{-1}, which could still retain the capacity of 100 mAh g^{-1} after 500 cycles. Yang et al.[203] also fabricated a high pyridine N-doped porous carbon anode derived from ZIF-67, which deliver excellent electrochemical K storage performances, such as the outstanding specific capacity (587.6 mA h g^{-1} at 50 mA g^{-1}), long cycling performance (231.6 mA h g^{-1} after 2000 cycles at 500 mA g^{-1}), and stable rate capability (186.2 mA h g^{-1} at 2 A g^{-1}). Sun et al.[204] further reported a novel composite architecture, defined as ZIF-8@ZIF-67 derived N-doped porous carbon confined with CoP nanoparticles (NC@CoP/NC), after a complex nucleation, carbonization and phosphorization process successively. Inspiring by the multiple effects of porous structures, N dopants, and uniformly distributed CoP, the NC@CoP/NC architecture anode exhibits an improved capacity of 200 mAh g^{-1} at 2 A g^{-1} in PIBs and maintains a capacity retention of 93% after 100 cycles at 100 mA g^{-1}. Other MOFs, e.g. NH2-MIL-101(Al)[205], Bi-MOF[206], were also introduced and carbonized into various hard carbon as the anode with high reversible capacities and stable long-cycling capacity retention in PIBs. Liu et al.[206] developed a novel composite architecture, ultrathin carbon film@carbon nanorods@Bi nanoparticle (UCF@CNs@BiN), by directly annealing the Bi-MOF at 700 °C in Ar. The carbon nanorods could provide high-speed channels for ion transport and accommodate the volume change of Bi nanoparticles during the $Bi \leftrightharpoons KBi_2 \leftrightharpoons K_3Bi_2 \leftrightharpoons K_3Bi$ potassiation/depotassiation processes. The resulted reversible capacity is presented to be 425 mAh g^{-1} at 100 mA g^{-1} with a discharge capacity of 327 mAh g^{-1} over 600 cycles. Due to the abundant variety of MOFs materials, the future studies should focus on the design of novel hard carbon structure to improve the specific capacity and initial Coulomb efficiency.

In order to understand the relationship between structure characteristics of these porous carbon (e.g. pore structure and interlayer distance) and electrochemical performances, Lin et al.[207] designed a series of porous carbon materials with various pore structures via a solvothermal method in the autoclaves, using 1-Dodecanol as the carbon source. Combining the various characterization and DFT calculation, they found an interesting result that the intercalation capacity ang adsorption capacity of K^+ ions are positively correlated with I_G/I_D ratio and mesopore volume, respectively. The interlayer distance, surface area, and pore size play comparatively far less important roles in the K ion storage. Moreover, the mesopores can also promote K ions migration, serve as active sites for the adsorption of K ions, and accommodate the volume expansion during the potassiation/depotassiation process. Integrated analysis indicates that the as-prepared sample with the largest mesopore volume and appropriate surface area could display a high capacity (633 mAh g^{-1} at 50 mA g^{-1}) and long cycling stability (263.9 mAh g^{-1} at 1 A g^{-1} after 1000 cycles), which could provide a new avenue to design novel carbonaceous materials as high performance anodes for practical PIBs.

Different with the widely studied carbon materials including graphite, graphene, and hard carbon, the rarely reported soft carbon owns unique advantages of highly tunable crystallinity and lattice interlayer spacing, exhibiting the structural integrity for high energy density and stability in

the battery field. Cao et al.[208] reported a pitch-derived soft carbon sample by carbonizing the pitch powder at 1200 ºC in Ar, existing as big aggregates of micro-sized particles. The TEM, XRD, and Raman results indicate an increasing graphitic crystallization degree for the pitch-derived soft carbon, which changes the main K^+ storage mechanism from surface adsorption to lattice intercalation with a lower capacity. However, the intercalation of K^+ ions always occurred at low voltage bellow 1 V, which could ensure a high battery voltage and high energy density in the full buttery in comparison with other non-graphitic carbons. Moreover, the turbostratic lattices with wide interlayer spacing could be formed by regulating the heating temperatures, which leads to a randomly dispersion of active carbon layers for the flexible K storages. Specifically, the in situ XRD analysis on the K^+ storage mechanism of the soft carbon sample and commercial graphite indicates that the intercalation compounds (e.g. KC_{24}), requiring long range-ordered carbon layers, diminish along with high transportation kinetics for soft carbon. When compared to the graphite, the former could present a higher structural resilience against mechanical failure during structural deformation. After structural optimization on the soft carbon materials for PIBs, they could exhibit the higher reversible specific capacity of 296 mAh g^{-1} at 28 mA g^{-1} than that of the graphite (273.6 mAh g^{-1}) or hard carbon (148.2 mAh g^{-1}). After 50 cycles, 93.2% the initial capacity could be remained for the soft carbon, while the retained value is only 82.6% for graphite. When the current density increases to 1.4 A g^{-1}, the capacity of the soft carbon could achieve about 115.2 mA h g^{-1}, while the hard carbon and graphite samples are valid without any capacities. The similar results could also be found in the cycling performances over 1000 cycles. These studies confirm the significant potential of soft carbon as a promising high-performance electrode in PIBs. Qiu et al.[209] prepared a high-performance soft carbon from the low-cost coal via a ball-milling, acid washing, oxidation, and carbonization process. The as-prepared coal-based carbon anode could deliver a reversible capacity of 260 mAh g^{-1} at 50 mA g^{-1} and a stable long cycling performance with the capacity of 118 mAh g^{-1} after 1200 cycles at 1 A g^{-1}. Ji and coworkers[210] systematically reported the electrochemical performance of hard-soft composite carbon microspheres with 20 wt% of soft carbon distributed in the hard carbon as an effective anode for PIBs, using the binder of sodium carboxymethyl cellulose. The experimental results found that hard-soft carbon can display better performances at high current density when compared to the hard carbon. For example, the hard-soft composite carbon exhibit a capacity of 190 mAh g^{-1} at 560 mA g^{-1}, which is higher than that of hard carbon (135 mAh g^{-1}). After 200 cycles at 280 mA g^{-1}, the composite carbon anode could maintain a specific capacity close to 200 mAh g^{-1} with the retention rate of 93%, which is much stable than the pure hard carbon and soft carbon materials.

As mentioned above, the soft carbon anode material has shown excellent rate performances for energy storage, among which the carbon nanotubes were also reported in recent years in PIBs.[211-214] The volume change of the K ions intercalation in the carbon nanotubes is about 61%, which might result in an obvious capacity decrease during the long cycling process. Han et al.[215] designed a multi-walled carbon nanotube material to solve these above-mentioned problems by regulating the synthetic parameters of CVD process. The special hierarchical structure of carbon nanotubes is that the inner layer of nanotube consists of dense graphitic carbon, while the outer layer is composed of disordered amorphous carbon which is beneficial for K^+ ions accommodation. The nanotubes are further interconnected together into a hyper porous sponge with high macropore volume, facilitating both the potassiation/depotassiation reaction kinetics and surface capacitive behavior. Finally, the as-prepared electrode could obtain a high reversible

specific capacity (232 mA h g^{-1}), excellent rate capability, and long cycling stability of at least 500 cycles. Cao and coworkers[216] further reported a porous-carbon aerogel as an anode for PIBs, constructing from the 1D porous-carbon nanotubes with a pore size distribution of around 0.8 nm. The long cycling stability and high rate capability with enhanced capacity retention are obtained due to the high surface capacitive mechanism. The sub-nanopores would also decrease the energy barrier of K ion diffusion and transport with negligible lattice change, providing a novel strategy for developing highly efficient carbon-based anodes for energy storage systems.

Heteroatom doping is also a common way to modify the K-storage capacity and cycling stability of no-graphite carbon materials. Chen et al.[217] prepared the nitrogen/oxygen co-doped mesoporous amorphous carbon octahedrons via a carbonization-etching process, using the renewable and readily available materials as reactants. The resulted samples process a hierarchical mesoporous structure, large specific surface area, and enlarged interlayer spacing. When the octahedrons are used as anodes for PIBs, they could deliver a superior reversible capacity (364 mAh g^{-1} over 50 cycles at 50 mA g^{-1}), and excellent cyclability (80 mAh g^{-1} after 3000 cycles at 2 A g^{-1}). The nitrogen and oxygen dual-doped amorphous carbon network materials were also synthesized for PIBs by Zheng et al.[218], which exhibits an excellent reversible capacity and outstanding ultra-long cycling performance. They reveal that superior performances are attributed to the unique ultra-stable network structure and the co-doping of N and O elements with the K-ion storage process of pseudocapacitive mechanism. Guo et al.[219] tuned the species and content of N elements in a honeycomb-like carbon structure co-doped with phosphorus. The sufficient pore defects and edges, originating from the porous structure and P-doping, could promote the formation of high-level pyridinic N in carbon and facilitate the interfacial adsorption reaction of K^+ ions. The outstanding reversible capacity (419.3 mAh g^{-1} at 100 mA g^{-1}) and excellent rate capability (270.4 mAh g^{-1} at 1 A g^{-1}) are finally achieved. Lei et al.[220] reported a highly nitrogen-doped carbon nanofiber electrode material by carbonizing the N-containing polypyrrole nanofibers at high temperature. After carbonization at 650 °C, the resulted sample (NCNF-650) obtains a nitrogen content of 13.8%, and further research indicates that the amounts of pyridinic N and pyrrolic N decrease with the increasing heating temperature, while that of quaternary N increases. However, according to the DFT calculation, the pyridinic N and pyrrolic N would promote the generation of defect sites and contribute to a higher K ions storage capacity than the quaternary N site. Among all the as-prepared N-doped carbon nanofiber, NCNF-650 shows the highest reversible specific capacity of 248 mAh g^{-1} at 25 mA g^{-1} and rate performance (101 mAh g^{-1} at 20 A g^{-1}). After 4000 discharge/charge cycles at 2 A g^{-1}, this electrode could remain a capacity of 146 mAh g^{-1} with the Coulomb efficiency of about 100%. Besides, the edge-N doping is also proposed as an effective approach to enhance the potassium storage performances of carbonaceous materials. Alshareef et al.[221] reported a molecular-scale site-selective doping strategy to produce a defect-rich and edge-N doped carbon anode via a copolymer pyrolysis procedure. The doping of N atoms could reach more than 10 at% in carbon with an edge-N ratio of 87.6%, delivering an excellent reversible potassium storage capacity (423 mA h g^{-1}), stable long cycle life (93.8 % retention after three months) and superior rate capability. Kaskel et al.[222] also proposed edge-enriched N-doped porous carbon nanosheets based on the pyrolysis-etching strategy of a pyridine-coordinated polymer. The optimized amorphous carbon with high surface area shows an edge-nitrogen content of 9.34 at%, showing an unbelievable potassium storage stability with a capacity retention of 94.5 % after 6000 cycles at the current density of 1 A g^{-1}. All

these studies could offer a potential approach to adjust the content of N active atoms in heteroatom-doped carbon materials for PIB energy storage systems.

Moreover, Deng et al.[223] prepared a high sulfur-doped (25.8 wt%) hard carbon by calcining the glucose in K_2SO_4@LiCl/KCl molten salt. The S-doped hard carbon anode exhibits a specific capacity of 361.4 mA h g^{-1} in initial cycle and retains 88% capacity over 100th cycle at 50 mA g^{-1}. Nan et al.[224] reported the S-doped bamboo charcoal anode materials for PIBs, using biomass bamboo and sulfur as raw materials. The doping S and residual O atoms in the bamboo charcoal could increase the conductivity and increase the content of active sites, delivering outstanding electrochemical potassium storage performance. In order to improve the low-voltage plateau capacity, the P-doped hard carbon was further synthesized at 1300 °C as the anode material for PIBs[225]. After P-doping into the lignin-derived hard carbon, the low-voltage capacity below 0.25 V can be improved from 153 to 192 mA h g^{-1}, and the specific capacity increases from 245 to 302 mA h g^{-1}, which is an important an effective strategy for designing high-energy-density PIBs anodes. Recently, we reported a carbonization-etching strategy for making a class of S and O co-doped porous hard carbon microspheres (PCMs) anode material for PIBs.[226] The amorphous PCMs possess a porous architecture with a large BET surface area of 983.2 m^2 g^{-1}, an enlarged interlayer distance of 0.393 nm, and abundant structural defects. These new features contribute to an excellent potassium ion storage, including a high capacity of 226.6 mA h g^{-1} at 50 mA g^{-1} over 100 cycles and a highly stable long cycling capacity of 108.4 mAh g^{-1} after 2000 cycles at 1 A g^{-1}. The reversible capacities at 50, 200, 500, 1000 mA g^{-1} are found to be 230, 213, 176, and 158 mAh g^{-1}, respectively. The DFT calculation demonstrates that the S/O co-doping can not only facilitate the adsorption of K ions on the active sites of PCMs electrode but also reduce the structural deformation during the potassiation/depotassiation process, thus improving the capacity and stability. In the latest report, [173] the S/N co-doped carbon could be optimized and increase the diffusion of K ions, exhibiting a high reversible specific capacity of 437 mAh g^{-1} at 0.1 A g^{-1} and the capacity retention rate of 75% after 3000 cycles at 2 A g^{-1}. Furthermore, an unique flower-like S/N/O multi-element tri-doped hard carbon structure has also been discovered by a facile sublime sulfur-vapor vulcanization process.[174] The 3D structure could offer rich surface areas to adsorb the K^+ ions and also promote the electron transportation, while the highly reactive -N-C_x-S- species can enhance the pseudo-capacitive behavior for K ions storage. As a result, the reversible specific capacity could be 423 mAh g^{-1} at a low current density of 0.05 A g^{-1}. Their rate capability (251 mAh g^{-1} at 1 A g^{-1}) and long cycling stability (362 mAh g^{-1} after 300 cycles at a current density of 0.5 A g^{-1}) are also much better than most carbonaceous materials, which provides an effective material design strategy for performance optimization of PIBs.

All these non-graphite carbon materials have shown outstanding reversible capacities and rate performances because of their special porous structure, large specific surface, and defects. Since the precursor are composed of C elements and various heteroatoms, e.g. N, S, P, and Q, the resulted carbon materials can also be in situ doped with these elements, further optimizing their electrochemical performances. However, the initial Coulombic efficiency and cycling stability are still desired to be improved for their practical application in commercial PIBs. Meanwhile, the relationship between compositions/structures/phases and electrochemical performances of the non-graphite carbon materials should be further studied deeply, which could offer novel ideas to enhance their properties and make the PIB energy storage technology become practical.

3.1.3 Other intercalation anode materials

In comparison with these carbonaceous materials, other layered metal compounds (transition metal oxides[227], sulfides[228-231], selenides[232-236], and carbonitride[237, 238]) have also exhibited attractive capacities and stability as anode materials for alkali metal ions storage due to their unique layered structure and excellent electronic conductivity. The layered intercalation compound $K_2Ti_4O_9$ was firstly reported as an anode material for PIBs by Munichandraiah et al.[239]. The charge and discharge process could be achieved by the oxidation and reduction of two Ti^{4+} to Ti^{3+} ions, however, the actual specific capacity of the $K_2Ti_4O_9$ is relatively low (80 mAh g^{-1} at 80 mA g^{-1}). The $K_2Ti_8O_{17}$ nanorods were subsequently reported as an anode material for PIBs, synthesizing via a facile hydrothermal method.[240] The lattice spacing of the (1 1 0) crystal layer is about 0.367 nm, which is slightly larger than that of graphite, exhibiting a reversible specific capacity of 181.5 mAh g^{-1} at 20 mA g^{-1}. After 50 discharge/charge cycles at a current density of 20 mA g^{-1}, the capacity retention rate is about 61%, while the capacity at 500 mA g^{-1} is only 44.2 mAh g^{-1}. Recently, Wang et al.[241] reported a carbon-coated $K_2Ti_2O_5$ microsphere (S-KTO@C) with porous microstructure via a simple spray drying method. The S-KTO@C shows excellent reversible discharge capacity of 155.1 mA h g^{-1} at 16 mA g^{-1}, rate capability, and cycling stability with a capacity retention of 77.1% at 160 mA g^{-1} after 1000 cycles. The authors reveal an enhancement of K^+ intercalation pseudocapacitive behavior due to the carbon coating through a CVD technology. Chen et al.[242] also designed a novel carbon-coated phosphate-based VPO_4 with different morphologies, via a thermal reduction process after intercalating isobutanol into the layered $VOPO_4{\cdot}2H_2O$. After optimization, the flower-like VPO_4 could deliver an outstanding capacity of 400 mAh g^{-1} at 50 mA g^{-1} with a stable long cycling stability (263 mAh g^{-1} at 500 mA g^{-1}) after 500 cycles. These results indicate that the special carbon-coated flower-like structure could accommodate the volume expansion during the potassiation/depotassiation process. Besides, the V_2O_5-based composite materials are also developed recently as the anodes for PIBs. Chen et al.[243] reported a carbon coated V_2O_3 hollow sphere via a facile solvothermal reaction, in which the hollow structure and the outer carbon coating could bear the volume change and improve the electronic conductivity, respectively. The resulted electrode displays a promising reversible capacity of 330 mAh g^{-1} at 100 mA g^{-1} after 500 cycles due to the combination of intercalation and pseudocapacitive effects. Xu et al.[244] firstly developed an oxynitride TiO_xN_y nanoparticles/carbon composite from $Ti_3C_2T_x$ MXene as anode material for PIBs. The composite electrode exhibits a stable capacity (150 mAh g^{-1} at 0.2 A g^{-1} after 1250 cycles) and impressive rate performance (72 mAh g^{-1} at 1.6 A g^{-1}), providing a new strategy for promising oxynitride-based anode material for PIBs.

The polyanionic compounds are also selected as the anode host materials for potassium ion storages. Xu et al.[245] prepared a novel $KTi_2(PO_4)_3$ nanocubic by a hydrothermal method with a subsequent heating treatment. After coating with carbon layer by a sugar-assisted process, the electrochemical performances could be further improved from 30 mAh g^{-1} to around 80 mAh g^{-1} after 100 cycles at 64 mA g^{-1}. Sun et al.[246] also developed a carbon coated inorganic-open-framework material $KTiOPO_4$ for PIBs, which owns K^+-transport kinetics about 10 times faster than those of Na-superionic conductors, such as the $KTi_2(PO_4)_3$. This compound obtains a reversible capacity of 102 mAh g^{-1} at 5 mA g^{-1} and a long lifespan with the capacity retention of ~77% over 200 cycles. The in situ XRD, XPS, and DFT calculation results reveal a biphasic and solid solution reaction mechanism and a smaller lattice volume change (9.5 %), improving the

capacity and cycling capability to some extent.

The metal sulfides, such as MoS_2, SnS_2, WS_2, TiS_2, ZnS, CoS, etc., also have attract much attentions in PIBs, due to their electrochemically structural stability, low redox potential, high specific capacities, and long lifetime. Among these sulfides, MoS_2 is mostly studied with a similar potassium storage mechanism with the graphite. Ren et al.[247] indicated that the K ions could intercalate into the MoS_2 lattice and form a hexagonal $K_{0.4}MoS_2$. Although the radius of K ions is much larger, the intercalation in MoS_2 is still stable, exhibiting a better cycle stability with a capacity retention rate of 97.5% after 200 cycles at 20 mA g^{-1}. When the value x in the K_xMoS_2 is higher than 0.4, the intercalated compounds are not stable, which limits the reversible capacity of practical PIBs. Li et al. [248] designed a tubular MoS_2-N/O co-doped carbon composite with an expanded interlayer spacing (0.92 nm), improved K^+ ions diffusion rate. The tubular could ensure a stable structural rigidity to mitigate the mechanical strain during the intercalation of K^+ ions. And the co-doping of N/O in carbon could not only improve the electronic conductivity and buffer the volume expansion, but also inhibit the dissolution of active components and the side reactions. Benefiting from the specially designed structure, the composite anode delivers a reversible capacity of 220 mAh g^{-1} after 300 cycles at 250 mA g^{-1}, and the capacity can remain at 176 mA h g^{-1} after 500 cycles at the higher current density of 1 A g^{-1}. Liu et al.[249] prepared a composite structure by anchoring nono-rose-like MoS_2 on the rGO for the PIB anode. Based on the strong chemical bonds (e.g. Mo-C and Mo-O-C) between MoS_2 and rGO, the structure stability could be well guaranteed during the potassiation/depotassiation process. The composite anode delivers an excellent initial capacity of 438.5 mAh g^{-1} at 100 mA g^{-1} with remarkable rate capability of 196.8 mAh g^{-1} at 2 A g^{-1}) and outstanding cycling stability without obvious fading after 1000 cycles at 500 mA g^{-1}. Further investigation indicates that outstanding capacity is contributed from combination of both intercalation and conversion K-ions insertion/extraction mechanisms via a four-electrons-transfer process. Liu et al.[250] proposed a self-loading of ultrathin MoS_2 nanosheets on the inner surface of hollow tubular carbon skeleton, and the interlayer distance is tuned by a step-by-step intercalation of organic molecules in various sizes. The hollow tubular structure and the expanded interlayer could facilitate the K^+ ions transition and storage, so that delivering a high specific capacity of 148.5 mAh g^{-1} after 10000 cycles at 2 A g^{-1}. In contrast, Huang et al.[251] reported a densified 1T-MoS_2/graphene composite bulk by tightening the hydrogel via a capillary tension theory. The K^+ ions can also be electrochemically stored in as-prepared electrode via similar intercalation and conversion mechanisms with fast K^+ ions kinetics and high transportation ability. The reversible capacities could be reached as high as 511 and 327 mA g^{-1} at 0.1 and 1 A g^{-1}, respectively. Besides, Lei et al.[252] proposed an unexpected intercalation-dominated process for potassium storage in the an der Waals gaps of WS_2 anode, exhibiting a reversible capacity of 103 mAh g^{-1} after 100 cycles at 100 mA g^{-1} with a decay rate of 0.07% per cycle. When the current density increases to 500 mA g^{-1}, the capacity could still keep stable up to at least 400 cycles. We recently reported ultrafine zinc sulfide (ZnS) nanorods nested in the tertiary hierarchical structure through a facile solvothermal-pyrolysis process as the anode material for PIBs[253]. The designed architectural can not only offer a stable diffusion path for both K^+ ions and electrons, but also construct a stable SEI and buffer the volume expansion during cycling. As a result, the stable specific capacities are obtained at 330 mAh g^{-1} (50 mA g^{-1}) and 208 mAh g^{-1} (500 mA g^{-1}) after 100 and 300 cycles, respectively. Shu et al.[254] designed a defect rich TiS_2 anode material by introducing abundant functional cation defects on the surface via a thermal annealing method. The

generated titanium vacancies (V_{Ti}) can not only weaken the microscopic stress and strain during the ion intercalation process, bout also regulate insertion sites of K ions and improve the kinetics. When using as the anode material in PIB, defect rich TiS_2 could possess 63.56% of the initial reversible capacity after 450 cycles. Other mono-sulfides and quasi 2D layered sulfides, such as ReS_2,[255] CoS[256], Co_9S_8,[257] FeS_2,[258] and $K_{0.36}(H_2O)_yWS_2$,[259] were also synthesized and cooperated with various carbon materials as superior PIB anodes for excellent K storage capacity, rate performance, and cycling stability.

Apart from these sulfide-based anodes, the research on selenide materials also show great interest for PIBs. Li et al.[260] demonstrated a facile strategy to achieve highly reversible potassium ions storage in the nanosized $MoSe_2$@carbon composites, exhibiting a high specific capacity, good cycling stability (267 mA g^{-1} with a capacity fading of 15.8% after 5000 cycles at 5 A g^{-1}), and rate capability (169 mA g^{-1} at 5 A g^{-1}). Zhang et al.[261] implanted the sheet-like $MoSe_2$ in the carbon nanofibers through an electrospinning and selenization route. The composite owns high structural stability and fast intercalation/deintercalation of K^+ ions, therefore displaying a high reversible capacity of 316 mA h g^{-1} after 100 cycles at 100 mA g^{-1}. Furthermore, Zhang et at.[262]. reported a flexible and freestanding anode by embedding the $Co_{0.85}Se$@carbon nanoboxes in carbon nanofibers films via a MOF-engaged electrospinning method following with a carbonization-selenidation process. The special nanoarchitecture can not only offer large surface area and void space to accommodate the volumetric expansion during the K^+ de/intercalation cycles, but also improve the electronic and ionic conductivity. The cycling stability, as an anode material for PIBs, could be 299 mAh g^{-1} after 400 cycles at 1 A g^{-1} and the specific capacity could still maintain 166 mA h g^{-1} at a high current density of 5 A g^{-1}. We also designed a unique structure by encapsulating the $Co_{0.85}Se$ quantum dots in mesoporous carbon matrix[263], which also shows an outstanding K-storage performance with a high capacity of 402 mAh g^{-1} after 100 cycles at 50 mA g^{-1}. Du et al.[264] synthesized a crystal-pillar-like CuSe material with cubic phase assembled by the nanosheets, which could store the K^+ ions fast and stably. The as-prepared electrode delivers a high specific capacity of 280 mAh g^{-1} at 5 A g^{-1} in PIBs without any obvious capacity decay after 340 cycles. The in situ XRD and ex situ TEM results indicate that the ionic storage process contains both the K^+ ions insertion reaction ($K_{0.5}CuSe$ phase) and conversion reaction (Cu and K_2Se phases). Shu et al.[265] reported a pretreated commercial $TiSe_2$ as an insertion-type anode for K ion storage with good cyclability and excellent rate performance. The $K_{0.24}TiSe_2$ phase is stably formed after the first cycle by in situ XRD, resulting a reversible insertion/extraction process of potassium ions. After fabrication into full cell with the as-pretreated PB, the Coulombic efficiency and cyclability could be further improved to promote the development of commercial PIBs. In the meantime, the $FeSe_2$/N-doped carbon composite[266], porous $FeSe_2$@C nanofiber[267], $NbSe_2$ sheet[268], and the graphene-wrapped corals-like $NiSe_2$ composite[269] were also prepared and applied as an anode material for potassium-ion batteries, demonstrating considerable potassium storage capacity and rate performance. In order to improve the electrochemical performances of selenide anode materials, ternary chalcogenides were further put forward recently. Wang et al.[270] firstly reported a few-layered ternary Ta_2NiSe_5 flake with an interlayer spacing of 1.1 nm, expanding by a facile ion-intercalation-mediated exfoliation method with Mg^{2+} cations and NO^{3-} anion. Because of the abundant Se sites, this electrode delivers superior K^+ ions storage performances, such as high specific capacity (315 mAh g^{-1} after 50 cycles at 50 mA g^{-1}), excellent rate capability (121 mAh g^{-1} at 1 A g^{-1}), and stable long-cycling

performance with a capacity retention of 81.4% after 1100 cycles. The DFT and experimental results elucidate that the enlarged interlayers with low diffusion barriers and large adsorption energy could result in a fast intercalation and high-efficiency adsorption of K^+ ions, contributing to the high-performance in PIBs. Huang et al.[271] incorporated dual anionic vacancies on MoSSe arrays on the carbon nanofiber membrane, improving the adsorption of K^+ ions than the vacancy-free MoSSe. The reversible capacity could be as high as 370.6 mAh g^{-1} after 60 discharge/charge cycles at 100 mA g^{-1}. Since the 3D porous structure of the vacancy-rich MoSSe arrays could remit the volume expansion during cycling, a high capacity retention could be achieved at 220.5 mAh g^{-1} after 1000 cycles at 500 mA g^{-1}. The vacancy designing for the optimization of K^+ ions storage could also open a feasible route to develop potential anode materials for practical PIBs.

In recent studies, the 2D layered MXenes, consisting of transition metal carbides and carbonitrides, have shown considerable electrochemical performances as anode materials in LIBs, SIBs, and capacitors[272-276]. Michael et al.[277] prepared the Ti_3CNT_z material with a specific capacity of 75 mAh g^{-1} after 100 cycles at 20 mA g^{-1}. Alshareef et al.[278] designed a general acid/alkali treatment strategy for preparing porous MXene materials to enhance the capacity of K^+ storage. The resulted K-V_2C anode displays an improved capacity of 195 mAh g^{-1} at a current density of 50 mA g^{-1}. When the current density increases to 3 A g^{-1}, the capacity could maintain at 70 mAh g^{-1} over 48 cycles. Xu et al.[279] fabricated a 2D $Ti_3C_2T_x$ MXene flakes combined flexible hard carbon composite electrode to increase the electrochemically active components for stable K-ion storage. The stable 3D architecture could effectively accommodate the volume expansion of hard carbon during the cycling process, delivering an enhanced capacity of 280.6 mAh g^{-1} at 30 mA g^{-1}, rate capability (102.2 mAh g^{-1} at 500 mA g^{-1}), and stable cycle performance. Yin et al.[280] further designed a Ti_3C_2 MXene and N-rich porous carbon nanosheets hybrids for high-performance PIBs via an electrostatic attraction self-assembly method (Fig. 12a). The composite hybrids could efficiently combine the advantages of all these components because of their intimate contact in the stacked structure. Along with the large specific surface area and abundant active sites because of the unique 3D porous interconnected structure, a high reversible capacity is obtained at 358.4 mA h g^{-1} after 300 cycles at 100 mA g^{-1}, (Fig. 12b) which is larger than both the Ti_3C_2 MXene and N-rich porous carbon nanosheets. Moreover, the high chemical stability and enlarged interlayer spacing can also facilitate the ionic/electronic transport and tolerance the volume change during the fast charge/discharge process, so that a durable rate capability (191.2 mAh g^{-1} at 2.0 A g^{-1}) and long cycling stability (151.2 mAh g^{-1} at 2.0 A g^{-1} after 2000 cycles) are obtained (Fig. 12c). Further DFT calculations and ex situ XRD results, as shown in Fig. 12d-f, indicate that electrochemical reaction mechanisms are the enhanced interfacial K^+ adsorption and the optimized potassiation/depotassiation process including the reactions of $8C + xK^+ + xe^- \leftrightarrow K_xC_8$ and $Ti_3C_2T_x + yK^+ + ye^- \leftrightarrow K_yTi_3C_2T_x$, which could help to explore coupled hybrids in advanced energy storage devices. Wu et al.[281] designed a novel black phosphorene@V_2CT_x MXene hybrid anode based on the van der Waals interactions to accelerate the K^+ transport and tolerate the cycling volume changes. The composite could achieve an outstanding reversible capacity of 593.6 mAh g^{-1} at 0.1 A g^{-1} and excellent cycling stability of 261 mAh g^{-1} with a retention ratio of 86% after 3000 cycles at 2.0 A g^{-1}. Based on the remarkable synergetic effect, several layered MXene-based composite electrode materials, such as the layered $Ti_3C_2T_x$ MXene/MoS_2 composites[282], carbon-coated $MoSe_2$/$Ti_3C_2T_x$ MXene hybrid nanosheets[283], 3D Fe_3C@porous graphite carbon

core-shell structures[284], N-doped graphene/$ReSe_2$/Ti_3C_2 MXene heterostructure frameworks[285], and mesoporous NbN/N-doped carbon hybrids[286], were also developed with enhanced electrochemical performances, confirming a new way to design high-performance anode materials for K ions storage.

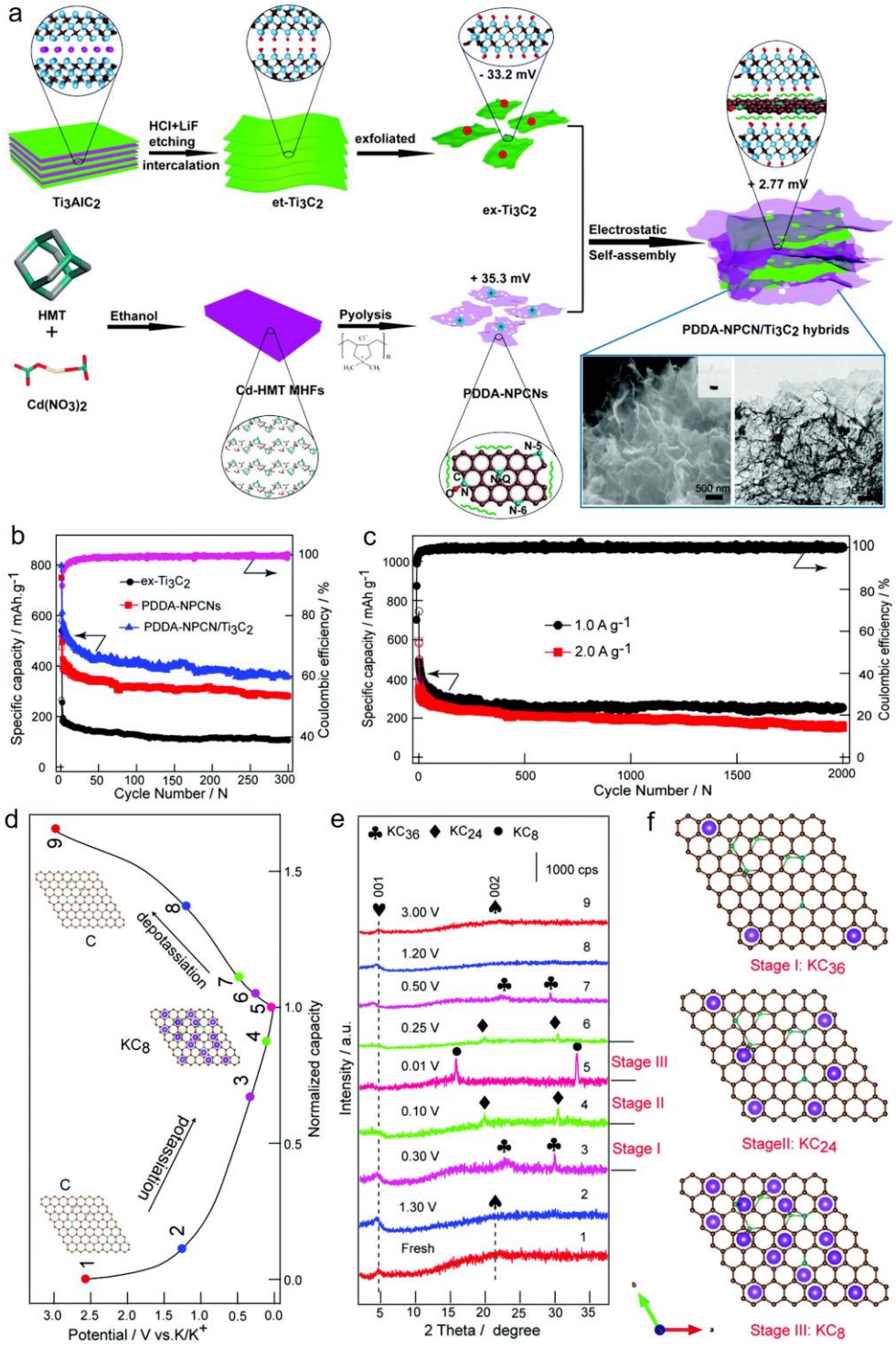

Fig. 12. (a) Schematic of the preparation of the Ti_3C_2 MXene and N-rich porous carbon nanosheets (PDDA-NPCN/Ti_3C_2) hybrids; (c) K^+ ion storage and (b) long cycling performances of the PDDA-NPCN/Ti_3C_2 hybrids at different current density for several cycles; (d) Voltage profile, (e) corresponding ex situ XRD patterns, and (f) supercells for the PDDA-NPCN/Ti_3C_2 anode at different stages during the initial

potassiation/depotassiation process.

Unlike those inorganic anode materials, organic materials also shows several advantages as the electrode materials for batteries, including the low toxic, low cost, abundant sources, and controllable chemical structure. For example, a layered organic dipotassium terephthalate (K_2TP)[287] crystal with cyclic moiety and conjugated structure for alkali metal ions storage were tried to be used as the PIB anodes. Chen et al. reported that the K_2TP could show an enhanced electrochemical performance in 1, 2-dimethoxyethane (DME) based electrolyte. Benefiting from the synergistic effect of abundant active carboxylate groups and stable SEI, the reversible capacity achieves 249 mAh g^{-1} at 200 mA g^{-1} and the capacity can still retain 94.6% of the initial capacity after 500 cycles at 1 A g^{-1}. After replacing the adjacent carbon close to the ester group by nitrogen[288], the superior electrochemical potassium storage performances could also be obtained in carbonate electrolyte. In addition to these organic materials, the 3,4,9,10-perylenetetracarboxylic diimide (PTCDI)[289] was developed as a high-rate anode for PIBs, due to its low charge-transfer resistance and fast K ion diffusion. The high specific capacity is found to be 208 mAh g^{-1} with only 20 mAh g^{-1} capacity loss after 320 cycles at a current density of 5 A g^{-1}. The ex situ IR and XRD results indicate a six-electron storage mechanism for the PTCDI anode during the K-ion insertion/extraction process. Besides, the few-layered boronic ester based covalent organic framework[290] (COF) material anchoring on CNTs is firstly used as an anode material for PIBs. This novel organic material could also exhibit outstanding reversible capacities of 288 mAh g^{-1} after 500 cycles at 0.1 A g^{-1} and 161 mAh g^{-1} after 4000 cycles at 1 A g^{-1}, because of the improved π-K^+ interaction between the potassium ions and conjugated π-electrons of benzene rings. Similar conjugated microporous polymers (CMPs) with π-conjugated skeletons were also employed as anodes for PIBs. Jiang et al.[291] studied the relationships between the structure and performances of the CMPs with delocalized lowest unoccupied molecular orbital (LUMO) distribution. By synthetic controlling the low LUMO energy level and narrow band gap along with porous structure of CMPs, all the electron conductivity, the number of active sites, and the accommodation of volume change during K intercalation could be enhanced and resulted in high electrochemical performances. As a result, the reversible capacity can reach 428 mAh g^{-1} at 30 mA g^{-1} with excellent cycling stability (272 mAh g^{-1} after 500 cycles at 50 mA g^{-1}). These examples could give promising green organic electrode candidates with large capacity and long cycling stability for PIBs. However, the poor electrical conductivity and the solubility of organic materials in the electrolyte still limit the practical application of PIBs, and the specific energy should be further improved in future studies.

3.2 Conversion anodes

The conversion reaction refers to a chemical reaction process in which the potassium ions react with other elements in the anodes and generate new compounds in the potassiation process. Because of the total reduction of transition metal ions to the metallic state during electrochemical reactions, the theoretical capacities of conversion anode materials are always much higher than the intercalation anodes. Along with the advantages of high redox reversibility, the recently reported conversion anodes for PIBs also include the metal oxides and transition metal dichalcogenides.

Several transition metal oxides have been considered as promising anodes because of their electrochemically reversible conversion process. Jiao and co-workers[292] synthesized the CuO nanoplates with a thickness of around 20 nm as high-performance anode materials for PIBs.

Benefiting from the ultrathin thickness, the CuO nanoplates afford a short K^+ ion diffusion distance and large electrode-electrolyte contact interface, resulting in a high reversible capacity of 342.5 mAh g^{-1} at 200 mA g^{-1}. Based on the conversion reactions mechanism between the as-formed Cu_2O and Cu, the theoretical reversible capacity could be calculated to be 374 mAh g^{-1}. Thus, when the current density increases to 1 A g^{-1}, the capacity could remain over 206 mAh g^{-1} after 100 cycles. Kim et al.[293] reported a Magnéli phase Ti_6O_{11}/CNT composite electrode through an in situ electrochemical reaction, which could show a reversible charge/discharge capacity of ~150 mAh g^{-1} at 50 mA g^{-1} in PIBs. The Ex situ XRD and TEM reveal that the K storage process also achieves via a conversion reaction during the K^+ insertion/deinsertion. Different with the simple oxide, Liang et al.[294] applied the β-FeOOH/conductive carbon composite as a new anode for PIBs, exhibiting high capacity and good cycling stability with a reversible capacity of 177.7 mAh g^{-1} at 100 mA g^{-1} after 100 cycles. The potassium storage mechanism is finally found to be that β-FeOOH in the composite firstly irreversibly turns into an amorphous structure and then remains stable in the amorphous state in the subsequent de/intercalation cycles. Nithya et al.[295] fabricated a $MnCO_3$ nanorods@rGO composite via a simple one-step hydrothermal method without any further heat treatment. Due to high surface area of the nano sized $MnCO_3$ nanorods with a diameter of 5-10 nm and the sheet-like rGO for conversion reaction, the composite delivers high capacity and superior long-term cycling stability (841 mAh g^{-1} after 500 cycles at 200 mA g^{-1}) as a anode material for PIBs. The conversation reaction, $MnCO_3+2K^++2e^-\leftrightarrow Mn+K_2CO_3$, contribute mostly for the outstanding performances. Sultana et al.[296] studied the potassium storage behavior of transition metal oxide anodes by conversion reactions, which indicates that the volume change and stress during the intercalation and conversion reactions would directly affect the performances and stability. Thus, they proposed the Co_3O_4-F_2O_3/C composite nanoparticles via a molten salt method to overcome these problems. Compared with the Co_3O_4-F_2O_3 nanoparticles without carbon, the Co_3O_4-F_2O_3/C composites present a higher specific surface area and porosity, delivering a reversible capacity of 220 mAh g^{-1} after 50 cycles at 50 mA g^{-1}. The in situ XRD results further indicate that the main potassium storage mechanism is the conversion reactions of Co_3O_4 and F_2O_3 in the Co_3O_4-F_2O_3/C composites including $Fe_2O_3+6K^++6e^-\leftrightarrow 2Fe+3K_2O$ and $Co_3O_4+8K^++8e^-\leftrightarrow 3Co+4K_2O$. These studies could offer meaningful strategies for developing high performance, environmental benignity, and earth-abundant transition metal oxide anodes in practical PIBs.

In addition, conversion-based transition metal dichalcogenides have gradually emerged for PIBs in recent years. Metal sulfides have good electrical conductivity and electrochemical activity. However, pure metal sulfides have poor electrochemical performance due to volume changes due to transformation reactions and conversion reactions. Researchers have tried to solve these problems by making these metal sulfides into composite systems with carbon, obtaining great improvement in electrochemical performances. For example, The carbon-coated Co_3O_4 and MoS_2 composite electrode (Co_3O_4@C@MoS_2) has been reported,[297] with designed layered structure to accommodate the volume expansion. The composite anode delivers a specific capacity of 256 mAh g^{-1} with the capacity retention rate of 88.3% after 500 cycles at 500 mA g^{-1}. Simultaneously, rGO was used as a carrier by Xie et al.[298] to stabilize the MoS_2 in a rose shape. The electrode has ultra-high potassium storage specific capacities of 679 mAh g^{-1} and 178 mAh g^{-1} at 20 mA g^{-1} and 500 mA g^{-1}, respectively. After 100 cycles under the current density of 100 mA g^{-1}, the specific capacity still remains above 380 mAh g^{-1}. Interestingly, they reveal that the K^+ ions storage

mechanism of MoS_2@rGO undergoes both the intercalation reaction and conversion reactions by the in-situ Raman results, such as $MoS_2+xK^++xe^-\leftrightarrow K_xMoS_2$ (above 0.54 *vs*. K/K^+), $K_xMoS_2+(4-x)K^++(4-x)\ e^-\leftrightarrow Mo+K_2S$ (below 0.54 *vs*. K/K^+).

Similarly, studies like growing nanosized SnS_2 and Sb_2S_3on the rGO have also been carried out recently.[299, 300] Although the specific capacity is improved in comparison to the pure SnS_2 and Sb_2S_3, the cycling stability is still need to be improved. For example, the capacity retention rate of SnS_2-rGO is only about 70% after 30 cycles at 25 mA g^{-1}, while the capacity retention rate of the Sb_2S_3-S/N co-doped graphene is about 89% after 100 cycles at 50 mA g^{-1}. The bulk Sb_2S_3 crystal owns a lamellar structure paralleling to the b axis, which makes it possible to fabricate the 2D Sb_2S_3 sheets. Compared to the bulk Sb_2S_3, the 2D Sb_2S_3 nanosheets can effectively accommodate the large volume change during the potassiation/depotassiation reactions. Guo et al.[301] successfully peeled and prepared a few-layered Sb_2S_3 material with a thickness of 6.8 nm by the high-shear peeling method using a certain ratio (2:1) of water and ethanol as a solvent. Ethanol is used to in situ carbonize to carbon and finally obtain the Sb_2S_3/C anode material for PIBs. The Sb_2S_3/C electrode displays an excellent reversible specific capacity (404 mAh g^{-1} after 200 cycles at 500 mA g^{-1}) and rate performance (the capacity retention rate is about 76% when the current density increases from 50 to 500 mA g^{-1}). The K_3Sb and K_2S_3 might be formed during the charge/discharge process, which means that Sb_2S_3/C undergoes the intercalation reaction, conversion reaction, and alloying reaction in the course of cycling.

Since the nanosized metal sulfide particles are supported on graphene, the nanoparticles might also agglomerate and smash during the electrochemical process, which will significantly reduce the cycling performance. Based on this problem, Zhao et al.[302] improved the electrochemical performance of the metal sulfide FeS_2 (G@Y-S FeS_2@C) in PIBs by adjusting the microstructure of the active material. The composite electrode has a shell structure with enlarged gap. When the internal active material expands during the conversion reaction, the gap is sufficient to support their volume changes, thereby avoiding agglomeration and smash of the active material. The as-prepared anode materials could display the specific capacities of 270 mAh g^{-1} and 162 mAh g^{-1} after 1000 cycles at current densities of 0.3 A g^{-1} and 1 A g^{-1}, respectively. When the current density increase to high rates of 1, 2, 4, 6, 10 A g^{-1}, the anode also shows excellent rate performance with the capacities of 360, 315, 266, 240, and 203 mAh g^{-1}, respectively. The study mainly proposes that the intercalation and phase transformation mechanism for the G@Y-S FeS_2@C composite include the reactions $K_xFeS_2\leftrightarrow K_yFeS_2\leftrightarrow Fe+K_2S$. In terms of iron-based conversion anodes, Yang et al.[303] synthesized a FeP@C nanobox with carbon shell (FeP@CNBs) by the phosphorylation strategy using the yolk shell structural Fe_2O_3 nanobox as precursor. The conductive carbon shell improves the conductivity of the electrode, and the yolk shell structure adapts the volume expansion of FeP during the electrochemical process, so that exhibiting a better cycle stability and rate performance. As a result, the FeP@CNBs anode shows the reversible capacities of 201, 156, 101, 65 and 37 mAh g^{-1} at 0.1, 0.2, 0.5, 1, and 2 A g^{-1}, respectively. Moreover, our design also tried to improve the conductivity and structural stability of FeP as anode for PIBs[304]. We fabricated a 3D foam-like graphitic carbon scaffold incorporated with FeP nanoparticles (FeP@FGCS) through a simple pyrolysis-blowing and phosphorization approach. The FeP nanoparticles are evenly incorporated and tightly fixed by the strong P-C chemical bonds to the carbon scaffold, which not only serves as a conductive pathway to accelerate the transport of K ions and electron, but also alleviates the volume variation of FeP

nanoparticles to preserve their integrity during the K ions intercalation. Moreover, the elaborately selected ether-based electrolyte and binder also facilitate the cycle stability of the FeP electrode. Thus, the FeP@FGCS composite exhibits superior electrochemical activity in PIBs with a high specific capacity of 382 mAh g^{-1} at 100 mA g^{-1}. More importantly, the cycle stability could be further improved due to the uniform construction of a stable inorganic SEI layer on the surface of FeP@FGCS electrode in the ether-based electrolyte (1.0 M KFSI in DME). Consequently, the FeP@FGCS displays an outstanding cycling performance for potassium storage with the capacity of 183 mAh g^{-1} retained for over 1000 cycles at 3 A g^{-1}, which could rival most reported anode materials for PIBs.

NiS, as a member of transition metal sulfides, is rarely reported in PIBs due to the disadvantages of low conductivity and large volume expansion. By coating the precursor with a carbon source, the core-shell structure NiS@C composite materials were provided after in situ carbonization to buffer the volume expansion during the potassiation/depotassiation cycles.[305] The K-ion storage capacity can retain 171 mAh g^{-1} at 1 A g^{-1} after 300 cycles. In addition, nickel selenide $NiSe_2$ has the advantages of small band gap (0.54 eV), low diffusion barrier (0.05 eV), and high carrier mobility (1658 cm^2 V s), rendering a high-performance anode candidate for PIBs.[306] Wang et al. reported that the as-prepared 2D T-$NiSe_2$ shows a larger specific capacity of 247 mAh g^{-1} witrh good cycling stability than that of most 2D anode materials for PIBs. Moreover, the average voltage of the T-$NiSe_2$ is 0.49 V, which is also in the energy range for promising anode materials.

Recently, the Cu-based conversion anodes, such as CuS and Cu_2S, have been developed as electrodes for electrochemical energy storage with impressive performance[307-310]. One of the copper sulfides, Cu_2S, owns several superiorities for the suitable PIB anode, including non-toxic, low-cost, and high electrical conductivity. Yu et al.[311] designed a uniform N-doped carbon coated Cu_2S hollow nanocube as an anode material for the PIBs, via an anion exchange process following with a PDA coating and carbonization process in Ar (Fig. 13a-d). As shown in Fig. 13e, the special composite nanocage could possess enough inner cavity to relieve the volume expansion during cycles, high specific surface area for electrolyte soaking, and short diffusion length of potassium ions/electrons. Further replacing the conventional electrolyte by high-concentration ether-based electrolyte, a more stable and uniform SEI could also be achieved along with lower interface impedance (Fig. 13g). As a result, the Cu_2S@NC anode displays an impressive reversible capacity (372 mAh g^{-1} at 100 mA g^{-1} after 530 cycles), outstanding cycle performance (317 mAh g^{-1} after 1200 cycles at 1 A g^{-1}), and excellent rate capacity (257 mAh g^{-1} at 6 A g^{-1}) in a PIB half-cell (Fig. 13f). The ex situ TEM and ex situ XRD demonstrate the complex conversion reaction mechanism of Cu_2S@NC anode during the charge/discharge cycles.

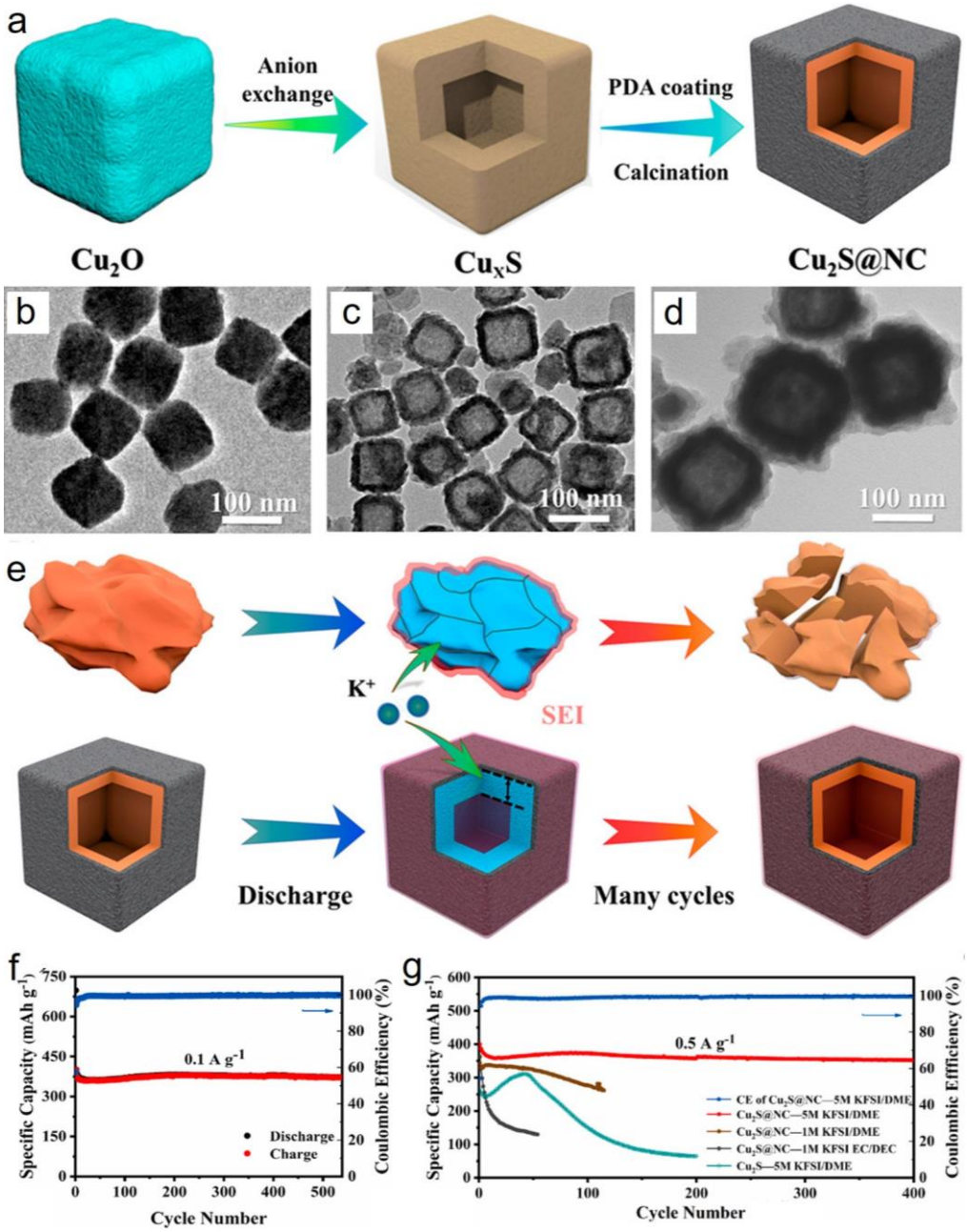

Fig. 13. (a) Schematic for the synthesis of Cu_2S@NC; (b-d) SEM images of Cu_2O precursors, Cu_xS, and Cu_2S@NC, respectively; (e) Schematic for the degradation mechanisms of Cu_2S blocks and Cu_2S@NC composite during the charge/discharge process; (f) Cycling stability for the potassium-ion storage behavior of Cu_2S@NC anode at 100 mA g^{-1}; (g) Cycling performance of the Cu_2S@NC anode at 500 mA g^{-1} in different electrolytes.

Zn-based conversion anodes, e.g. ZnS, are very promising anodes in terms of energy storage due to their advantages of safety, non-toxicity, high natural abundance, and low cost.[312-315] In our recently published results, we designed an open ZnSe/C nanocage composed of sub-10 nm nanoparticles with a multi-hierarchy stress-buffering effect as anode materials for PIBs.[316] The synergistic effect of all the ultrafine nanoparticles, the open structure, and the hollow structure effectively reduces the diffusion-induced stresses and greatly enhances the structural integrity. Meanwhile, the coated carbon layer can also enhance the electronic conductivity and suppress the agglomeration of ZnSe nanoparticles. Owing to these merits, the ZnSe/C nanocages deliver a high reversible capacity of 318 mAh g^{-1} at 50 mAh g^{-1} as well as excellent cyclability of 189 mAh g^{-1}

up to 1000 cycles at 500 mA g^{-1}, which could provide new research ideas for the Zn-based conversion anodes in practical potassium storage. Meanwhile, various Fe-based anodes have also been carried out for PIBs, such as hollow Fe_xO nanospheres anchoring on the 3D N-doped few-layer graphene framework[317], amorphous $FeVO_4$[318], 3D N-doped porous graphene framework decorating with Fe_3O_4 nanoparticles[319], 3D carbon framework-supported FeSe[320], and multicore-shell Fe_2N nanoparticle impregnated N-doped carbon nanofiber bundles[321], and hierarchical Fe_9S_{10}@MoS_2@C composite[322]. The potassium ion storage performances of all these electrodes are studied in detail, and similar optimization strategies have also been utilized to improve their reversible capacity and cycling stbilty.

Besides, quantum dots with high specific surface area and reactivity are also expected to be used as energy storage materials. Gao et al.[323] reported, for the first time, the CoS and GO composite PIB anode material. Four samples with different contents of GO (0, 10, 15, 20%) are prepared by a two-step hydrothermal method by in situ vulcanizing the as-prepared $Co(OH)_2$ nanosheets with GO. During the vulcanization process, the $Co(OH)_2$ nanosheets transfer into CoS quantum dot nanoclusters in the surface of GO, exhibiting a larger surface area, high electrical conductivity, structural stability, and excellent electrochemical energy storage performance. At a current density of 500 mA g^{-1}, the electrode displays a high specific capacity of 310.8 mAh g^{-1} after 100 cycles. Moreover, Li et al.[324] reported a novel 3D structural self-supported $NiCo_2S_4$@N-C composite material by anchoring the tapered rod-shaped $NiCo_2S_4$ nanomaterial on the N-doped hollow carbon nanofibers via a carbonization and hydrothermal method. The as-prepared electrode materials deliver a high capacity of 263.7 mAh g^{-1} after 200 cycles at 100 mA g^{-1} and an outstanding stability with a capacity 134.3 mAh g^{-1} after 600 cycles at 3.2 A g^{-1}.

Generally, the reaction mechanisms of these aforementioned transition metal oxides and dichalcogenides are mostly based on the intercalation, conversion, and alloying process along with large volume changes during the potassiation/depotassiation reactions. As a result, the aggregation and pulverization of these active materials severely limit their rate performances and cycling stability. The previous studies have tried to overcome these problems by designing various complex nanostructure and composite heterojunction with carbon materials. The performance optimization mainly attributes to the combined advantages of nanostructure and carbon, such as large contact area, abundant reaction sites, short diffusion path, high electronic conductivity, and adequate resilience to alleviate the volume changes and agglomeration during cycling. However, both the low initial CE from large irreversible capacity loss and the high and sloping operating voltage plateau hamper their practical application in PIBs. Thus, the future studies should focus more attention on understanding the working mechanisms between various structures and performances, therefore designing more efficient conversion electrodes with novel structure for energy storage.

The MOFs are also considered directly as potential anode candidates because of the potential polyelectron transfer by oxidizing/reducing of both the inorganic metal and organic linkers. Along with the advantages of high controllability, porosity with controlled pore size, and high specific surface area, the MOFs could accelerate the diffusion rate of K^+ ions and exhibit promising electrochemical performances for potassium storage. For example, Deng and co-workers[325] reported a low-cost microporous iron based organic framework (MOF-235) as novel anode materials for PIBs. After composited with multiwall-carbon nanotubes, the composite electrode exhibit a specific capacity of 132 mAh g^{-1} over 200 cycles at 200 mA g^{-1} with remarkable rate

capability. The enhanced electron conductivity from the carbon nanotubes and the active site from the organic terephthalate moiety account for the high performance. Wang et al.[326] proposed a non-redox-metal potassium MOF (K-MOF) to directly investigate the redox reaction of organic pyridine dicarboxylate in PIBs. A unique and reversible three-step redox reaction from $[C_7H_3KNO_4]_n$ to $[C_7H_3K_2NO_4]_n$ is observed in the organic anode, resulting in a moderate average capacity of 115 mA h g^{-1} in 300 cycles at 100 mA g^{-1} with the capacity retention of 92%. The potassium perylene-3,4,9,10-tetracarboxylate (K_4PTC)[327] was also reported as a new two-electron redox-active organic anode for PIBs. Since the strong multiple K-O bonds could prevent the solubility of organic materials in electrolyte, the K_4PTC anode displays the capacity of 100 mAh g^{-1} for 500 cycles at 50 mA g^{-1}. Wang et al.[328] further discovered an organic azobenzene-4,4′-dicarboxylic acid potassium salt with an azo group as the redox center to reversibly react with K^+ ions. Because of the surface reaction-controlled mechanism, this electrode could display a high reversible capacity of 109 mAh g^{-1} over 400 cycles at 155 mA g^{-1}. However, the reversible capacity and cycling stability of MOFs are still far from practical application. Thus, more effective strategies should be developed to enhance the electrochemical performances for promising electrode materials in PIBs.

3.3 Alloying anodes

Similar to the research history of LIBs and SIBs, partial Group IVA and VA elements (e.g. Si, P, Ge, Sn, Sb, Pb, and Bi etc.) and their compounds (e.g., oxides, sulfides, and phosphides) have also attracted much attention due to the low operating voltage and high theoretical specific capacities for PIBs.[329-332] Because of the alloying reaction mechanism, K-rich intermetallic compounds are formed with great potential for high-energy PIBs. For instance, Sb possesses a final alloying product of K_3Sb with a remarkable theoretical capacity of 660 mAh g^{-1} for PIBs, which is much higher than the carbonaceous anode materials. The most important obstacle for the commercialization of alloy-based anodes is the rapid capacity fading due to the large volume variations and the sluggish kinetics during cycling. Moreover, new surfaces of active materials are always exposed after pulverization because of the huge volume changes, so that the SEI layers would form continuously in the next cycle, which further impedes the charge transfer and fades the reversible capacity. Recently, several effective strategies have been developed to overcome these problems, including designing special nanostructure, introducing protective matrix, and employing suitable electrolytes. Herein, the research progress about different alloy-based anodes with enhanced potassium storage capacity is presented based on the recent literatures.

Tin (Sn) is an attractive alloy-based anode material for LIBs and SIBs with considerable theoretical capacities of 990 mA h·g^{-1} ($Li_{22}Sn_5$ as the final phase) and 847 mAh·g^{-1} ($Na_{15}Sn_4$ as the product), respectively[333]. However, the Sn anodes suffer significant volume change during cycles in both the LIBs (420%) and SIBs (260%), which lead to the structural pulverization and fast capacity fading. Similarity, the Sn anode presents a moderate theoretical capacity in PIBs, but the electrode also easily pulverizes upon potassiation/depotassiation reactions.[334] Most reported researches are devoted to develop novel electrodes to solve these obstacles. The commonly used method is to incorporate the nano-size Sn with carbon materials including the porous carbon, graphite, and graphene. Lrin et al.[335] prepared the Sn-C alloy by mechanical ball milling with a weight ratio of 7:3 in Ar atmosphere. The alloy is used as an anode material for PIBs, delivering a reversible specific capacity of about 150 mAh g^{-1}. Huang and co-workers[336] reported a 3D

hierarchical Sn/porous carbon composite anode for PIBs via a high temperature solid state method using the NaCl as the template. The Sn nanoparticles with sizes of 22-94 nm could homogeneously anchor on the porous carbon matrix after carbonization in different temperatures. The reversible capacity could be optimized to be 276.4 mAh g^{-1} at 50 mA g^{-1} after 100 cycles under 650 °C. When the current density increases to 500 mA g^{-1}, the capacity can still maintain at 150 mAh g^{-1}. Meanwhile, the submicron Sn particles were also encapsulated into the 3D porous rGO networks[337], displaying a reversible capacity of 123.6 mAh g^{-1} after 500 cycles at 500 mA g^{-1}. Moreover, the Sn-based compounds also exhibit promising electrochemical performances as electrode materials for PIBs[338, 339]. For example, Zhou and co-workers[340] synthesized homogeneous SnO_2 nanocrystals with a size of 2-6 nm embedded in porous carbon via a hydrothermal method. Because of the well-restrained ultrasmall SnO_2 nanoparticles in porous carbon matrix, the composite electrode could present an excellent reversible capacity of 300 mA h g^{-1} after 100 cycles. Even after 10000 cycles at a high current density of 1 A g^{-1}, an outstanding reversible capacity of 108.3 mA h g^{-1} can still maintain. Xia et al.[341] fabricated the few-layered SnS_2 nanosheets on the rGO matrix, which presents a high specific capacity of 448 mAh g^{-1} at 50 mA g^{-1}. The high capacity is revealed to be attributed from the sequential conversion (SnS_2 to Sn) and alloying (Sn to K_4Sn_{23} and KSn) reactions of SnS_2 nanosheets during the potassiation process. Along with the fast K storage kinetics and excellent structure integrity, a stable long cycling performance with a capacity retention of 73% after 300 cycles is remarkably promoted by structure engineering. In order to further improve the attenuation of this specific capacity, Ci et al.[342] prepared an alloyed-based composite electrode SnS_2@C@rGO by restraining the SnS_2 in porous carbon networks with an in situ rGO shell. As a result, the volume expansion during the alloying process is reduced obviously, delivering a high reversible capacity of 298.1 mAh g^{-1} and 170.9 mAh g^{-1} after 500 cycles at the current density of 0.2 and 0.5 A g^{-1}, respectively. Based on the above investigation, although these Sn-based carbon composite materials manifest better specific capacity and cycling stability than the pure Sn anode, the reversible capacity is still much lower than the theoretical capacity. More studies should be investigated on the Sn-based electrodes for PIBs to improve their reversible capacity and CE in the future.

Antimony (Sb) is also well known for its good conductivity and alloying ability with alkali metal elements. For example, Sb could alloy with the Li and Na to form the Li_3Sb and Na_3Sb final phases with high capacities. Wang et al.[343] detailly investigated the phase changes of Sb anode during the potassiation process by DFT calculation. In combination with the CV measurement, they reveal a phase transformation from Sb to KSb_2, KSb, K_5Sb_4, and K_3Sb sequentially with the increasing potential during the potassiation/depotassiation process, showing a high theoretical capacity of 660 mAh·g^{-1}. However, the volume expansion of 407% is much larger, which easily results in a rapid capacity fading. The authors further design a Sb@CSN composite by encapsulating Sb nanoparticles in a carbon sphere network to tackle this issue. Using the concentrated 4 M KTFSI/EC + DEC as electrolyte, the as-prepared anode could deliver an outstanding capacity of 551 mA h g^{-1} after 100 cycles at 100 mA g^{-1}. Thus, introducing a carbon matrix to form various Sb-based carbon composites seems to be a common strategy to improve its comprehensive electrochemical properties, which could efficiently accommodate the volume change of Sb and promote the fast electronic/ionic diffusion[344]. For example, Lin et al.[345] embedded the Sb nanoparticles with an average size of 14.0 nm on the surface of the 18.6 nm thick ultrathin carbon nanosheets by a one-step solvothermal “metathesis” chemical reaction. The

composite anode display a reversible capacity of 247 mA h g^{-1} after 600 cycles at 200 mA g^{-1}, which fades only 10% of the initial capacity. The novel Sb-based composites with unique microstructures, such as 3D macroporous Sb@carbon composite[346] and segment-like Sb nanorod encapsulated in N-doping hollow carbon tube[347], are also reported with greatly improved electrochemical performance. Moreover, the Sb nanoparticles are also incorporated with the conductive and flexible MXene paper to form a flexible and freestanding MXene@Sb anodes[348], delivering a high reversible capacity of 516.8 mA h g^{-1} at 50 mA g^{-1} and a stable long-term cycling capability with a capacity fading rate of only 0.042% per cycle. Ou et al.[349] firstly impregnated the Sb nanoparticles into few-layered MoS_2 nanosheets, and then encapsulated the MoS_2/Sb heterostructure into N-doped graphene framework as a complex anode material for PIBs. Due to the synergistic coupling effect of MoS_2 nanosheets and N-doped graphene in the chrysanthemum-like structure, the hierarchical composite electrode could prevent the coarsening of alloyed Sb nanograins, alleviate the volume expansion during de/potassiation cycles, and promote the electron/ion conductivity, which results in a high reversible capacity of 359.5 mAh g^{-1} at 50 mA g^{-1} and outstanding cycling stability with a reversible capacity of 170.1 mAh g^{-1} over 1000 cycles at 2 A g^{-1}. Furthermore, the strategy of forming intermetallic alloys with other elements has recently aroused great attention in Sb-based anodes for PIBs[350]. Xu et al.[351] reported w a composite nanosheet by embedding the Bi-Sb alloy nanoparticles in a porous carbon matrix via a freeze-drying and pyrolysis method. The Bi and carbon can effectively buffer the volume change during charge/discharge process, delivering a reversible capacity of 320 mA h g^{-1} at 500 mA g^{-1} over 600 cycles from the reversible alloying reaction mechanism of (Bi,Sb) ↔K(Bi,Sb) ↔K_3(Bi,Sb). When the as-prepared composite is fabricated into a full PIB with the PB cathode, it can still deliver a high capacity of 360 mAh g^{-1} after 70 cycles. Besides, the Sb-based compounds, e.g. Sb_2Se_3, are also developed as stable two step conversion/alloying anodes for PIBs[351, 352]. By combining with carbon materials (such as rGO and N-doped carbon layer), the volume expansion of Sb_2Se_3 nanoparticles could be relieved, so that enhancing the reversible specific capacity and stability. And a bimetallic oxide Sb_2MoO_6 supported on rGO is further reported as the PIB anode material by Lu et al[353]. The discharge capacity could be 402 mAh g^{-1} at 100 mA g^{-1}, and the capacity can still keep stable at 247 mAh g^{-1} after 100 cycles when the current density increases to 100 mA g^{-1}. The in situ XRD, TEM, and DFT calculation indicate that the majority of the high capacity is from the alloying/dealloying of Sb, which stems from the irreversible reduction of Sb_2MoO_6. Meanwhile, the resulted amorphous Mo could improve the conductivity of electrode and relieve the volume change of Sb during cycling. Although different methods have been proposed to enhance the electrochemical performances, the cyclic stability and initial CE are still unsatisfactory. So that future research should focus more on the fundamental of capacity fading and improvement of cyclic stability and rate performance for the Sb-based PIB anodes.

Similar to the metal Sn and Sb, bismuth (Bi) is a promising metal anode which can also alloy with three K ions due to its unique layered crystal structure with a large interlayer spacing of 3.95 Å. The Bi-based electrodes could deliver a higher theoretical capacity of 385 mAh g^{-1}, however, these electrodes still attract little attention in PIBs. The main reason might be their low CE and fast capacity fading. Guo et al.[354] reported that the de/alloying process consists two typical multi-phase reactions to form K_3Bi in the initial potassiation process and a reversible stepwise K_3Bi↔K_3Bi_2↔KBi_2↔Bi mechanism in the following de/potassiation cycles. The volume

expansion of phase transformation from Bi to K_3Bi is found to be as high as 406%, which is much larger than that of the Na_3Bi (≈244%) and Li_3Bi (≈106%). Thus, the nanostructural design method, such as the 2D few layered bismuthene[355], has been proposed to improve the performances of PIB anodes due to its fast ion diffusion, electrolyte penetration, and the ability to buffer the volume change along the c-axis. The excellent rate capacity of the bismuthene anode for PIBs indicates that the capacity could keep highly stable with the capacity values of 423, 356, 275, and 227 mAh g^{-1} at 2.5, 5, 10, and 15 A g^{-1}, respectively. When the current density increases to 20 A g^{-1}, a long-term cycling stability with the capacity of 200 mAh g^{-1} is obtained at 2 A g^{-1}. In addition, the introduction of various carbon materials is also a commonly efficient way to accommodate the huge volume expansion during the alloying/dealloying process. For example, Tai and co-workers[356] developed a hierarchical bismuth nanodots/graphene composite by a facial in situ spontaneous reduction. The Bi nanodots with a size of 3 nm are well confined in the graphene layers, which could not only accommodate the volume change but can also provide ionic transport channels. As the result, the composite electrode displays an impressive reversible capacity of 213 mA h g^{-1} after 500 cycles at 5 A g^{-1} and even provides a stable rate capability of 200 mA h g^{-1} at 10 A g^{-1}. Qu et al.[357] fabricated the hollow Bi@N-doped C nanorods via a simple evaporation method, in which the hollow structure can buffer the volume changes of Bi during de/potassiation cycles and the outer conductive carbon shells could promote the electron transfer. The reversible capacity of 353 mAh g^{-1} can be achieved at 50 mA g^{-1}, and the capacity retention rate is 80.3% after 300 cycles at 500 mA g^{-1}. Jian et al.[358] reported a hollow structured N-doped carbon coated Bi nanorods, which also exhibits a stable high-rate capability and excellent long-term cycling performance. The Bi-based compounds, such as chalcogenides, oxides, and oxyhalides, were also reported for high-performance PIB anodes via the conversion and alloying reactions successively. For example, Neeraj et al.[359] reported a tetradymite-type Bi_2Te_3 anode for rechargeable Li, Na and K-ion batteries, which exhibit the first discharge capacities of 480, 498, and 456 mAh g^{-1}, respectively. Similar to the bimetallic oxide Sb_2MoO_6, the nanoplates-assembled Bi_2MoO_6 microsphere is also unveiled as a novel anode for high performance PIBs by Zhang et al[360]. Without hybridizing with conductive carbon materials, the Bi_2MoO_6 microsphere can still achieve a stable reversible capacity of 121.7 mAh g^{-1} over 600 cycles at 100 mA·g^{-1}. Lei et al.[361] firstly found the layered bismuth oxyhalides, which are promising photocatalysts in environmental protection field, could also be used as anodes in PIBs. The as-prepared BiOCl nanoflakes delivers a high specific capacity of 367 mAh g^{-1} at 50 mA g^{-1} due to the formation of K-Bi alloys during potassiation reaction. Lu et al.[362] further dispersed the bimetallic oxychloride $Bi_{0.51}Sb_{0.49}OCl$ nanosheets on rGO nanosheets, which could integrate the advantages of both $Bi_{0.51}Sb_{0.49}OCl$ and rGO nanosheets. Based on the potassium ion storage mechanism of $Bi_{0.51}Sb_{0.49}OCl \rightarrow (Bi,Sb) \rightleftharpoons K(Bi,Sb) \rightleftharpoons K_3(Bi,Sb)$ reactions, the as-prepared electrode exhibits a low charge/discharge plateaus and high discharge capacity of 360 mAh g^{-1} after running 1000 cycles at 100 mA g^{-1}. When the current density increases to 1 A g^{-1}, the discharge capacity can still remain as high as 319 mAh g^{-1}. These studies could not only shed light on the mechanisms for K^+ ion storage in Bi-based composite heterostructures, but also pave the potential strategy for the practical application of PIBs.

The phosphorus (P) can also form a binary phase K_3P with potassium via a three-electron reaction mechanism. Along with its light atomic quality, the P anode material exhibits the highest theoretical capacity of 2596 mAh g^{-1} for PIBs, which is like that in LIBs and SIBs. Among the

allotropes of P elements, the white phosphorus can hardly be used for electrochemical energy storage because of its toxicity and flammability in air. But the performance of red phosphorus is stable, and the low electronic conductivity can also reduce the electrochemical redox reactions. While the 2D black phosphorus possesses the highest stability and electron mobility. The red and black phosphorus seems to be potential anode materials for PIBs in theory. However, the practical reactivity of these pure P-based materials is hard to trigger and the initial CE is quite low with negligible capacity after few cycles. Thus, the carbon materials are also introduced to improve their intrinsic insulating electronic performance and finally optimize their cycling stability. For example, Sultana et al.[363] initially found that, when encapsulating pure black phosphorus in a carbon matrix, the cycle performance is related to the mass ratio of black phosphorus to carbon. When the mass ratio of black phosphorous to carbon is 7:3, the specific capacity drops to nearly 0 mAh g^{-1} after 50 cycles at 50 mA g^{-1}. When the mass ratio is 1:1, the composite exhibits a specific capacity of 270 mAh g^{-1} after 50 cycles under the same current density, and the capacity retention rate is 60%. In a recently published paper, Yu and co-workers[364] reported an outstanding PIB anode by encapsulating red phosphorus into N-doped porous hollow carbon nanofibers (red P@N-PHCNF) via a vaporization-condensation strategy (Fig. 14a). The SEM and TEM images indicate that the tubular structured composites exhibit an amorphous characteristic without any red P nanoparticles on the surface of carbon nanofiber (Fig. 14b-d). The special structure could buffer the volume expansion, while the P-C bonds and the adsorption of P atoms at N-doped site can facilitate the transfer and diffusion of K^+ ions (Fig. 14e, f). The rationally designed electrode delivers an ultra-high reversible specific capacity of 650 mAh g^{-1} after 100 cycles at a low current density of 100 mA g^{-1} (Fig. 14g). After 800 cycles at the high current density of 2 A g^{-1}, a specific capacity still maintains 465 mAh g^{-1} (Fig. 14h). In addition, the composite anode also realizes an excellent rate performance with a capacity of 342 mAh g^{-1} at 5 A g^{-1} (Fig. 14h). The in situ Raman and ex situ XRD results confirm that the final discharge product of red P in this composite is the K_4P_3 alloy phase via the reversible $4K + 3P \leftrightarrows K_4P_3$ reaction. The ball-milling method is also a common strategy to the red P-carbon composite material. For example, the red P particles could be dispersed into the multiwall CNTs by this ball-milling method[365], however, their reversible capacity and cycling performance are lower than the aforementioned vaporization-condensation method. Moreover, the polypyrrole layer was further coated on the surface of P-activated carbon composite to offer a dual protection of red P material, so that the air stability and reversible capacities could be enhanced[366]. In addition, various metal phosphides are developed as PIB anodes, such as hierarchically porous carbon supported Sn_4P_3[367], trigonal SnP@C[368], SnP_3/C nanocomposite[369], yolk-shell structured FeP@C nanoboxes[303, 370], MoP@N/P-codoped carbon nanofibers[371], and Se_3P_4@mesoporous carbon composite[372]. Among these compounds, the Se_3P_4@C composite obtains an excellent electrochemical performance as an anode material for PIBs[372]. An outstanding reversible initial capacity of 1036.8 mAh g^{-1} is obtained at 50 mA g^{-1} with an initial CE of 68.9%. But the CE value quickly increases to 97.5% and stabilizes at about 99.3% in the following cycles. An exceptional cycling stability with a capacity retention of 78.9% is also achieved after 300 cycles at 1000 mA g^{-1}. The researchers reveal that the high capacity detailly relates to the reversible potassiation process $Se_3P_4 + (18-4x)\ K^+ + 18\ e^- \rightarrow 4K_{3-x}P + 3K_2Se$, and the synergistic effect between Se and P elements provides a buffering effect to reduce the volume change and retain the cycling stability. As mentioned, the capacity is proportional to the P contents in electrode, while the cycling performance is inversely proportionate to the P loadings in the

composite. Thus, it is difficult to find a suitable balance between the capacity and cyclic stability in PIBs. In future work, the main direction for the P-based anode is still the optimization of electrochemical performances.

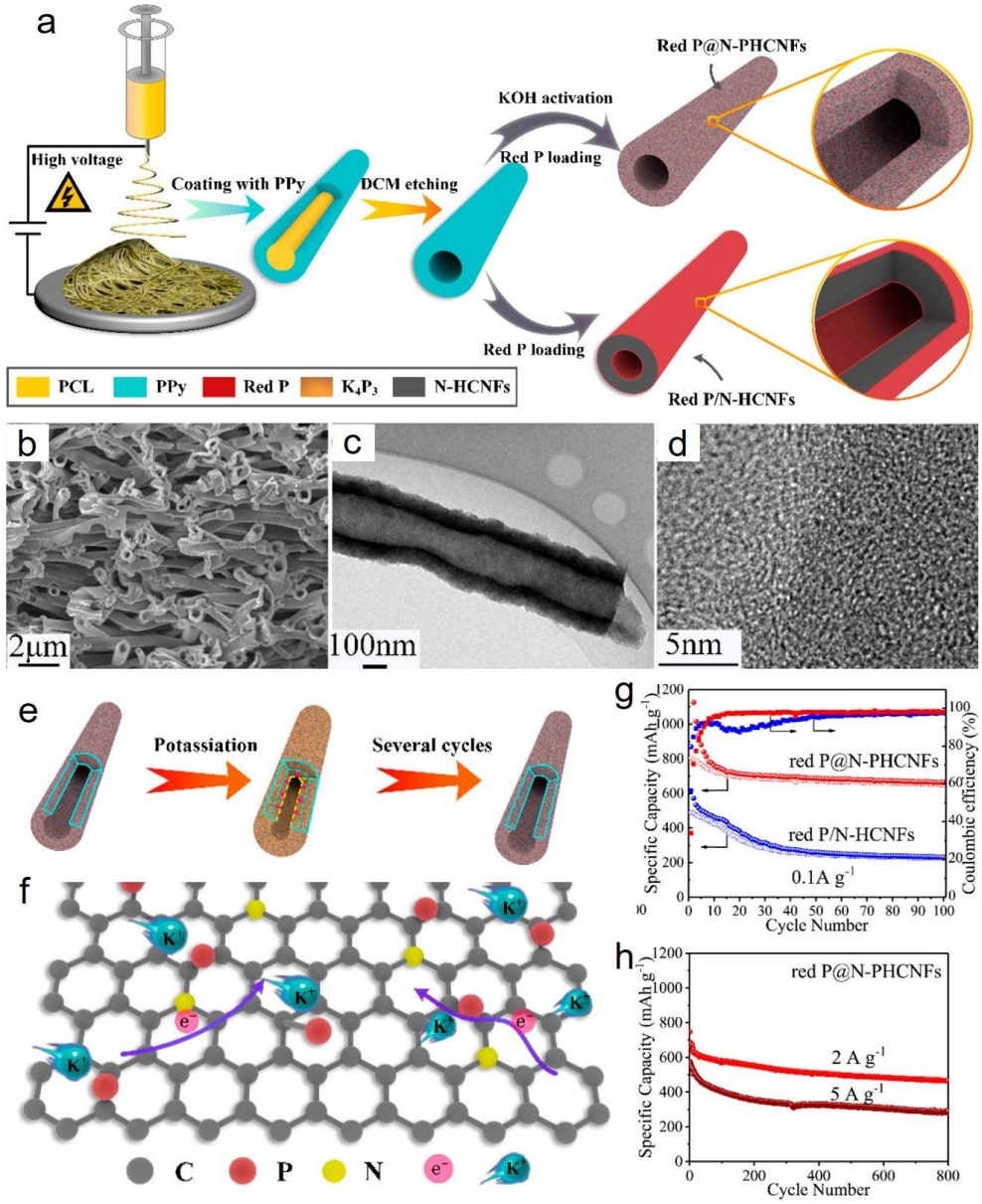

Fig. 14. (a) Schematic illustration of the synthesis process the red P@N-PHCNF sample; (b-d) The SEM, TEM, and HRTEM images of the red P@N-PHCNF; (e, f) The de/potassiation process and charge transfer in the red P@N-PHCNF sample; (g, h) Cycling performance at 0.1 A g^{-1}, 2 A g^{-1}, and 5 A g^{-1}, respectively.

On the other hand, the rational use of electrolyte and binder is an effective approach to optimize the performance of alloying anodes. In practical studies, the anode materials, such as metals Sn, Sb, and Bi, that perform potassium storage through alloying reactions have a large volume expansion during the reaction. The expansion rate of Sb and Bi metal during the reaction is about 300% and 406%, respectively, leading to a poor cycling performance in PIBs. By choosing potassium bis(fluorosulfonyl)imide (KFSI) to replace potassium hexafluorophosphate (KPF_6) in the EC and DEC (1:1 volume) mixture, Guo et al.[354] reported that the Bi/rGO anode

could deliver an higher initial charge capacity of 441 mAh g^{-1} and maintain a more stable reversible capacity of 290 mAh g^{-1} after 50 cycles in KFSI electrolyte. Further studies indicate that the FSI^- anion could inhibit the electrolyte decomposition, modify the surface passivation, and form a more uniform, conductive, stable, and robust SEI, so that improving the cycling stability. More importantly, the KFSI salt is very versatile and can significantly promote the electrochemical performance of other alloy-based anode materials, such as the Sn/C and Sb/C composite. Furthermore, the above-mentioned resutls by Lei and Huang et al.[373, 374] are based on the non-carbonate electrolyte DME. The interaction between DME molecules and Bi in this electrolyte promotes the potassiation/depotassiation cycling. 3D structure might be formed during the alloying process, which could also improve the cycle performance of the anode in PIBs. These electrolyte and binder can not only promote the ion transfer between anode and cathode, but also enhances the electronic contact between the active material and matrix. More and more researches in future should be focus more on the electrolyte and binder for performance optimization of each new electrode materials.

4. Summary and perspectives 第 2-3 部分一般都是大众的描述，第 4 部分其实是最重要的，编辑审稿人主要是看这里我们能有什么好的观点。我加了几句话，是从三个维度来写，晶格-界面-形貌，这个如果你们有时间也可以扩充，在第一段以及 4.1 4.2 4.3 等部分，都可以扩充，没时间就按照目前的写法也行。

With the exponentially growing consumption of lithium resources in recent years, it is significantly vital to develop alternative technologies for large-scale energy storage to compete with the commercialized LIBs systems. Among the reported rechargeable batteries, the PIBs based on using the earth-abundant K element as the charge carrier are considered suitable for the next generation energy storage systems. As graphite is commonly used as an anode for LIBs and SIBs, it was the first choice anode for PIBs, promoting safety and cycling stability according to some reports. However, the theoretical and practical issues of PIBs are different from LIBs and SIBs because of the larger ionic radius and the higher reactivity of potassium. Hence, the design of electrode materials and the fabrication of full cells have distinctive features. The adjusting of lattice structures (such as enlarged interlayer spacing, increased transport channels, low K-intercalation energy barrier, etc.) of the active materials to facilitate the large-radius K^+ transport is unprecedentedly significant. On a larger scale, the morphological control of the electrode materials is another way to enhance the battery behavior by means of boosting the kinetics of K^+ and electron, accommodating the volume change, avoiding the agglomeration of the particles and restraining active materials' dissolution and dispersion. Beyond one particle dimension, the interface interactions (including the electrode-electrolyte interface, single-phase particles interface, different-phases interface, etc.) are also of great importance to the thermodynamics and kinetics characteristics of the electrode during cycling. Thus, in-depth researches are still needed to meet the requirements for further practical application of high-performance PIBs.

Based on the type of the electrochemical reactions, the active cathode materials can be

categorized into insertion and conversion cathode types. For the insertion cathodes, where K+ ions are inserted between the layers of the crystals and then removed in the second half-cycle, materials such as Prussian blue and its analogues, layered transition metal oxides, and the flexible organic materials can be used. In this case, a crystal structure, that can accommodate the sizeable volumetric change during the K+ ions insertion/desertion, is crucial for determining the cathode cycle life. Unfortunately, most of the active materials investigated so far cannot sustain the substantial volumetric changes, and also exhibited limited storage capacity and poor electronic conductivity. In future research, exploring novel flexible structures combining with theoretical prediction would be one of the most effective ways to tolerate the inevitable structural deformation. Also, crystal structure optimization, such as lattice optimization, cationic/anion substitution, and heteroatom doping, could also be necessary strategies to adjust the crystal lattice parameters, improve the structural stability, and optimize the Fermi level, which accordingly enhance their reversible capacity and long-term cyclability. These methods may also be a potential direction to change the one-electron transfer process of the most promising PB and PB analogues cathodes into a multi-electron storage per formula unit with higher capacity and stability. To further improve the electronic conductivity of electrodes, the electronic conductive agents (e.g. carbon-based materials) might be a good option to be added into the materials, which could also help to buffer the volumetric changes during cycling. Developing intrinsically conductive cathode materials, probably by using potassium-rich phases, may also help to reduce the electrode resistance and minimize the parasitic reactions. Moreover, the reinforcement on the thermal stability of the PB analogs and organic cathode materials is also required for further commercial applications. Last, but definitely not least, the essential characteristic and mechanism of the reversibility of K+ ion insertion/extraction in insertion-type cathodes should be studied much more in-depth to provide a reference for the further development on new high-performance cathode materials.

Similar to the studies on LIBs and SIBs, the capacities of the conversion cathodes are achieved by the solid-state redox reactions with repeated breaking and reforming of chemical bonds during potassiation/depotassiation cycling. These cathode materials, including metal fluorides and chlorides, sulfur, selenium, iodine, and oxygen, always own high theoretical capacity and volumetric capacities. Most of these materials have been used in LIBs and SIBs with better success. Although using them in PIBs is still at an early stage, results thus far showing poor cycling stability as a result of three competing factors; the poor electrical conductivity, the severe side reactions, and the possible intermediates (e.g. polysulfide) dissolution. Like the more-established researches in LIBs and SIBs, the K-S, K-Se, K-I2, and K-O2 systems, with the superiority of high specific energy capacities and low cost, could also be considered as promising candidates for practical application of PIBs. Future studies of these conversion-type cathodes could focus on designing novel low-dimensional nanostructures that can minimize the detrimental effect of the repeated phase changes. Another future direction would be investigating new multi-structure composites that can buffer the contentious changes in the active material, such as carbon yolk-shell structure; or introducing two competing processes, such as mixing two or more active materials. Developing suitable electrolytes and electrolyte additives for the corresponding systems will also help to improve the cycling stability and promote the application of PIBs in large-scale energy storage. Indeed, optimizing the cathode production method is necessary to reduce the cost and to achieve a high energy density before practical application.

The research on the anode materials is still dominated by the carbon-based materials, with some attempts to use alloy-based materials, layered metal compounds, metal organic frame materials, and organic materials. The selection of these materials is mainly based on their reported success with LIBs, with few attempts to design anode materials specifically for the potassium systems. Despite the clear efforts, there are still several challenges to developing suitable carbon-based electrode materials with reasonable potassium-storage capability. Some metal-based compound anodes, such as titanium-based compounds, have shown high reversible capacities, and good cycling stability, but their low energy density still limits their practical applications. Anodes based on materials that can alloy with potassium exhibited high specific capacities and energy density. However, they present finite cycling stability due to the serious volume and phases variations with further particle pulverization and aggregation. The dwindling contact among particles fades their capacity rapidly. Intercalation-based anodes would probably be ruled out as candidates for PIBs shortly since the defined interlayer space, and the large size of K+ will make any improvement in their performance incremental. To facilitate the commercial visability of PIBs, future research should focus on improving the storage capacity and long-term stability based on conventional anode materials. Some perspectives are outlined as follows:

(1) Nano-architectural design and engineering for more robust anode structures: Firstly, the material design and preparation of low-dimensional nanostructure (including 0D, 1D and 2D architecture) should be investigated more with focus on improving the cycling and rate performance. The new designs should be able to tolerate the sizeable volume variation, resist pulverization, and increase the electrode/electrolyte interface area. Engineering the low dimensional materials into porous 3D architectures may help to buffer the volumetric changes and shorten the diffusion pathway. With increasing the specific surface areas, more active sites could be exposed to the electrolyte, which facilities the K+ reaction with the anode. Multi-structure design and morphology optimization on heterostructure composite electrodes, including all kinds of hierarchical structure, hollow structure, coating structure, sandwich-type structure, yolk-shell structure etc., could become a promising strategy to alleviate the mechanical stress during charge/discharge cycling. The formed internal electric field at the interfaces of the coupled materials could bring a rapid diffusion while improving the electronic/ionic conductivity and the electrochemical activity. Functionalized the anode materials to have more target groups on the surface is another way to enhance the K+ kinetics by reducing the adsorption energy. Of course, the preparation process of the designed nano-architectural materials should be low cost, simple to control, and easy to automatic fabrication for further practical application.

(2) Composition design and optimization: Since the development of entirely new active materials is difficult, compositional design and optimization seems more practical. Heteroatom doping of the anode materials, typically with normally including N, S, O, P, F, and/or B, has shown great potential with LIBs and SIBs anodes and can also be applied to PIBs. The defects or vacancies forming in the vicinity of heteroatom doping sites would rearrange the electrons, and change the electronic structure or hybridization states, which can improve the reaction kinetics and the electrode electrical conductivity. Doping carbonaceous materials with nitrogen, especially pyridinic N, is known to enhance the K-C adsorption bond around the nitrogen doping sites. Some reports have linked the nitrogen doping to improved reversible capacity in all alkali-ions batteries. Density functional theory (DFT) calculations suggest improvement in the electron transfer when carbon-based materials are doped with P, S, F, and B atoms, which might lead to stabilizing the

structures and improve the theoretical capacities. However, no experimental data has been published yet. The so-called co-doping (doping by more than one element) such as binary or ternary elements doped anodes, can improve the electrode performance by synergistic effects of all the dopants. For example, the co-doping of nitrogen and oxygen into hard carbon material could enhance the capacity and cycling performance simultaneously. The DFT calculation and further experimental research on varied multi-elements doped electrodes, such as N/S doped, N/P doped, S/O doped, P/B doped, and N/P/S doped carbon should be investigated carefully in the near future.

(3) More theoretical and experimental studies are needed in order to gain more insights on the mechanism of the electrochemical reaction and the changes in the electrode during the charge/discharge. Of particular interest, the mechanism of forming SEI in the nonaqueous solvents should receive more attention. Engineering a robust SEI through ALD, CVD or similar techniques would undoubtedly help to prevent unwanted reactions on the electrode/electrolyte interface, preventing sever electrolyte decomposition and improving the overall stability of the electrode in general. In the nearly future, the advanced in-situ spectroscopic characterization technologies, (e.g. cryogenic electron microscopy, HRTEM, STEM, Raman spectroscopy, and Fourier transform infrared microscopy) with supporting DFT calculations could help to understand the K ion transportation and storage mechanism, as well as get more details on the side reactions and SEI formation process, thus helping to develop viable anode systems.

To date, most of the researches are focused on the active materials, with the majority of the lab tests are conducted on half-cell configuration using potassium metal as the counter electrode. In this case, it is known that the exact cycling behavior of the working electrode might be concealed by the side reactions between the potassium metal electrode and electrolytes. For instance, the Coulombic efficiency of the carbon-based anodes (e.g. hard carbon, CNT, graphene) is always less than 70%, which, of course, severely limits their practical application. In order to move the PIBs closer to commercial use, other areas, such as electrolytes, electrolyte additives, and binders should also be investigated. More focus should also be paid to optimizing the full cell using the best-known electrolyte and electrode materials. To the best of our knowledge, there is only one commercial use of a full potassium ion cell by the Chinese company Starsway Electronics to power media player portable device.

The electrolytes, as the window for electrochemical reactions by connecting the electrodes, should be significantly important for the development of commercial PIBs. On the interface of the electrolytes and electrodes, the solid electrolyte interphase (SEI) layer passivation film is usually formed on the electrode surface because of the irreversible reduction of electrolytes. In PIBs, the SEI layer is reported to be thick, implying poor ionic diffusion kinetics and thus high resistances. One route to improve the ionic conductivity of the SEI layer is by optimizing the electrolyte (alkali salts and solvents) as well as investigate new additives to manage the SEI formation. Suppressing the dendrites growth and minimizing the side reactions are also need to be considered in the whole process of new electrolytes systems development. Since the amount of the electrolyte in the actual full cell is limited, the issues relegated to dendrites formation, SEI layer and the side reactions would have a significant influence on the overall performance of the cell. Reports have shown that KFSI electrolyte has higher conductivity than KPF6, but issues related to the homogeneity of the composition should be addressed. Electrolytes that use ether-based solvents (e.g. DMC, DME, and diglyme) are reported to form more stable SEI layer with higher initial

Coulombic efficiency than the carbonate-based electrolytes (e.g. EC, DEC, and PC) due to their strong chemical adsorption and charge-transfer kinetics. Some binary or ternary solvent mixtures (e.g. KFSI-DME electrolyte), polymer electrolytes, and potassium ionic liquid could also promote the formation of stable SEI layers and suppress the dendrite growth. In addition, the SEI layer formed with some electrolyte additives, such as FEC, could also prevent the side reactions and stay more stable to a certain extent.

The electrode fabrication technology is a problem shared by all the alkali-metal ions batteries. One of the problems specifically related to PIBs is the type of the binder. Polyvinylidene fluoride (PVDF) binder, commonly used in LIBs, cannot sustain the large volumetric changes associated with the potassium ions insertion/stripping. As a result, exfoliating the key functional components away from the metal foil current collector is very common in PIBs, leading to fast capacity fading and poor electronic conductivity. Therefore, more studies focusing on exploring new binders with excellent elasticity is necessary to improve the mechanical integrity of the electrodes for practical PIBs. Further development for the separators is also desirable to optimize their performances. Modifying the sides of the separators that faces the anode or the cathode could be viable approaches to suppress the parasitic reactions and the dentate formations.

Although PIBs have shown lower susceptibility to thermal runaway and in general release less heat when compared to LIBs, the safety of PIBs remain a problem due to the flammable organic electrolytes and poor thermal stability of SEI layers. Using thermally stable separators, polymer electrolytes, solid-state electrolytes, and adding flame-retardants into the liquid electrolytes or electrode materials may help to improve the batteries safety. Besides, the theoretical and experimental studies should also be utilized to build an efficient kinetic model of the complex thermal runaway process, facilitating the unique structural design for high-safety PIBs.

References

1. Tarascon, J. M.; Armand, M., Issues and challenges facing rechargeable lithium batteries. *Nature* **2001,** *414* (6861), 359-367.
2. Goodenough, J. B.; Park, K.-S., The Li-Ion Rechargeable Battery: A Perspective. *Journal of the American Chemical Society* **2013,** *135* (4), 1167-1176.
3. Etacheri, V.; Marom, R.; Elazari, R.; Salitra, G.; Aurbach, D., Challenges in the development of advanced Li-ion batteries: a review. *Energy & Environmental Science* **2011,** *4* (9), 3243-3262.
4. Larcher, D.; Tarascon, J. M., Towards greener and more sustainable batteries for electrical energy storage. *Nature Chemistry* **2015,** *7* (1), 19-29.
5. Liu, C.; Li, F.; Ma, L. P.; Cheng, H. M., Advanced materials for energy storage. *Adv. Mater.* **2010,** *22* (8), E28-62.
6. Lu, L.; Han, X.; Li, J.; Hua, J.; Ouyang, M., A review on the key issues for lithium-ion battery management in electric vehicles. *J. Power Sources* **2013,** *226*, 272-288.
7. Li, M.; Lu, J.; Chen, Z.; Amine, K., 30 Years of Lithium-Ion Batteries. *Adv. Mater.* **2018**, e1800561.
8. Wang Qiushu, Y. C., The global supply situation of lithium ore and sugestions on resources security in China. *China Mining Magazine* **2019,** *28* (5), 1-6.
9. Tarascon, J. M., Key challenges in future Li-battery research. *Philosophical Transactions of the*

Royal Society a-Mathematical Physical and Engineering Sciences **2010,** *368* (1923), 3227-3241.
10. Eftekhari, A., Lithium Batteries for Electric Vehicles: From Economy to Research Strategy. *Acs Sustainable Chemistry & Engineering* **2019,** *7* (6), 5602-5613.
11. Harper, G.; Sommerville, R.; Kendrick, E.; Driscoll, L.; Slater, P.; Stolkin, R.; Walton, A.; Christensen, P.; Heidrich, O.; Lambert, S.; Abbott, A.; Ryder, K. S.; Gaines, L.; Anderson, P., Recycling lithium-ion batteries from electric vehicles. *Nature* **2019,** *575* (7781), 75-86.
12. Zeng, X.; Li, M.; Abd El-Hady, D.; Alshitari, W.; Al-Bogami, A. S.; Lu, J.; Amine, K., Commercialization of Lithium Battery Technologies for Electric Vehicles. *Advanced Energy Materials* **2019,** *9* (27).
13. Hesse, H. C.; Schimpe, M.; Kucevic, D.; Jossen, A., Lithium-Ion Battery Storage for the Grid-A Review of Stationary Battery Storage System Design Tailored for Applications in Modern Power Grids. *Energies* **2017,** *10* (12).
14. Rahimi-Eichi, H.; Ojha, U.; Baronti, F.; Chow, M.-Y., Battery Management System An Overview of Its Application in the Smart Grid and Electric Vehicles. *Ieee Industrial Electronics Magazine* **2013,** *7* (2), 4-16.
15. Dunn, B.; Kamath, H.; Tarascon, J.-M., Electrical Energy Storage for the Grid: A Battery of Choices. *Science* **2011,** *334* (6058), 928-935.
16. Hwang, J.-Y.; Myung, S.-T.; Sun, Y.-K., Recent Progress in Rechargeable Potassium Batteries. *Adv. Funct. Mater.* **2018,** *28* (43).
17. Su, T.; Guo, M.; Liu, Z.; Li, Q., Comprehensive Review of Global Lithium Resources. *Journal of Salt Lake Research* **2019,** *27* (3), 104-111.
18. Li, X.; Mo, Y.; Qing, W.; Shao, S.; Tang, C. Y.; Li, J., Membrane-based technologies for lithium recovery from water lithium resources: A review. *J. Membr. Sci.* **2019,** *591*.
19. Liu, C.; Lin, J.; Cao, H.; Zhang, Y.; Sun, Z., Recycling of spent lithium-ion batteries in view of lithium recovery: A critical review. *Journal of Cleaner Production* **2019,** *228*, 801-813.
20. Eftekhari, A., Potassium secondary cell based on Prussian blue cathode. *J. Power Sources* **2004,** *126* (1-2), 221-228.
21. Eftekhari, A.; Jian, Z.; Ji, X., Potassium Secondary Batteries. *ACS Appl Mater Interfaces* **2017,** *9* (5), 4404-4419.
22. Jian, Z.; Xing, Z.; Bommier, C.; Li, Z.; Ji, X., Hard Carbon Microspheres: Potassium-Ion Anode Versus Sodium-Ion Anode. *Advanced Energy Materials* **2016,** *6* (3).
23. Slater, M. D.; Kim, D.; Lee, E.; Johnson, C. S., Sodium-Ion Batteries. *Adv. Funct. Mater.* **2013,** *23* (8), 947-958.
24. Yabuuchi, N.; Kubota, K.; Dahbi, M.; Komaba, S., Research development on sodium-ion batteries. *Chem Rev* **2014,** *114* (23), 11636-82.
25. Palomares, V.; Serras, P.; Villaluenga, I.; Hueso, K. B.; Carretero-Gonzalez, J.; Rojo, T., Na-ion batteries, recent advances and present challenges to become low cost energy storage systems. *Energy & Environmental Science* **2012,** *5* (3), 5884-5901.
26. Yabuuchi, N.; Kubota, K.; Dahbi, M.; Komaba, S., Research Development on Sodium-Ion Batteries. *Chem. Rev.* **2014,** *114* (23), 11636-11682.
27. Wenchao Zhang, Y. L., Zaiping Guo, Approaching high-performance potassium-ion batteries via advanced design strategies
and engineering. *Science Advances* **2019,** *5*, eaav7412—.
28. Li, M.; Lu, J.; Ji, X.; Li, Y.; Shao, Y.; Chen, Z.; Zhong, C.; Amine, K., Design

strategies for nonaqueous multivalent-ion and monovalent-ion battery anodes. *Nature Reviews Materials* **2020,** *5* (4), 276-294.

29. Marcus, Y., THERMODYNAMIC FUNCTIONS OF TRANSFER OF SINGLE IONS FROM WATER TO NONAQUEOUS AND MIXED-SOLVENTS .3. STANDARD POTENTIALS OF SELECTED ELECTRODES. *Pure Appl. Chem.* **1985,** *57* (8), 1129-1132.

30. Matsuura, N.; Umemoto, K.; Takeuchi, Z. i., Standard potentials of alkali metals, silver, and thallium metal/ion couples in N, N′-dimethylformamide, dimethyl sulfoxide, and propylene carbonate. *Bull. Chem. Soc. Jpn.* **1974,** *47* (4), 813-817.

31. Pramudita, J. C.; Sehrawat, D.; Goonetilleke, D.; Sharma, N., An Initial Review of the Status of Electrode Materials for Potassium-Ion Batteries. *Advanced Energy Materials* **2017,** *7* (24).

32. Kubota, K.; Dahbi, M.; Hosaka, T.; Kumakura, S.; Komaba, S., Towards K-Ion and Na-Ion Batteries as "Beyond Li-Ion". *Chem Rec* **2018,** *18* (4), 459-479.

33. Gabaudan, V.; Monconduit, L.; Stievano, L.; Berthelot, R., Snapshot on Negative Electrode Materials for Potassium-Ion Batteries. *Frontiers in Energy Research* **2019,** *7*.

34. Xu, Y.-S.; Duan, S.-Y.; Sun, Y.-G.; Bin, D.-S.; Tao, X.-S.; Zhang, D.; Liu, Y.; Cao, A.-M.; Wan, L.-J., Recent developments in electrode materials for potassium-ion batteries. *Journal of Materials Chemistry A* **2019,** *7* (9), 4334-4352.

35. Ferlay, S.; Mallah, T.; Ouahes, R.; Veillet, P.; Verdaguer, M., A room-temperature organometallic magnet based on Prussian blue. *Nature* **1995,** *378* (6558), 701-703.

36. Wessells, C. D.; Huggins, R. A.; Cui, Y., Copper hexacyanoferrate battery electrodes with long cycle life and high power. *Nature communications* **2011,** *2* (1), 1-5.

37. Karyakin, A. A., Prussian blue and its analogues: electrochemistry and analytical applications. *Electroanalysis: An International Journal Devoted to Fundamental and Practical Aspects of Electroanalysis* **2001,** *13* (10), 813-819.

38. Keggin, J.; Miles, F., Structures and formulae of the Prussian blues and related compounds. *Nature* **1936,** *137* (3466), 577-578.

39. Robin, M. B., The Color and Electronic Configurations of Prussian Blue. *Inorganic Chemistry* **1962,** *1* (2), 337-342.

40. You, Y.; Wu, X.-L.; Yin, Y.-X.; Guo, Y.-G., High-quality Prussian blue crystals as superior cathode materials for room-temperature sodium-ion batteries. *Energy & Environmental Science* **2014,** *7* (5), 1643-1647.

41. Nie, P.; Shen, L.; Luo, H.; Ding, B.; Xu, G.; Wang, J.; Zhang, X., Prussian blue analogues: a new class of anode materials for lithium ion batteries. *Journal of Materials Chemistry A* **2014,** *2* (16), 5852-5857.

42. Lu, Y.; Wang, L.; Cheng, J.; Goodenough, J. B., Prussian blue: a new framework of electrode materials for sodium batteries. *Chem Commun (Camb)* **2012,** *48* (52), 6544-6.

43. Wang, L.; Lu, Y.; Liu, J.; Xu, M.; Cheng, J.; Zhang, D.; Goodenough, J. B., A superior low-cost cathode for a Na-ion battery. *Angew. Chem. Int. Ed. Engl.* **2013,** *52* (7), 1964-7.

44. Lee, H. W.; Wang, R. Y.; Pasta, M.; Woo Lee, S.; Liu, N.; Cui, Y., Manganese hexacyanomanganate open framework as a high-capacity positive electrode material for sodium-ion batteries. *Nat Commun* **2014,** *5*, 5280.

45. Scholz, F.; Dostal, A., The formal potentials of solid metal hexacyanometalates. *Angewandte Chemie International Edition in English* **1996,** *34* (23-24), 2685-2687.

46. Yang, D.; Xu, J.; Liao, X.-Z.; Wang, H.; He, Y.-S.; Ma, Z.-F., Prussian blue without

coordinated water as a superior cathode for sodium-ion batteries. *Chem. Commun.* **2015,** *51* (38), 8181-8184.

47. Zhang, C.; Xu, Y.; Zhou, M.; Liang, L.; Dong, H.; Wu, M.; Yang, Y.; Lei, Y., Potassium Prussian Blue Nanoparticles: A Low-Cost Cathode Material for Potassium-Ion Batteries. *Adv. Funct. Mater.* **2017,** *27* (4).

48. Liu, C.; Luo, S.; Huang, H.; Wang, Z.; Hao, A.; Zhai, Y.; Wang, Z., K0. 67Ni0. 17Co0. 17Mn0. 66O2: a cathode material for potassium-ion battery. *Electrochem. Commun.* **2017,** *82*, 150-154.

49. Azhar, Z.; Fariati; Wijaya, H. W.; Jayanti, W. D.; Golhen, S.; Dasna, I. W. In *Synthesis and characterization of zinc-thiocyanato and chromium (III)-quinoline complex as K-ion battery material*, AIP Conf. Proc., AIP Publishing LLC: 2020; p 030004.

50. Huang, B.; Liu, Y.; Lu, Z.; Shen, M.; Zhou, J.; Ren, J.; Li, X.; Liao, S., Prussian Blue [K2FeFe (CN) 6] Doped with Nickel as a Superior Cathode: An Efficient Strategy To Enhance Potassium Storage Performance. *ACS Sustainable Chemistry & Engineering* **2019,** *7* (19), 16659-16667.

51. Wessells, C. D.; Peddada, S. V.; Huggins, R. A.; Cui, Y., Nickel Hexacyanoferrate Nanoparticle Electrodes For Aqueous Sodium and Potassium Ion Batteries. *Nano Lett.* **2011,** *11* (12), 5421-5425.

52. Xia, M.; Zhang, X.; Liu, T.; Yu, H.; Chen, S.; Peng, N.; Zheng, R.; Zhang, J.; Shu, J., Commercially Available Prussian Blue Get Energetic in Aqueous K-ion Batteries. *Chem. Eng. J.* **2020**, 124923.

53. Luo, Y.; Shen, B.; Guo, B.; Hu, L.; Xu, Q.; Zhan, R.; Zhang, Y.; Bao, S.; Xu, M., Potassium titanium hexacyanoferrate as a cathode material for potassium-ion batteries. *J. Phys. Chem. Solids* **2018,** *122*, 31-35.

54. Xue, L.; Li, Y.; Gao, H.; Zhou, W.; Lu, X.; Kaveevivitchai, W.; Manthiram, A.; Goodenough, J. B., Low-Cost High-Energy Potassium Cathode. *J. Am. Chem. Soc.* **2017,** *139* (6), 2164-2167.

55. Huang, B.; Shao, Y.; Liu, Y.; Lu, Z.; Lu, X.; Liao, S., Improving Potassium-Ion Batteries by Optimizing the Composition of Prussian Blue Cathode. *ACS Applied Energy Materials* **2019,** *2* (9), 6528-6535.

56. Xue, Q.; Li, L.; Huang, Y.; Huang, R.; Wu, F.; Chen, R., Polypyrrole-modified prussian blue cathode material for potassium ion batteries via in situ polymerization coating. *ACS applied materials & interfaces* **2019,** *11* (25), 22339-22345.

57. Husmann, S.; Zarbin, A. J.; Dryfe, R. A., High-performance aqueous rechargeable potassium batteries prepared via interfacial synthesis of a Prussian blue-carbon nanotube composite. *Electrochim. Acta* **2020**, 136243.

58. Lopes, L. C.; Husmann, S.; Zarbin, A. J., Chemically synthesized graphene as a precursor to Prussian blue-based nanocomposite: A multifunctional material for transparent aqueous K-ion battery or electrochromic device. *Electrochim. Acta* **2020**, 136199.

59. He, P.; Yu, H.; Li, D.; Zhou, H., Layered lithium transition metal oxide cathodes towards high energy lithium-ion batteries. *J. Mater. Chem.* **2012,** *22* (9).

60. Sathiya, M.; Abakumov, A. M.; Foix, D.; Rousse, G.; Ramesha, K.; Saubanère, M.; Doublet, M. L.; Vezin, H.; Laisa, C. P.; Prakash, A. S.; Gonbeau, D.; VanTendeloo, G.; Tarascon, J. M., Origin of voltage decay in high-capacity layered oxide electrodes. *Nature Materials* **2014,** *14* (2), 230-238.

61. Carlier, D.; Cheng, J. H.; Berthelot, R.; Guignard, M.; Yoncheva, M.; Stoyanova, R.; Hwang, B. J.; Delmas, C., The P2-Na(2/3)Co(2/3)Mn(1/3)O2 phase: structure, physical properties and electrochemical behavior as positive electrode in sodium battery. *Dalton Trans* **2011,** *40* (36), 9306-12.
62. Xie, M.; Luo, R.; Lu, J.; Chen, R.; Wu, F.; Wang, X.; Zhan, C.; Wu, H.; Albishri, H. M.; Al-Bogami, A. S.; El-Hady, D. A.; Amine, K., Synthesis-microstructure-performance relationship of layered transition metal oxides as cathode for rechargeable sodium batteries prepared by high-temperature calcination. *ACS Appl Mater Interfaces* **2014,** *6* (19), 17176-83.
63. Vaalma, C.; Giffin, G. A.; Buchholz, D.; Passerini, S., Non-Aqueous K-Ion Battery Based on Layered K0.3MnO2and Hard Carbon/Carbon Black. *J. Electrochem. Soc.* **2016,** *163* (7), A1295-A1299.
64. Choi, J. U.; Park, Y. J.; Jo, J. H.; Jung, Y. H.; Ahn, D.-C.; Jeon, T.-Y.; Lee, K.-S.; Kim, H.; Lee, S.; Kim, J.; Myung, S.-T., An optimized approach toward high energy density cathode material for K-ion batteries. *Energy Storage Materials* **2020,** *27*, 342-351.
65. Kim, H.; Seo, D. H.; Kim, J. C.; Bo, S. H.; Liu, L.; Shi, T.; Ceder, G., Investigation of Potassium Storage in Layered P3-Type K0. 5MnO2 Cathode. *Adv. Mater.* **2017,** *29* (37), 1702480.
66. Zhang, Q.; Didier, C.; Pang, W. K.; Liu, Y.; Wang, Z.; Li, S.; Peterson, V. K.; Mao, J.; Guo, Z., Structural Insight into Layer Gliding and Lattice Distortion in Layered Manganese Oxide Electrodes for Potassium-Ion Batteries. *Advanced Energy Materials* **2019,** *9* (30), 1900568.
67. Choi, J. U.; Kim, J.; Hwang, J.-Y.; Jo, J. H.; Sun, Y.-K.; Myung, S.-T., K0. 54 [Co0. 5Mn0. 5] O2: New cathode with high power capability for potassium-ion batteries. *Nano Energy* **2019,** *61*, 284-294.
68. Zhang, X.; Yang, Y.; Qu, X.; Wei, Z.; Sun, G.; Zheng, K.; Yu, H.; Du, F., Layered P2-Type K0. 44Ni0. 22Mn0. 78O2 as a High-Performance Cathode for Potassium-Ion Batteries. *Adv. Funct. Mater.* **2019,** *29* (49), 1905679.
69. Jo, J. H.; Choi, J. U.; Park, Y. J.; Jung, Y. H.; Ahn, D.; Jeon, T. Y.; Kim, H.; Kim, J.; Myung, S. T., P2-K0. 75 [Ni1/3Mn2/3] O2 Cathode Material for High Power and Long Life Potassium-Ion Batteries. *Advanced Energy Materials* **2020,** *10* (7), 1903605.
70. Liu, C.-l.; Luo, S.-h.; Huang, H.-b.; Liu, X.; Zhai, Y.-c.; Wang, Z.-w., Fe-doped layered P3-type K0. 45Mn1− xFexO2 (x≤ 0.5) as cathode materials for low-cost potassium-ion batteries. *Chem. Eng. J.* **2019,** *378*, 122167.
71. Liu, C.-l.; Luo, S.-h.; Huang, H.-b.; Zhai, Y.-c.; Wang, Z.-w., Influence of Na-substitution on the structure and electrochemical properties of layered oxides K0.67Ni0.17Co0.17Mn0.66O2 cathode materials. *Electrochim. Acta* **2018,** *286*, 114-122.
72. Yu, Q.; Hu, J.; Wang, W. A.; Li, Y.; Suo, G.; Zhang, L.; Xi, K.; Lai, F.; Fang, D., K0. 6CoO2-xNx Porous Nanoframe: a Co-enhanced Ionic and Electronic Transmission for Potassium Ion Batteries. *Chem. Eng. J.* **2020**, 125218.
73. Hironaka, Y.; Kubota, K.; Komaba, S., P2-and P3-K x CoO 2 as an electrochemical potassium intercalation host. *Chem. Commun.* **2017,** *53* (26), 3693-3696.
74. Masese, T.; Yoshii, K.; Kato, M.; Kubota, K.; Huang, Z.-D.; Senoh, H.; Shikano, M., A high voltage honeycomb layered cathode framework for rechargeable potassium-ion battery: P2-type K2/3Ni1/3Co1/3Te1/3O2. *Chem. Commun.* **2019,** *55* (7), 985-988.
75. Jo, J. H.; Hwang, J.-Y.; Choi, J. U.; Kim, H. J.; Sun, Y.-K.; Myung, S.-T., Potassium vanadate as a new cathode material for potassium-ion batteries. *J. Power Sources* **2019,** *432*, 24-29.
76. Yuan, K.; Ning, R.; Bai, M.; Hu, N.; Zhang, K.; Gu, J.; Li, Q.; Huang, Y.; Shen, C.;

Xie, K., Prepotassiated V2O5 as the Cathode Material for High-Voltage Potassium-Ion Batteries. *Energy Technology* **2020,** *8* (1), 1900796.

77. Kim, H.; Kim, J. C.; Bo, S.-H.; Shi, T.; Kwon, D.-H.; Ceder, G., K-Ion Batteries Based on a P2-Type K0.6CoO2 Cathode. *Advanced Energy Materials* **2017,** *7* (17).

78. Kim, H.; Seo, D.-H.; Urban, A.; Lee, J.; Kwon, D.-H.; Bo, S.-H.; Shi, T.; Papp, J. K.; McCloskey, B. D.; Ceder, G., Stoichiometric Layered Potassium Transition Metal Oxide for Rechargeable Potassium Batteries. *Chem. Mater.* **2018,** *30* (18), 6532-6539.

79. Naveen, N.; Han, S. C.; Singh, S. P.; Ahn, D.; Sohn, K.-S.; Pyo, M., Highly stable P′ 3-K0. 8CrO2 cathode with limited dimensional changes for potassium ion batteries. *J. Power Sources* **2019,** *430*, 137-144.

80. Gao, A.; Li, M.; Guo, N.; Qiu, D.; Li, Y.; Wang, S.; Lu, X.; Wang, F.; Yang, R., K-Birnessite Electrode Obtained by Ion Exchange for Potassium-Ion Batteries: Insight into the Concerted Ionic Diffusion and K Storage Mechanism. *Advanced Energy Materials* **2019,** *9* (1), 1802739.

81. Jo, J. H.; Hwang, J.-Y.; Choi, J.; Sun, Y.-K.; Myung, S.-T., Layered K0. 28MnO2· 0.15 H2O as a Cathode Material for Potassium-Ion Intercalation. *ACS applied materials & interfaces* **2019,** *11* (46), 43312-43319.

82. Lin, B.; Zhu, X.; Fang, L.; Liu, X.; Li, S.; Zhai, T.; Xue, L.; Guo, Q.; Xu, J.; Xia, H., Birnessite Nanosheet Arrays with High K Content as a High-Capacity and Ultrastable Cathode for K-Ion Batteries. *Adv. Mater.* **2019,** *31* (24), 1900060.

83. Recham, N.; Rousse, G.; Sougrati, M. T.; Chotard, J.-N.; Frayret, C.; Mariyappan, S.; Melot, B. C.; Jumas, J.-C.; Tarascon, J.-M., Preparation and Characterization of a Stable FeSO4F-Based Framework for Alkali Ion Insertion Electrodes. *Chem. Mater.* **2012,** *24* (22), 4363-4370.

84. Rousse, G.; Tarascon, J. M., Sulfate-Based Polyanionic Compounds for Li-Ion Batteries: Synthesis, Crystal Chemistry, and Electrochemistry Aspects. *Chem. Mater.* **2013,** *26* (1), 394-406.

85. Subban, C. V.; Ati, M.; Rousse, G.; Abakumov, A. M.; Van Tendeloo, G.; Janot, R.; Tarascon, J. M., Preparation, structure, and electrochemistry of layered polyanionic hydroxysulfates: LiMSO4OH (M = Fe, Co, Mn) electrodes for Li-ion batteries. *J. Am. Chem. Soc.* **2013,** *135* (9), 3653-61.

86. Yamada, A.; Chung, S. C.; Hinokuma, K., Optimized LiFePO4 for Lithium Battery Cathodes. *J. Electrochem. Soc.* **2001,** *148* (3).

87. Shoufeng Yang, Y. S., Peter Y. Zavalij, M. Stanley Whittingham, Reactivity, stability and electrochemical behavior of lithium iron phosphates. *Electrochem. Commun.* **2002,** *4* (3), 239-244.

88. Mathew, V.; Kim, S.; Kang, J.; Gim, J.; Song, J.; Baboo, J. P.; Park, W.; Ahn, D.; Han, J.; Gu, L.; Wang, Y.; Hu, Y.-S.; Sun, Y.-K.; Kim, J., Amorphous iron phosphate: potential host for various charge carrier ions. *NPG Asia Materials* **2014,** *6* (10), e138-e138.

89. Zhong, S.; Li, F.; Liu, J.; Li, Y.; Deng, X., Preparation and electrochemical studies of Y-doped LiVPO4F cathode materials for lithium-ion batteries. *Journal of Wuhan University of Technology-Mater. Sci. Ed.* **2009,** *24* (4), 552-556.

90. Nishimura, S.; Nakamura, M.; Natsui, R.; Yamada, A., New lithium iron pyrophosphate as 3.5 V class cathode material for lithium ion battery. *J. Am. Chem. Soc.* **2010,** *132* (39), 13596-7.

91. Prabeer Barpanda, S.-i. N., Atsuo Yamada, High-Voltage Pyrophosphate Cathodes. *Advanced Energy Materials* **2012,** *2* (7), 841-859.

92. Park, Y.-U.; Seo, D.-H.; Kim, H.; Kim, J.; Lee, S.; Kim, B.; Kang, K., A Family of

High-Performance Cathode Materials for Na-ion Batteries, Na-3(VO1-xPO4)(2) F1+2x (0 <= x <= 1): Combined First-Principles and Experimental Study. *Adv. Funct. Mater.* **2014,** *24* (29), 4603-4614.

93. Recham, N.; Chotard, J. N.; Dupont, L.; Delacourt, C.; Walker, W.; Armand, M.; Tarascon, J. M., A 3.6 V lithium-based fluorosulphate insertion positive electrode for lithium-ion batteries. *Nature Materials* **2010,** *9* (1), 68-74.

94. Han, J.; Li, G. N.; Liu, F.; Wang, M.; Zhang, Y.; Hu, L.; Dai, C.; Xu, M., Investigation of K3V2(PO4)3/C nanocomposites as high-potential cathode materials for potassium-ion batteries. *Chem Commun (Camb)* **2017,** *53* (11), 1805-1808.

95. Zheng, S.; Cheng, S.; Xiao, S.; Hu, L.; Chen, Z.; Huang, B.; Liu, Q.; Yang, J.; Chen, Q., Partial replacement of K by Rb to improve electrochemical performance of K3V2(PO4)(3) cathode material for potassium-ion batteries. *J. Alloys Compd.* **2020,** *815*.

96. Lin, X.; Huang, J.; Tan, H.; Huang, J.; Zhang, B., K3V2(PO4)(2)F-3 as a robust cathode for potassium-ion batteries. *Energy Storage Materials* **2019,** *16*, 97-101.

97. Chihara, K.; Katogi, A.; Kubota, K.; Komaba, S., KVPO4F and KVOPO4 toward 4 volt-class potassium-ion batteries. *Chem Commun (Camb)* **2017,** *53* (37), 5208-5211.

98. Liao, J.; Hu, Q.; Che, B.; Ding, X.; Chen, F.; Chen, C., Competing with other polyanionic cathode materials for potassium-ion batteries via fine structure design: new layered KVOPO4 with a tailored particle morphology. *Journal of Materials Chemistry A* **2019,** *7* (25), 15244-15251.

99. Liao, J.; Hu, Q.; He, X.; Mu, J.; Wang, J.; Chen, C., A long lifespan potassium-ion full battery based on KVPO4F cathode and VPO4 anode. *J. Power Sources* **2020,** *451*.

100. Tan, H.; Du, X.; Huang, J.-Q.; Zhang, B., KVPO4F as a novel insertion-type anode for potassium ion batteries. *Chem. Commun.* **2019,** *55* (75), 11311-11314.

101. Park, W. B.; Han, S. C.; Park, C.; Hong, S. U.; Han, U.; Singh, S. P.; Jung, Y. H.; Ahn, D.; Sohn, K.-S.; Pyo, M., KVP2O7 as a Robust High-Energy Cathode for Potassium-Ion Batteries: Pinpointed by a Full Screening of the Inorganic Registry under Specific Search Conditions. *Advanced Energy Materials* **2018,** *8* (13).

102. Park, H.; Kim, H.; Ko, W.; Jo, J. H.; Lee, Y.; Kang, J.; Park, I.; Myung, S.-T.; Kim, J., Development of K4Fe3(PO4)(2)(P2O7) as a novel Fe-based cathode with high energy densities and excellent cyclability in rechargeable potassium batteries. *Energy Storage Materials* **2020,** *28*, 47-54.

103. Voronina, N.; Jo, J. H.; Konarov, A.; Kim, J.; Myung, S.-T., KTi2(PO4)(3) Electrode with a Long Cycling Stability for Potassium-Ion Batteries. *Small* **2020,** *16* (20).

104. Fedotov, S. S.; Luchinin, N. D.; Aksyonov, D. A.; Morozov, A. V.; Ryazantsev, S. V.; Gaboardi, M.; Plaisier, J. R.; Stevenson, K. J.; Abakumov, A. M.; Antipov, E. V., Titanium-based potassium-ion battery positive electrode with extraordinarily high redox potential. *Nature Communications* **2020,** *11* (1).

105. Kim, H.; Shakoor, R. A.; Park, C.; Lim, S. Y.; Kim, J.-S.; Jo, Y. N.; Cho, W.; Miyasaka, K.; Kahraman, R.; Jung, Y.; Choi, J. W., Na2FeP2O7 as a Promising Iron-Based Pyrophosphate Cathode for Sodium Rechargeable Batteries: A Combined Experimental and Theoretical Study. *Adv. Funct. Mater.* **2013,** *23* (9), 1147-1155.

106. Hailong Chen, Q. H., Olivera Zivkovic, Geoffroy Hautier, Lin-Shu Du, Yuanzhi Tang, Yan-Yan Hu, Xiaohua Ma, Clare P. Grey, Gerbrand Ceder, Sidorenkite (Na3MnPO4CO3): A New Intercalation Cathode Material for Na-Ion Batteries. *Chem. Mater.* **2013,** *25* (14), 2777-2786.

107. Ji, B.; Yao, W.; Zheng, Y.; Kidkhunthod, P.; Zhou, X.; Tunmee, S.; Sattayaporn, S.; Cheng, H.-M.; He, H.; Tang, Y., A fluoroxalate cathode material for potassium-ion batteries with

ultra-long cyclability. *Nature communications* **2020,** *11* (1), 1225-1225.

108. Wang, F.; Liu, S.; Jiang, Q.; Feng, K.; Yang, X.; Li, X.; Zhang, H.; Xia, M.; Zhang, H., K2Fe3(SO4)(3)(OH)(2)(H2O)(2): A new high-performance hydroxysulfate cathode material for alkali metal ion batteries. *J. Power Sources* **2020,** *452*.

109. Chen, Y.; Luo, W.; Carter, M.; Zhou, L.; Dai, J.; Fu, K.; Lacey, S.; Li, T.; Wan, J.; Han, X.; Bao, Y.; Hu, L., Organic electrode for non-aqueous potassium-ion batteries. *Nano Energy* **2015,** *18*, 205-211.

110. Xing, Z.; Jian, Z.; Luo, W.; Qi, Y.; Bommier, C.; Chong, E. S.; Li, Z.; Hu, L.; Ji, X., A perylene anhydride crystal as a reversible electrode for K-ion batteries. *Energy Storage Materials* **2016,** *2*, 63-68.

111. Jian, Z.; Liang, Y.; Rodríguez-Pérez, I. A.; Yao, Y.; Ji, X., Poly(anthraquinonyl sulfide) cathode for potassium-ion batteries. *Electrochem. Commun.* **2016,** *71*, 5-8.

112. Fan, L.; Liu, Q.; Xu, Z.; Lu, B., An Organic Cathode for Potassium Dual-Ion Full Battery. *ACS Energy Letters* **2017,** *2* (7), 1614-1620.

113. Tang, M.; Wu, Y.; Chen, Y.; Jiang, C.; Zhu, S.; Zhuo, S.; Wang, C., An organic cathode with high capacities for fast-charge potassium-ion batteries. *Journal of Materials Chemistry A* **2019,** *7* (2), 486-492.

114. Xiong, M.; Tang, W.; Cao, B.; Yang, C.; Fan, C., A small-molecule organic cathode with fast charge-discharge capability for K-ion batteries. *Journal of Materials Chemistry A* **2019,** *7* (35), 20127-20131.

115. Hu, Y.; Tang, W.; Yu, Q.; Wang, X.; Liu, W.; Hu, J.; Fan, C., Novel Insoluble Organic Cathodes for Advanced Organic K-Ion Batteries. *Adv. Funct. Mater.* **2020,** *30* (17).

116. Obrezkov, F. A.; Ramezankhani, V.; Zhidkov, I.; Traven, V. F.; Kurmaev, E. Z.; Stevenson, K. J.; Troshin, P. A., High-Energy and High-Power-Density Potassium Ion Batteries Using Dihydrophenazine-Based Polymer as Active Cathode Material. *Journal of Physical Chemistry Letters* **2019,** *10* (18), 5440-5445.

117. Tong, Z.; Tian, S.; Wang, H.; Shen, D.; Yang, R.; Lee, C.-S., Tailored Redox Kinetics, Electronic Structures and Electrode/Electrolyte Interfaces for Fast and High Energy-Density Potassium-Organic Battery. *Adv. Funct. Mater.* **2020,** *30* (5).

118. Tian, B.; Zheng, J.; Zhao, C.; Liu, C.; Su, C.; Tang, W.; Li, X.; Ning, G.-H., Carbonyl-based polyimide and polyquinoneimide for potassium-ion batteries. *Journal of Materials Chemistry A* **2019,** *7* (16), 9997-10003.

119. Fang, C.; Huang, Y.; Yuan, L.; Liu, Y.; Chen, W.; Huang, Y.; Chen, K.; Han, J.; Liu, Q.; Huang, Y., A Metal-Organic Compound as Cathode Material with Superhigh Capacity Achieved by Reversible Cationic and Anionic Redox Chemistry for High-Energy Sodium-Ion Batteries. *Angew. Chem. Int. Ed.* **2017,** *56* (24), 6793-6797.

120. Ma, J.; Zhou, E.; Fan, C.; Wu, B.; Li, C.; Lu, Z. H.; Li, J., Endowing CuTCNQ with a new role: a high-capacity cathode for K-ion batteries. *Chem Commun (Camb)* **2018,** *54* (44), 5578-5581.

121. Liang, Y.; Luo, C.; Wang, F.; Hou, S.; Liou, S.-C.; Qing, T.; Li, Q.; Zheng, J.; Cui, C.; Wang, C., An Organic Anode for High Temperature Potassium-Ion Batteries. *Advanced Energy Materials* **2019,** *9* (2).

122. Zhao, Q.; Wang, J.; Lu, Y.; Li, Y.; Liang, G.; Chen, J., Oxocarbon Salts for Fast Rechargeable Batteries. *Angewandte Chemie-International Edition* **2016,** *55* (40), 12528-12532.

123. Li, J.; Gao, J.; Thai, P. K.; Shypanski, A.; Nieradzik, L.; Mueller, J. F.; Yuan, Z.; Jiang, G., Experimental Investigation and Modeling of the Transformation of Illicit Drugs in a Pilot-Scale Sewer System. *Environmental Science & Technology* **2019,** *53* (8), 4556-4565.
124. Chen, L.; Zhao, Y., Exploration of p-Na2C6H2O6 -based organic electrode materials for sodium-ion and potassium-ion batteries. *Mater. Lett.* **2019,** *243*, 69-72.
125. Li, B.; Zhao, J.; Zhang, Z.; Zhao, C.; Sun, P.; Bai, P.; Yang, J.; Zhou, Z.; Xu, Y., Electrolyte-Regulated Solid-Electrolyte Interphase Enables Long Cycle Life Performance in Organic Cathodes for Potassium-Ion Batteries. *Adv. Funct. Mater.* **2019,** *29* (5).
126. Wang, X.; Xu, X.; Niu, C.; Meng, J.; Huang, M.; Liu, X.; Liu, Z.; Mai, L., Earth Abundant Fe/Mn-Based Layered Oxide Interconnected Nanowires for Advanced K-Ion Full Batteries. *Nano Lett.* **2017,** *17* (1), 544-550.
127. Deng, T.; Fan, X.; Chen, J.; Chen, L.; Luo, C.; Zhou, X.; Yang, J.; Zheng, S.; Wang, C., Layered P2-Type K0.65Fe0.5Mn0.5O2 Microspheres as Superior Cathode for High-Energy Potassium-Ion Batteries. *Adv. Funct. Mater.* **2018,** *28* (28).
128. Deng, Q.; Zheng, F.; Zhong, W.; Pan, Q.; Liu, Y.; Li, Y.; Chen, G.; Li, Y.; Yang, C.; Liu, M., P3-type K0.5Mn0.72Ni0.15Co0.13O2 microspheres as cathode materials for high performance potassium-ion batteries. *Chem. Eng. J.* **2020,** *392*.
129. Wang, Q.; Zhao, B.; Zhang, S.; Gao, X.; Deng, C., Superior sodium intercalation of honeycomb-structured hierarchical porous Na3V2(PO4)(3)/C microballs prepared by a facile one-pot synthesis. *Journal of Materials Chemistry A* **2015,** *3* (15), 7732-7740.
130. Genorio, B.; Pirnat, K.; Cerc-Korosec, R.; Dominko, R.; Gaberscek, M., Electroactive Organic Molecules Immobilized onto Solid Nanoparticles as a Cathode Material for Lithium-Ion Batteries. *Angewandte Chemie-International Edition* **2010,** *49* (40), 7222-7224.
131. Nokami, T.; Matsuo, T.; Inatomi, Y.; Hojo, N.; Tsukagoshi, T.; Yoshizawa, H.; Shimizu, A.; Kuramoto, H.; Komae, K.; Tsuyama, H.; Yoshida, J.-i., Polymer-Bound Pyrene-4,5,9,10-tetraone for Fast-Charge and -Discharge Lithium-Ion Batteries with High Capacity. *Journal of the American Chemical Society* **2012,** *134* (48), 19694-19700.
132. Wu, Z. S.; Ren, W.; Xu, L.; Li, F.; Cheng, H. M., Doped graphene sheets as anode materials with superhigh rate and large capacity for lithium ion batteries. *ACS Nano* **2011,** *5* (7), 5463-71.
133. Yoo, E.; Kim, J.; Hosono, E.; Zhou, H. S.; Kudo, T.; Honma, I., Large reversible Li storage of graphene nanosheet families for use in rechargeable lithium ion batteries. *Nano Lett.* **2008,** *8* (8), 2277-82.
134. Xu, J.; Dou, Y.; Wei, Z.; Ma, J.; Deng, Y.; Li, Y.; Liu, H.; Dou, S., Recent Progress in Graphite Intercalation Compounds for Rechargeable Metal (Li, Na, K, Al)-Ion Batteries. *Adv Sci (Weinh)* **2017,** *4* (10), 1700146.
135. Liu, Q.; Li, S.; Wang, S.; Zhang, X.; Zhou, S.; Bai, Y.; Zheng, J.; Lu, X., Kinetically Determined Phase Transition from Stage II (LiC12) to Stage I (LiC6) in a Graphite Anode for Li-Ion Batteries. *Journal of Physical Chemistry Letters* **2018,** *9* (18), 5567-5573.
136. Senyshyn, A.; Muehlbauer, M. J.; Dolotko, O.; Ehrenberg, H., Low-temperature performance of Li-ion batteries: The behavior of lithiated graphite. *J. Power Sources* **2015,** *282*, 235-240.
137. Jian, Z.; Luo, W.; Ji, X., Carbon Electrodes for K-Ion Batteries. *Journal of the American Chemical Society* **2015,** *137* (36), 11566-11569.
138. Schleede A, W. M., Notiz über die herstellung eines lindemannglases für kapillaren zwecks aufnahme von luftempfindlichen substanzen mit langwelliger röntgenstrahlung[J]. Zeitschrift für

Kristallographie. *Crystalline Materials* **1932,** *83*, 148-149.
139. Liu, D.; Yang, Z.; Li, W.; Qiu, S.; Luo, Y., Electrochemical intercalation of potassium into graphite in KF melt. *Electrochim. Acta* **2010,** *55* (3), 1013-1018.
140. Pramudita, J. C.; Peterson, V. K.; Kimpton, J. A.; Sharma, N., Potassium-ion intercalation in graphite within a potassium-ion battery examined using in situ X-ray diffraction. *Powder Diffr.* **2017,** *32*, S43-S48.
141. Luo, W.; Wan, J.; Ozdemir, B.; Bao, W.; Chen, Y.; Dai, J.; Lin, H.; Xu, Y.; Gu, F.; Barone, V.; Hu, L., Potassium Ion Batteries with Graphitic Materials. *Nano Lett.* **2015,** *15* (11), 7671-7.
142. Wang, Z.; Selbach, S. M.; Grande, T., Van der Waals density functional study of the energetics of alkali metal intercalation in graphite. *Rsc Advances* **2014,** *4* (8), 4069-4079.
143. Wang, Z.; Ratvik, A. P.; Grande, T.; Selbach, S. M., Diffusion of alkali metals in the first stage graphite intercalation compounds by vdW-DFT calculations. *Rsc Advances* **2015,** *5* (21), 15985-15992.
144. Cao, B.; Zhang, Q.; Liu, H.; Xu, B.; Zhang, S.; Zhou, T.; Mao, J.; Pang, W. K.; Guo, Z.; Li, A.; Zhou, J.; Chen, X.; Song, H., Graphitic Carbon Nanocage as a Stable and High Power Anode for Potassium-Ion Batteries. *Advanced Energy Materials* **2018,** *8* (25).
145. Tai, Z.; Liu, Y.; Zhang, Q.; Zhou, T.; Guo, Z.; Liu, H. K.; Dou, S. X., Ultra-light and flexible pencil-trace anode for high performance potassium-ion and lithium-ion batteries. *Green Energy & Environment* **2017,** *2* (3), 278-284.
146. Choi, S. H.; Baucom, J.; Li, X.; Shen, L.; Seong, Y.-H.; Han, I. S.; Choi, Y. J.; Ko, Y. N.; Kim, H. J.; Lu, Y., Porous carbon microspheres with highly graphitized structure for potassium-ion storage. *J. Colloid Interface Sci.* **2020,** *577*, 48-53.
147. Zhang, W.; Ming, J.; Zhao, W.; Dong, X.; Hedhili, M. N.; Costa, P. M. F. J.; Alshareef, H. N., Graphitic Nanocarbon with Engineered Defects for High-Performance Potassium-Ion Battery Anodes. *Adv. Funct. Mater.* **2019,** *29* (35).
148. Xing, Z.; Qi, Y.; Jian, Z.; Ji, X., Polynanocrystalline Graphite: A New Carbon Anode with Superior Cycling Performance for K-Ion Batteries. *Acs Applied Materials & Interfaces* **2017,** *9* (5), 4343-4351.
149. Tai, Z.; Zhang, Q.; Liu, Y.; Liu, H.; Dou, S., Activated carbon from the graphite with increased rate capability for the potassium ion battery. *Carbon* **2017,** *123*, 54-61.
150. An, Y.; Fei, H.; Zeng, G.; Ci, L.; Xi, B.; Xiong, S.; Feng, J., Commercial expanded graphite as a low–cost, long-cycling life anode for potassium–ion batteries with conventional carbonate electrolyte. *J. Power Sources* **2018,** *378*, 66-72.
151. Lee, C.; Wei, X.; Kysar, J. W.; Hone, J., Measurement of the elastic properties and intrinsic strength of monolayer graphene. *Science* **2008,** *321* (5887), 385-8.
152. Chen, J.-H.; Jang, C.; Xiao, S.; Ishigami, M.; Fuhrer, M. S., Intrinsic and extrinsic performance limits of graphene devices on SiO2. *Nature Nanotechnology* **2008,** *3* (4), 206-209.
153. Balandin, A. A.; Ghosh, S.; Bao, W.; Calizo, I.; Teweldebrhan, D.; Miao, F.; Lau, C. N., Superior thermal conductivity of single-layer graphene. *Nano Lett.* **2008,** *8* (3), 902-7.
154. Ju, Z.; Zhang, S.; Xing, Z.; Zhuang, Q.; Qiang, Y.; Qian, Y., Direct Synthesis of Few-Layer F-Doped Graphene Foam and Its Lithium/Potassium Storage Properties. *ACS Appl Mater Interfaces* **2016,** *8* (32), 20682-90.
155. Zhao, Y.; Yang, L.; Ma, C.; Han, G., One-Step Fabrication of Fluorine-Doped Graphite Derived from a Low-Grade Microcrystalline Graphite Ore for Potassium-Ion Batteries. *Energy & Fuels* **2020**.

156. Wu, S.; Mo, J.; Zeng, Y.; Wang, Y.; Rawal, A.; Scott, J.; Su, Z.; Ren, W.; Chen, S.; Wang, K.; Chen, W.; Zhang, Y.; Zhao, C.; Chen, X., Shock Exfoliation of Graphene Fluoride in Microwave. *Small* **2020,** *16* (12).
157. Lu, J.; Wang, C.; Yu, H.; Gong, S.; Xia, G.; Jiang, P.; Xu, P.; Yang, K.; Chen, Q., Oxygen/Fluorine Dual-Doped Porous Carbon Nanopolyhedra Enabled Ultrafast and Highly Stable Potassium Storage. *Adv. Funct. Mater.* **2019,** *29* (49).
158. Share, K.; Cohn, A. P.; Carter, R.; Rogers, B.; Pint, C. L., Role of Nitrogen-Doped Graphene for Improved High-Capacity Potassium Ion Battery Anodes. *ACS Nano* **2016,** *10* (10), 9738-9744.
159. Ju, Z.; Li, P.; Ma, G.; Xing, Z.; Zhuang, Q.; Qian, Y., Few layer nitrogen-doped graphene with highly reversible potassium storage. *Energy Storage Materials* **2018,** *11*, 38-46.
160. Liu, C.; Xiao, N.; Li, H.; Dong, Q.; Wang, Y.; Li, H.; Wang, S.; Zhang, X.; Qiu, J., Nitrogen-doped soft carbon frameworks built of well-interconnected nanocapsules enabling a superior potassium-ion batteries anode. *Chem. Eng. J.* **2020,** *382*.
161. Li, J.; Li, Y.; Ma, X.; Zhang, K.; Hu, J.; Yang, C.; Liu, M., A honeycomb-like nitrogen-doped carbon as high-performance anode for potassium-ion batteries. *Chem. Eng. J.* **2020,** *384*.
162. Zhou, X.; Chen, L.; Zhang, W.; Wang, J.; Liu, Z.; Zeng, S.; Xu, R.; Wu, Y.; Ye, S.; Feng, Y.; Cheng, X.; Peng, Z.; Li, X.; Yu, Y., Three-Dimensional Ordered Macroporous Metal-Organic Framework Single Crystal-Derived Nitrogen-Doped Hierarchical Porous Carbon for High-Performance Potassium-Ion Batteries. *Nano Lett.* **2019,** *19* (8), 4965-4973.
163. Yang, W.; Zhou, J.; Wang, S.; Zhang, W.; Wang, Z.; Lv, F.; Wang, K.; Sun, Q.; Guo, S., Freestanding film made by necklace-like N-doped hollow carbon with hierarchical pores for high-performance potassium-ion storage. *Energy & Environmental Science* **2019,** *12* (5), 1605-1612.
164. Chang, X.; Zhou, X.; Ou, X.; Lee, C.-S.; Zhou, J.; Tang, Y., Ultrahigh Nitrogen Doping of Carbon Nanosheets for High Capacity and Long Cycling Potassium Ion Storage. *Advanced Energy Materials* **2019**.
165. An, Y.; Tian, Y.; Li, Y.; Xiong, S.; Zhao, G.; Feng, J.; Qian, Y., Green and tunable fabrication of graphene-like N-doped carbon on a 3D metal substrate as a binder-free anode for high-performance potassium-ion batteries. *Journal of Materials Chemistry A* **2019,** *7* (38), 21966-21975.
166. Zeng, S.; Chen, X.; Xu, R.; Wu, X.; Feng, Y.; Zhang, H.; Peng, S.; Yu, Y., Boosting the potassium storage performance of carbon anode via integration of adsorption-intercalation hybrid mechanisms. *Nano Energy* **2020**, 104807.
167. Sun, Y.; Zhu, D.; Liang, Z.; Zhao, Y.; Tian, W.; Ren, X.; Wang, J.; Li, X.; Gao, Y.; Wen, W.; Huang, Y.; Li, X.; Tai, R., Facile renewable synthesis of nitrogen/oxygen co-doped graphene-like carbon nanocages as general lithium-ion and potassium-ion batteries anode. *Carbon* **2020,** *167*, 685-695.
168. Li, J.; Qin, W.; Xie, J.; Lei, H.; Zhu, Y.; Huang, W.; Xu, X.; Zhao, Z.; Mai, W., Sulphur-doped reduced graphene oxide sponges as high-performance free-standing anodes for K-ion storage. *Nano Energy* **2018,** *53*, 415-424.
169. Ding, J.; Zhang, H.; Zhou, H.; Feng, J.; Zheng, X.; Zhong, C.; Paek, E.; Hu, W.; Mitlin, D., Sulfur-grafted hollow carbon spheres for potassium-ion battery anodes. *Adv. Mater.* **2019,** *31* (30), 1900429.
170. Ma, G.; Huang, K.; Ma, J.-S.; Ju, Z.; Xing, Z.; Zhuang, Q.-c., Phosphorus and oxygen

dual-doped graphene as superior anode material for room-temperature potassium-ion batteries. *Journal of Materials Chemistry A* **2017,** *5* (17), 7854-7861.

171. Yang, W.; Zhou, J.; Wang, S.; Wang, Z.; Lv, F.; Zhang, W.; Zhang, W.; Sun, Q.; Guo, S., A Three-Dimensional Carbon Framework Constructed by N/S Co-doped Graphene Nanosheets with Expanded Interlayer Spacing Facilitates Potassium Ion Storage. *ACS Energy Letters* **2020,** *5* (5), 1653-1661.

172. Li, Y.; Zhong, W.; Yang, C.; Zheng, F.; Pan, Q.; Liu, Y.; Wang, G.; Xiong, X.; Liu, M., N/S codoped carbon microboxes with expanded interlayer distance toward excellent potassium storage. *Chem. Eng. J.* **2019,** *358*, 1147-1154.

173. Tao, L.; Yang, Y.; Wang, H.; Zheng, Y.; Hao, H.; Song, W.; Shi, J.; Huang, M.; Mitlin, D., Sulfur-nitrogen rich carbon as stable high capacity potassium ion battery anode: Performance and storage mechanisms. *Energy Storage Materials* **2020,** *27*, 212-225.

174. Li, W.; Wang, D.; Gong, Z.; Guo, X.; Liu, J.; Zhang, Z.; Li, G., Superior potassium-ion storage properties by engineering pseudocapacitive sulfur/nitrogen-containing species within three-dimensional flower-like hard carbon architectures. *Carbon* **2020,** *161*, 97-107.

175. Lv, C.; Xu, W.; Liu, H.; Zhang, L.; Chen, S.; Yang, X.; Xu, X.; Yang, D., 3D Sulfur and Nitrogen Codoped Carbon Nanofiber Aerogels with Optimized Electronic Structure and Enlarged Interlayer Spacing Boost Potassium-Ion Storage. *Small* **2019,** *15* (23), 1900816.

176. Qiu, W.; Xiao, H.; Li, Y.; Lu, X.; Tong, Y., Nitrogen and Phosphorus Codoped Vertical Graphene/Carbon Cloth as a Binder-Free Anode for Flexible Advanced Potassium Ion Full Batteries. *Small* **2019,** *15* (23), 1901285.

177. Liu, L.; Lin, Z.; Chane-Ching, J.-Y.; Shao, H.; Taberna, P.-L.; Simon, P., 3D rGO aerogel with superior electrochemical performance for K–Ion battery. *Energy Storage Materials* **2019,** *19*, 306-313.

178. Han, J.; Zhang, C.; Kong, D.; He, X.; Xiao, J.; Chen, F.; Tao, Y.; Wan, Y.; Yang, Q.-H., Flowable sulfur template induced fully interconnected pore structures in graphene artefacts towards high volumetric potassium storage. *Nano Energy* **2020**, 104729.

179. Liu, Z.; Wang, J.; Jia, X.; Li, W.; Zhang, Q.; Fan, L.; Ding, H.; Yang, H.; Yu, X.; Li, X., Graphene armored with a crystal carbon shell for ultrahigh-performance potassium ion batteries and aluminum batteries. *ACS nano* **2019,** *13* (9), 10631-10642.

180. Zhang, E.; Jia, X.; Wang, B.; Wang, J.; Yu, X.; Lu, B., Carbon Dots@ rGO Paper as Freestanding and Flexible Potassium-Ion Batteries Anode. *Advanced Science* **2020**, 2000470.

181. Wang, W.; Zhou, J.; Wang, Z.; Zhao, L.; Li, P.; Yang, Y.; Yang, C.; Huang, H.; Guo, S., Short-Range Order in Mesoporous Carbon Boosts Potassium-Ion Battery Performance. *Advanced Energy Materials* **2018,** *8* (5).

182. Kamiyama, A.; Kubota, K.; Nakano, T.; Fujimura, S.; Shiraishi, S.; Tsukada, H.; Komaba, S., High-Capacity Hard Carbon Synthesized from Macroporous Phenolic Resin for Sodium-Ion and Potassium-Ion Battery. *ACS Applied Energy Materials* **2019,** *3* (1), 135-140.

183. Tao, L.; Liu, L.; Chang, R.; He, H.; Zhao, P.; Liu, J., Structural and interface design of hierarchical porous carbon derived from soybeans as anode materials for potassium-ion batteries. *J. Power Sources* **2020,** *463*, 228172.

184. Cui, R. C.; Xu, B.; Dong, H. J.; Yang, C. C.; Jiang, Q., N/O Dual-Doped Environment-Friendly Hard Carbon as Advanced Anode for Potassium-Ion Batteries. *Advanced Science* **2020,** *7* (5), 1902547.

185. Wu, Z.; Wang, L.; Huang, J.; Zou, J.; Chen, S.; Cheng, H.; Jiang, C.; Gao, P.; Niu, X., Loofah-derived carbon as an anode material for potassium ion and lithium ion batteries. *Electrochim. Acta* **2019,** *306*, 446-453.
186. Wang, Q.; Gao, C.; Zhang, W.; Luo, S.; Zhou, M.; Liu, Y.; Liu, R.; Zhang, Y.; Wang, Z.; Hao, A., Biomorphic carbon derived from corn husk as a promising anode materials for potassium ion battery. *Electrochim. Acta* **2019,** *324*.
187. Cao, W.; Zhang, E.; Wang, J.; Liu, Z.; Ge, J.; Yu, X.; Yang, H.; Lu, B., Potato derived biomass porous carbon as anode for potassium ion batteries. *Electrochim. Acta* **2019,** *293*, 364-370.
188. Yang, M.; Dai, J.; He, M.; Duan, T.; Yao, W., Biomass-derived carbon from Ganoderma lucidum spore as a promising anode material for rapid potassium-ion storage. *J. Colloid Interface Sci.* **2020,** *567*, 256-263.
189. Wang, B.; Yuan, F.; Wang, J.; Zhang, D.; Li, W.; Wang, Q.; Sun, H., Multi-forks hierarchical porous amorphous carbon with N-Doping for high-performance potassium-ion batteries. *Electrochim. Acta* **2020,** *354*, 136627.
190. Wang, H.; Artemova, A.; Yang, G.; Wang, H.; Zhang, L.; Cao, X.; Arkhipova, E.; Liu, J.; Huang, Y.; Lin, J.; Shen, Z., Lotus root-like porous carbon for potassium ion battery with high stability and rate performance. *J. Power Sources* **2020,** *466*.
191. Xu, B.; Qi, S.; Li, F.; Peng, X.; Cai, J.; Liang, J.; Ma, J., Cotton-derived oxygen/sulfur co-doped hard carbon as advanced anode material for potassium-ion batteries. *Chin. Chem. Lett.* **2020,** *31* (1), 217-222.
192. Luo, H.; Chen, M.; Cao, J.; Zhang, M.; Tan, S.; Wang, L.; Zhong, J.; Deng, H.; Zhu, J.; Lu, B., Cocoon Silk-Derived, Hierarchically Porous Carbon as Anode for Highly Robust Potassium-Ion Hybrid Capacitors. *Nano-Micro Letters* **2020,** *12* (1).
193. Li, W.; Li, Z.; Zhang, C.; Liu, W.; Han, C.; Yan, B.; An, S.; Qiu, X., Hard carbon derived from rice husk as anode material for high performance potassium-ion batteries. *Solid State Ionics* **2020,** *351*.
194. Verma, R.; Park, C.-J., Synthesis of Mesoporous Carbon Using Waste Orange Peel As an Anode Material for Potassium-Ion Batteries with Long Cyclability. *ECS Meeting Abstracts* **2019**.
195. Huang, F.; Liu, W.; Wang, Q.; Wang, F.; Yao, Q.; Yan, D.; Xu, H.; Xia, B. Y.; Deng, J., Natural N/O-doped hard carbon for high performance K-ion hybrid capacitors. *Electrochim. Acta* **2020,** *354*, 136701.
196. Chen, J.; Yang, B.; Li, H.; Ma, P.; Lang, J.; Yan, X., Candle soot: onion-like carbon, an advanced anode material for a potassium-ion hybrid capacitor. *Journal of Materials Chemistry A* **2019,** *7* (15), 9247-9252.
197. Nanjundan, A. K.; Gaddam, R. R.; Farokh Niaei, A. H.; Annamalai, P. K.; Dubal, D. P.; Martin, D. J.; Yamauchi, Y.; Searles, D. J.; Zhao, X. S., Potassium-Ion Storage in Cellulose-Derived Hard Carbon: The Role of Functional Groups. *Batteries & Supercaps n/a* (n/a).
198. Hao, R.; Lan, H.; Kuang, C.; Wang, H.; Guo, L., Superior potassium storage in chitin-derived natural nitrogen-doped carbon nanofibers. *Carbon* **2018,** *128*, 224-230.
199. Chen, C.; Wang, Z.; Zhang, B.; Miao, L.; Cai, J.; Peng, L.; Huang, Y.; Jiang, J.; Huang, Y.; Zhang, L.; Xie, J., Nitrogen-rich hard carbon as a highly durable anode for high-power potassium-ion batteries. *Energy Storage Materials* **2017,** *8*, 161-168.
200. Zhang, K.; He, Q.; Xiong, F.; Zhou, J.; Zhao, Y.; Mai, L.; Zhang, L., Active sites enriched hard carbon porous nanobelts for stable and high-capacity potassium-ion storage. *Nano*

Energy **2020**, 105018.
201. Zhang, W.; Jiang, X.; Zhao, Y.; Carné-Sánchez, A.; Malgras, V.; Kim, J.; Kim, J. H.; Wang, S.; Liu, J.; Jiang, J.-S., Hollow carbon nanobubbles: monocrystalline MOF nanobubbles and their pyrolysis. *Chemical science* **2017,** *8* (5), 3538-3546.
202. Xiong, P.; Zhao, X.; Xu, Y., Nitrogen-Doped Carbon Nanotubes Derived from Metal–Organic Frameworks for Potassium-Ion Battery Anodes. *ChemSusChem* **2018,** *11* (1), 202-208.
203. Li, Y.; Yang, C.; Zheng, F.; Ou, X.; Pan, Q.; Liu, Y.; Wang, G., High pyridine N-doped porous carbon derived from metal–organic frameworks for boosting potassium-ion storage. *Journal of Materials Chemistry A* **2018,** *6* (37), 17959-17966.
204. Yi, Y.; Zhao, W.; Zeng, Z.; Wei, C.; Lu, C.; Shao, Y.; Guo, W.; Dou, S.; Sun, J., ZIF-8@ ZIF-67-Derived Nitrogen-Doped Porous Carbon Confined CoP Polyhedron Targeting Superior Potassium-Ion Storage. *Small* **2020,** *16* (7), 1906566.
205. Yang, J.; Ju, Z.; Jiang, Y.; Xing, Z.; Xi, B.; Feng, J.; Xiong, S., Enhanced capacity and rate capability of nitrogen/oxygen dual-doped hard carbon in capacitive potassium-ion storage. *Adv. Mater.* **2018,** *30* (4), 1700104.
206. Su, S.; Liu, Q.; Wang, J.; Fan, L.; Ma, R.; Chen, S.; Han, X.; Lu, B., Control of SEI formation for stable potassium-ion battery anodes by Bi-MOF-derived nanocomposites. *ACS applied materials & interfaces* **2019,** *11* (25), 22474-22480.
207. Qian, Y.; Jiang, S.; Li, Y.; Yi, Z.; Zhou, J.; Tian, J.; Lin, N.; Qian, Y., Understanding mesopore volume-enhanced extra-capacity: Optimizing mesoporous carbon for high-rate and long-life potassium-storage. *Energy Storage Materials* **2020**.
208. Liu, Y.; Lu, Y. X.; Xu, Y. S.; Meng, Q. S.; Gao, J. C.; Sun, Y. G.; Hu, Y. S.; Chang, B. B.; Liu, C. T.; Cao, A. M., Pitch-Derived Soft Carbon as Stable Anode Material for Potassium Ion Batteries. *Adv. Mater.* **2020,** *32* (17), 2000505.
209. Xiao, N.; Zhang, X.; Liu, C.; Wang, Y.; Li, H.; Qiu, J., Coal-based carbon anodes for high-performance potassium-ion batteries. *Carbon* **2019,** *147*, 574-581.
210. Jian, Z.; Hwang, S.; Li, Z.; Hernandez, A. S.; Wang, X.; Xing, Z.; Su, D.; Ji, X., Hard-Soft Composite Carbon as a Long-Cycling and High-Rate Anode for Potassium-Ion Batteries. *Adv. Funct. Mater.* **2017,** *27* (26).
211. Gu, D.; Li, W.; Wang, F.; Bongard, H.; Spliethoff, B.; Schmidt, W.; Weidenthaler, C.; Xia, Y.; Zhao, D.; Schueth, F., Controllable Synthesis of Mesoporous Peapod-like Co3O4@Carbon Nanotube Arrays for High-Performance Lithium-Ion Batteries. *Angewandte Chemie-International Edition* **2015,** *54* (24), 7060-7064.
212. Miao, W.; Zhao, X.; Wang, R.; Liu, Y.; Li, L.; Zhang, Z.; Zhang, W., Carbon shell encapsulated cobalt phosphide nanoparticles embedded in carbon nanotubes supported on carbon nanofibers: A promising anode for potassium ion battery. *J. Colloid Interface Sci.* **2019,** *556*, 432-440.
213. Peng, S.; Wang, L.; Zhu, Z.; Han, K., Electrochemical performance of reduced graphene oxide/carbon nanotube hybrid papers as binder-free anodes for potassium-ion batteries. *J. Phys. Chem. Solids* **2020,** *138*.
214. Wu, R.; Wang, D. P.; Rui, X.; Liu, B.; Zhou, K.; Law, A. W. K.; Yan, Q.; Wei, J.; Chen, Z., In-Situ Formation of Hollow Hybrids Composed of Cobalt Sulfides Embedded within Porous Carbon Polyhedra/Carbon Nanotubes for High-Performance Lithium-Ion Batteries. *Adv. Mater.* **2015,** *27* (19), 3038-3044.
215. Wang, Y.; Wang, Z.; Chen, Y.; Zhang, H.; Yousaf, M.; Wu, H.; Zou, M.; Cao, A.;

Han, R. P. S., Hyperporous Sponge Interconnected by Hierarchical Carbon Nanotubes as a High-Performance Potassium-Ion Battery Anode. *Adv. Mater.* **2018,** *30* (32), e1802074.

216. Zhao, W.; Shen, Y.; Zhang, H.; Wang, Y.; Wu, Y.; Wu, H.; Zou, M.; Wang, Q.; Li, Y.; Cao, A., Porous-carbon aerogels with tailored subnanopores for high cycling stability and rate capability potassium ion battery anodes. *ACS Applied Materials & Interfaces* **2020**.

217. Xia, G.; Wang, C.; Jiang, P.; Lu, J.; Diao, J.; Chen, Q., Nitrogen/oxygen co-doped mesoporous carbon octahedrons for high-performance potassium-ion batteries. *Journal of Materials Chemistry A* **2019,** *7* (19), 12317-12324.

218. Ruan, J.; Zhao, Y.; Luo, S.; Yuan, T.; Yang, J.; Sun, D.; Zheng, S., Fast and stable potassium-ion storage achieved by in situ molecular self-assembling N/O dual-doped carbon network. *Energy Storage Materials* **2019,** *23*, 46-54.

219. He, H.; Huang, D.; Tang, Y.; Wang, Q.; Ji, X.; Wang, H.; Guo, Z., Tuning nitrogen species in three-dimensional porous carbon via phosphorus doping for ultra-fast potassium storage. *Nano Energy* **2019,** *57*, 728-736.

220. Xu, Y.; Zhang, C.; Zhou, M.; Fu, Q.; Zhao, C.; Wu, M.; Lei, Y., Highly nitrogen doped carbon nanofibers with superior rate capability and cyclability for potassium ion batteries. *Nat Commun* **2018,** *9* (1), 1720.

221. Zhang, W. L.; Cao, Z.; Wang, W. X.; Alhajji, E.; Emwas, A. H.; Costa, P.; Cavallo, L.; Alshareef, H. N., A Site-Selective Doping Strategy of Carbon Anodes with Remarkable K-Ion Storage Capacity. *Angewandte Chemie-International Edition* **2020,** *59* (11), 4448-4455.

222. Xu, F.; Zhai, Y.; Zhang, E.; Liu, Q.; Jiang, G.; Xu, X.; Qiu, Y.; Liu, X.; Wang, H.; Kaskel, S., Ultrastable surface-dominated pseudocapacitive potassium storage enabled by edge-enriched N-doped porous carbon nanosheets. *Angew. Chem. Int. Ed.* **2020**.

223. Zhang, Y.; Li, L.; Xiang, Y.; Zou, G.; Hou, H.; Deng, W.; Ji, X., High Sulfur-Doped Hard Carbon with Advanced Potassium Storage Capacity via a Molten Salt Method. *ACS Applied Materials & Interfaces* **2020**.

224. Tian, S.; Guan, D.; Lu, J.; Zhang, Y.; Liu, T.; Zhao, X.; Yang, C.; Nan, J., Synthesis of the electrochemically stable sulfur-doped bamboo charcoal as the anode material of potassium-ion batteries. *J. Power Sources* **2020,** *448*, 227572.

225. Alvin, S.; Chandra, C.; Kim, J., Extended plateau capacity of phosphorus-doped hard carbon used as an anode in Na-and K-ion batteries. *Chem. Eng. J.* **2019**, 123576.

226. Chen, M.; Wang, W.; Liang, X.; Gong, S.; Liu, J.; Wang, Q.; Guo, S.; Yang, H., Sulfur/Oxygen Codoped Porous Hard Carbon Microspheres for High-Performance Potassium-Ion Batteries. *Advanced Energy Materials* **2018,** *8* (19).

227. Jin, Y.; Xu, Y.; Lin, J.; He, S.; Zhang, B., Novel Mn-based Li-rich layered oxide 0.3 Li2MnO3· 0.7 LiNi1/3Co1/3Mn1/3O2 as anode material for lithium-ion batteries. *Mater. Lett.* **2018,** *210*, 223-226.

228. Geng, P.; Zheng, S.; Tang, H.; Zhu, R.; Zhang, L.; Cao, S.; Xue, H.; Pang, H., Transition Metal Sulfides Based on Graphene for Electrochemical Energy Storage. *Advanced Energy Materials* **2018,** *8* (15).

229. Hu, Z.; Tai, Z.; Liu, Q.; Wang, S.-W.; Jin, H.; Wang, S.; Lai, W.; Chen, M.; Li, L.; Chen, L.; Tao, Z.; Chou, S.-L., Ultrathin 2D TiS2 Nanosheets for High Capacity and Long-Life Sodium Ion Batteries. *Advanced Energy Materials* **2019,** *9* (8).

230. Yu, Q.; Hu, J.; Qian, C.; Gao, Y.; Wang, W.; Yin, G., CoS/N-doped carbon core/shell

nanocrystals as an anode material for potassium-ion storage. *J. Solid State Electrochem.* **2019,** *23* (1), 27-32.

231. Zhu, C.; Kopold, P.; Li, W.; van Aken, P. A.; Maier, J.; Yu, Y., A General Strategy to Fabricate Carbon-Coated 3D Porous Interconnected Metal Sulfides: Case Study of SnS/C Nanocomposite for High-Performance Lithium and Sodium Ion Batteries. *Advanced Science* **2015,** *2* (12).

232. Ali, Z.; Asif, M.; Huang, X.; Tang, T.; Hou, Y., Hierarchically Porous Fe2CoSe4 Binary-Metal Selenide for Extraordinary Rate Performance and Durable Anode of Sodium-Ion Batteries. *Adv. Mater.* **2018,** *30* (36).

233. Chu, J.; Yu, Q.; Yang, D.; Xing, L.; Lao, C.-Y.; Wang, M.; Han, K.; Liu, Z.; Zhang, L.; Du, W.; Xi, K.; Bao, Y.; Wang, W., Thickness-control of ultrathin bimetallic Fe-Mo selenide@N-doped carbon core/shell "nano-crisps" for high-performance potassium-ion batteries. *Applied Materials Today* **2018,** *13*, 344-351.

234. Hitz, E.; Wan, J.; Patel, A.; Xu, Y.; Meshi, L.; Dai, J.; Chen, Y.; Lu, A.; Davydoy, A. V.; Hu, L., Electrochemical Intercalation of Lithium Ions into NbSe2 Nanosheets. *Acs Applied Materials & Interfaces* **2016,** *8* (18), 11390-11395.

235. Wang, W.; Li, P.; Zheng, H.; Liu, Q.; Lv, F.; Wu, J.; Wang, H.; Guo, S., Ultrathin Layered SnSe Nanoplates for Low Voltage, High-Rate, and Long-Life Alkali-Ion Batteries. *Small* **2017,** *13* (46).

236. Yu, Q.; Jiang, B.; Hu, J.; Lao, C.-Y.; Gao, Y.; Li, P.; Liu, Z.; Suo, G.; He, D.; Wang, W.; Yin, G., Metallic Octahedral CoSe2 Threaded by N-Doped Carbon Nanotubes: A Flexible Framework for High-Performance Potassium-Ion Batteries. *Advanced Science* **2018,** *5* (10).

237. Chen, Y.; Li, C.; Wang, Y.; Zhang, Q.; Xu, C.; Wei, B.; An, L., Self-assembled carbon–silicon carbonitride nanocomposites: high-performance anode materials for lithium-ion batteries. *J. Mater. Chem.* **2011,** *21* (45), 18186-18190.

238. Du, F.; Tang, H.; Pan, L.; Zhang, T.; Lu, H.; Xiong, J.; Yang, J.; Zhang, C. J., Environmental friendly scalable production of colloidal 2D titanium carbonitride MXene with minimized nanosheets restacking for excellent cycle life lithium-ion batteries. *Electrochim. Acta* **2017,** *235*, 690-699.

239. Kishore, B.; G, V.; Munichandraiah, N., K2Ti4O9: A Promising Anode Material for Potassium Ion Batteries. *J. Electrochem. Soc.* **2016,** *163* (13), A2551-A2554.

240. Han, J.; Xu, M.; Niu, Y.; Li, G. N.; Wang, M.; Zhang, Y.; Jia, M.; Li, C. M., Exploration of K2Ti8O17 as an anode material for potassium-ion batteries. *Chem Commun (Camb)* **2016,** *52* (75), 11274-11276.

241. Zhao, S.; Dong, L.; Sun, B.; Yan, K.; Zhang, J.; Wan, S.; He, F.; Munroe, P.; Notten, P. H.; Wang, G., K2Ti2O5@ C Microspheres with Enhanced K+ Intercalation Pseudocapacitance Ensuring Fast Potassium Storage and Long-Term Cycling Stability. *Small* **2020,** *16* (4), 1906131.

242. Liao, J.; Hu, Q.; Mu, J.; He, X.; Wang, S.; Jiemin, D.; Chen, C., In situ carbon coated flower-like VPO 4 as an anode material for potassium-ion batteries. *Chem. Commun.* **2019,** *55* (92), 13916-13919.

243. Chen, F.; Wang, S.; dong He, X.; Liao, J.; Hu, Q.; Chen, C., Hollow sphere structured V2O3@ C as an anode material for high capacity potassium-ion batteries. *Journal of Materials Chemistry A* **2020**.

244. Tao, M.; Du, G.; Zhang, Y.; Gao, W.; Liu, D.; Luo, Y.; Jiang, J.; Bao, S.; Xu, M., TiOxNy nanoparticles/C composites derived from MXene as anode material for potassium-ion batteries. *Chem. Eng. J.* **2019,** *369*, 828-833.

245. Han, J.; Niu, Y.; Bao, S. J.; Yu, Y. N.; Lu, S. Y.; Xu, M., Nanocubic KTi2(PO4)3 electrodes for potassium-ion batteries. *Chem Commun (Camb)* **2016,** *52* (78), 11661-11664.

246. Zhang, R.; Huang, J.; Deng, W.; Bao, J.; Pan, Y.; Huang, S.; Sun, C. F., Safe, Low-Cost, Fast-Kinetics and Low-Strain Inorganic-Open-Framework Anode for Potassium-Ion Batteries. *Angew. Chem. Int. Ed.* **2019,** *58* (46), 16474-16479.

247. Ren, X.; Zhao, Q.; McCulloch, W. D.; Wu, Y., MoS2 as a long-life host material for potassium ion intercalation. *Nano Research* **2017,** *10* (4), 1313-1321.

248. Zheng, N.; Jiang, G.; Chen, X.; Mao, J.; Zhou, Y.; Li, Y., Rational design of a tubular, interlayer expanded MoS 2–N/O doped carbon composite for excellent potassium-ion storage. *Journal of Materials Chemistry A* **2019,** *7* (15), 9305-9315.

249. Chong, S.; Sun, L.; Shu, C.; Guo, S.; Liu, Y.; Wang, W. A.; Liu, H. K., Chemical bonding boosts nano-rose-like MoS2 anchored on reduced graphene oxide for superior potassium-ion storage. *Nano Energy* **2019,** *63*, 103868.

250. Cui, Y.; Liu, W.; Feng, W.; Zhang, Y.; Du, Y.; Liu, S.; Wang, H.; Chen, M.; Zhou, J., Controlled Design of Well-Dispersed Ultrathin MoS2 Nanosheets inside Hollow Carbon Skeleton: Toward Fast Potassium Storage by Constructing Spacious “Houses” for K Ions. *Adv. Funct. Mater.* **2020,** *30* (10), 1908755.

251. Yao, K.; Xu, Z.; Ma, M.; Li, J.; Lu, F.; Huang, J., Densified Metallic MoS2/Graphene Enabling Fast Potassium-Ion Storage with Superior Gravimetric and Volumetric Capacities. *Adv. Funct. Mater.* **2020**, 2001484.

252. Wu, Y.; Xu, Y.; Li, Y.; Lyu, P.; Wen, J.; Zhang, C.; Zhou, M.; Fang, Y.; Zhao, H.; Kaiser, U., Unexpected intercalation-dominated potassium storage in WS 2 as a potassium-ion battery anode. *Nano Research* **2019,** *12* (12), 2997-3002.

253. Chu, J.; Wang, W. A.; Feng, J.; Lao, C.-Y.; Xi, K.; Xing, L.; Han, K.; Li, Q.; Song, L.; Li, P., Deeply nesting zinc sulfide dendrites in tertiary hierarchical structure for potassium ion batteries: enhanced conductivity from interior to exterior. *ACS nano* **2019,** *13* (6), 6906-6916.

254. Liu, T.; Zhang, X.; Xia, M.; Yu, H.; Peng, N.; Jiang, C.; Shui, M.; Xie, Y.; Yi, T.-F.; Shu, J., Functional cation defects engineering in TiS2 for high-stability anode. *Nano Energy* **2020,** *67*, 104295.

255. Minglei Mao, C. C., Mingguang Wu, Ming Zhang, Tao Gao, Xiulin Fan, Ji Chen, Taihong Wang, Jianmin Ma, Chunsheng Wang, Flexible ReS2 nanosheets:N-doped carbon nanofibers-based paper as a universal anode for alkali (Li, Na, K) ion battery. *Nano Energy* **2018,** *45*, 346-352.

256. Yu, Q.; Hu, J.; Qian, C.; Gao, Y.; Wang, W. A.; Yin, G., CoS/N-doped carbon core/shell nanocrystals as an anode material for potassium-ion storage. *J. Solid State Electrochem.* **2019,** *23* (1), 27-32.

257. Ma, G.; Xu, X.; Feng, Z.; Hu, C.; Zhu, Y.; Yang, X.; Yang, J.; Qian, Y., Carbon-coated mesoporous Co 9 S 8 nanoparticles on reduced graphene oxide as a long-life and high-rate anode material for potassium-ion batteries. *Nano Research* **2020**, 1-8.

258. Zhao, Z.; Hu, Z.; Jiao, R.; Tang, Z.; Dong, P.; Li, Y.; Li, S.; Li, H., Tailoring multi-layer architectured FeS2@ C hybrids for superior sodium-, potassium-and aluminum-ion storage. *Energy Storage Materials* **2019,** *22*, 228-234.

259. Mao, Y.; Xie, M.; Zhao, W.; Yuan, K.; Fang, Y.; Huang, F., K 0.36 (H 2 O) y WS 2: a new layered compound for reversible hydrated potassium ion intercalation in aqueous electrolyte. *RSC Advances* **2019,** *9* (55), 32323-32327.
260. Zhao, Z.; Hu, Z.; Liang, H.; Li, S.; Wang, H.; Gao, F.; Sang, X.; Li, H., Nanosized MoSe2@ Carbon Matrix: A Stable Host Material for the Highly Reversible Storage of Potassium and Aluminum Ions. *ACS Applied Materials & Interfaces* **2019,** *11* (47), 44333-44341.
261. Shen, Q.; Jiang, P.; He, H.; Chen, C.; Liu, Y.; Zhang, M., Encapsulation of MoSe 2 in carbon fibers as anodes for potassium ion batteries and nonaqueous battery–supercapacitor hybrid devices. *Nanoscale* **2019,** *11* (28), 13511-13520.
262. Etogo, C. A.; Huang, H.; Hong, H.; Liu, G.; Zhang, L., Metal–organic-frameworks-engaged formation of Co0. 85Se@ C nanoboxes embedded in carbon nanofibers film for enhanced potassium-ion storage. *Energy Storage Materials* **2020,** *24*, 167-176.
263. Liu, Z.; Han, K.; Li, P.; Wang, W.; He, D.; Tan, Q.; Wang, L.; Li, Y.; Qin, M.; Qu, X., Tuning Metallic Co 0.85 Se Quantum Dots/Carbon Hollow Polyhedrons with Tertiary Hierarchical Structure for High-Performance Potassium Ion Batteries. *Nano-Micro Letters* **2019,** *11* (1), 96.
264. Lin, H.; Li, M.; Yang, X.; Yu, D.; Zeng, Y.; Wang, C.; Chen, G.; Du, F., Nanosheets-Assembled CuSe Crystal Pillar as a Stable and High-Power Anode for Sodium-Ion and Potassium-Ion Batteries. *Advanced Energy Materials* **2019,** *9* (20), 1900323.
265. Yu, H.; Cheng, X.; Xia, M.; Liu, T.; Ye, W.; Zheng, R.; Long, N.; Shui, M.; Shu, J., Pretreated commercial TiSe2 as an insertion-type potassium container for constructing “Rocking-Chair” type potassium ion batteries. *Energy Storage Materials* **2019,** *22*, 154-159.
266. Liu, Y.; Yang, C.; Li, Y.; Zheng, F.; Li, Y.; Deng, Q.; Zhong, W.; Wang, G.; Liu, T., FeSe2/nitrogen-doped carbon as anode material for Potassium-ion batteries. *Chem. Eng. J.* **2020,** *393*, 124590.
267. Wang, T.; Guo, W.; Wang, G.; Wang, H.; Bai, J.; Wang, B., Highly dispersed FeSe2 nanoparticles in porous carbon nanofibers as advanced anodes for sodium and potassium ion batteries. *J. Alloys Compd.* **2020**, 155265.
268. Xu, B.; Ma, X.; Tian, J.; Zhao, F.; Liu, Y.; Wang, B.; Yang, H.; Xia, Y., Layer-structured NbSe 2 anode material for sodium-ion and potassium-ion batteries. *Ionics* **2019,** *25* (9), 4171-4177.
269. Chu, J.; Yu, Q.; Han, K.; Xing, L.; Bao, Y.; Wang, W. A., A novel graphene-wrapped corals-like NiSe2 for ultrahigh-capacity potassium ion storage. *Carbon* **2020,** *161*, 834-841.
270. Tian, H.; Yu, X.; Shao, H.; Dong, L.; Chen, Y.; Fang, X.; Wang, C.; Han, W.; Wang, G., Unlocking Few-Layered Ternary Chalcogenides for High-Performance Potassium-Ion Storage. *Advanced Energy Materials* **2019,** *9* (29), 1901560.
271. Tian, Z.; Chui, N.; Lian, R.; Yang, Q.; Wang, W.; Yang, C.; Rao, D.; Huang, J.; Zhang, Y.; Lai, F., Dual anionic vacancies on carbon nanofiber threaded MoSSe arrays: A free-standing anode for high-performance potassium-ion storage. *Energy Storage Materials* **2020,** *27*, 591-598.
272. Chen, C.; Xie, X.; Anasori, B.; Sarycheva, A.; Makaryan, T.; Zhao, M.; Urbankowski, P.; Miao, L.; Jiang, J.; Gogotsi, Y., MoS2-on-MXene Heterostructures as Highly Reversible Anode Materials for Lithium-Ion Batteries. *Angewandte Chemie-International Edition* **2018,** *57* (7), 1846-1850.
273. Xie, Y.; Dall'Agnese, Y.; Naguib, M.; Gogotsi, Y.; Barsoum, M. W.; Zhuang, H. L.; Kent, P. R. C., Prediction and Characterization of MXene Nanosheet Anodes for Non-Lithium-Ion Batteries.

Acs Nano **2014,** *8* (9), 9606-9615.
274. Xiong, D.; Li, X.; Bai, Z.; Lu, S., Recent Advances in Layered Ti3C2Tx MXene for Electrochemical Energy Storage. *Small* **2018,** *14* (17).
275. Yu, P.; Cao, G.; Yi, S.; Zhang, X.; Li, C.; Sun, X.; Wang, K.; Ma, Y., Binder-free 2D titanium carbide (MXene)/carbon nanotube composites for high-performance lithium-ion capacitors. *Nanoscale* **2018,** *10* (13), 5906-5913.
276. Zhao, M.-Q.; Xie, X.; Ren, C. E.; Makaryan, T.; Anasori, B.; Wang, G.; Gogotsi, Y., Hollow MXene Spheres and 3D Macroporous MXene Frameworks for Na-Ion Storage. *Adv. Mater.* **2017,** *29* (37).
277. Naguib, M.; Adams, R. A.; Zhao, Y.; Zemlyanov, D.; Varma, A.; Nanda, J.; Pol, V. G., Electrochemical performance of MXenes as K-ion battery anodes. *Chem. Commun.* **2017,** *53* (51), 6883-6886.
278. Ming, F.; Liang, H.; Zhang, W.; Ming, J.; Lei, Y.; Emwas, A.-H.; Alshareef, H. N., Porous MXenes enable high performance potassium ion capacitors. *Nano Energy* **2019,** *62*, 853-860.
279. Sun, N.; Zhu, Q.; Anasori, B.; Zhang, P.; Liu, H.; Gogotsi, Y.; Xu, B., MXene-Bonded Flexible Hard Carbon Film as Anode for Stable Na/K-Ion Storage. *Adv. Funct. Mater.* **2019,** *29* (51), 1906282.
280. Zhao, R.; Di, H.; Hui, X.; Zhao, D.; Wang, R.; Wang, C.; Yin, L., Self-assembled Ti 3 C 2 MXene and N-rich porous carbon hybrids as superior anodes for high-performance potassium-ion batteries. *Energy & Environmental Science* **2020,** *13* (1), 246-257.
281. Wu, X.; Wang, H.; Zhao, Z.; Huang, B., Interstratification-assembled 2D black phosphorene and V 2 CT x MXene as superior anodes for boosting potassium-ion storage. *Journal of Materials Chemistry A* **2020,** *8* (25), 12705-12715.
282. Li, J.; Rui, B.; Wei, W.; Nie, P.; Chang, L.; Le, Z.; Liu, M.; Wang, H.; Wang, L.; Zhang, X., Nanosheets assembled layered MoS2/MXene as high performance anode materials for potassium ion batteries. *J. Power Sources* **2020,** *449*, 227481.
283. Huang, H.; Cui, J.; Liu, G.; Bi, R.; Zhang, L., Carbon-coated MoSe2/MXene hybrid nanosheets for superior potassium storage. *ACS nano* **2019,** *13* (3), 3448-3456.
284.Han, K.; Liu, Z.; Li, P.; Yu, Q.; Wang, W. A.; Lao, C.-Y.; He, D.; Zhao, W.; Suo, G.; Guo, H., High-throughput fabrication of 3D N-doped graphenic framework coupled with Fe3C@ porous graphite carbon for ultrastable potassium ion storage. *Energy Storage Materials* **2019,** *22*, 185-193.
285. Xia, Z.; Chen, X.; Ci, H.; Fan, Z.; Yi, Y.; Yin, W.; Wei, N.; Cai, J.; Zhang, Y.; Sun, J., Designing N-doped graphene/ReSe2/Ti3C2 MXene heterostructure frameworks as promising anodes for high-rate potassium-ion batteries. *Journal of Energy Chemistry* **2020**.
286. Lee, J.; Kim, S.; Park, J.-H.; Jo, C.; Chun, J.; Sung, Y.-E.; Lim, E.; Lee, J., A small-strain niobium nitride anode with ordered mesopores for ultra-stable potassium-ion batteries. *Journal of Materials Chemistry A* **2020,** *8* (6), 3119-3127.
287. Lei, K.; Li, F.; Mu, C.; Wang, J.; Zhao, Q.; Chen, C.; Chen, J., High K-storage performance based on the synergy of dipotassium terephthalate and ether-based electrolytes. *Energy & environmental science* **2017,** *10* (2), 552-557.
288. Deng, Q.; Pei, J.; Fan, C.; Ma, J.; Cao, B.; Li, C.; Jin, Y.; Wang, L.; Li, J., Potassium salts of para-aromatic dicarboxylates as the highly efficient organic anodes for low-cost K-ion batteries. *Nano Energy* **2017,** *33*, 350-355.

289. Bai, Y.; Fu, W.; Chen, W.; Chen, Z.; Pan, X.; Lv, X.; Wu, J.; Pan, X., Perylenetetracarboxylic diimide as a high-rate anode for potassium-ion batteries. *Journal of Materials Chemistry A* **2019,** *7* (42), 24454-24461.
290. Chen, X.; Zhang, H.; Ci, C.; Sun, W.; Wang, Y., Few-layered boronic ester based covalent organic frameworks/carbon nanotube composites for high-performance K-organic batteries. *ACS nano* **2019,** *13* (3), 3600-3607.
291. Zhang, C.; Qiao, Y.; Xiong, P.; Ma, W.; Bai, P.; Wang, X.; Li, Q.; Zhao, J.; Xu, Y.; Chen, Y., Conjugated microporous polymers with tunable electronic structure for high-performance potassium-ion batteries. *ACS nano* **2019,** *13* (1), 745-754.
292. Cao, K.; Liu, H.; Li, W.; Han, Q.; Zhang, Z.; Huang, K.; Jing, Q.; Jiao, L., CuO Nanoplates for High-Performance Potassium-Ion Batteries. *Small* **2019,** *15* (36).
293. Lee, G.-W.; Park, B. H.; Nazarian-Samani, M.; Kim, Y. H.; Roh, K. C.; Kim, K.-B., Magneli Phase Titanium Oxide as a Novel Anode Material for Potassium-Ion Batteries. *Acs Omega* **2019,** *4* (3), 5304-5309.
294. Shi, X.; Qin, L.; Xu, G.; Guo, S.; Ma, S.; Zhao, Y.; Zhou, J.; Liang, S., beta-FeOOH: a new anode for potassium-ion batteries. *Chem. Commun.* **2020,** *56* (26), 3713-3716.
295. Nithya, C.; Lee, J. H.; Kim, N. H., Hydrothermal fabrication of MnCO3@rGO: A promising anode material for potassium-ion batteries. *Appl. Surf. Sci.* **2019,** *484*, 1161-1167.
296. Sultana, I.; Rahman, M. M.; Mateti, S.; Ahmadabadi, V. G.; Glushenkov, A. M.; Chen, Y., K-ion and Na-ion storage performances of Co3O4-Fe2O3 nanoparticle-decorated super P carbon black prepared by a ball milling process. *Nanoscale* **2017,** *9* (10), 3646-3654.
297. Qin, G.; Liu, Y.; Han, P.; Liu, F.; Yang, Q.; Wang, C., Dispersed MoS2 nanosheets in core shell Co3O4@C nanocubes for superior potassium ion storage. *Appl. Surf. Sci.* **2020,** *514*.
298. Xie, K.; Yuan, K.; Li, X.; Lu, W.; Shen, C.; Liang, C.; Vajtai, R.; Ajayan, P.; Wei, B., Superior Potassium Ion Storage via Vertical MoS2 "Nano-Rose" with Expanded Interlayers on Graphene. *Small* **2017,** *13* (42).
299. Lakshmi, V.; Chen, Y.; Mikhaylov, A. A.; Medvedev, A. G.; Sultana, I.; Rahman, M. M.; Lev, O.; Prikhodchenko, P. V.; Glushenkov, A. M., Nanocrystalline SnS2 coated onto reduced graphene oxide: demonstrating the feasibility of a non-graphitic anode with sulfide chemistry for potassium-ion batteries. *Chem Commun (Camb)* **2017,** *53* (59), 8272-8275.
300. Yanying, L.; Jun, C., Robust self-supported anode by integrating Sb2S3 nanoparticles with S,N-codoped graphene to enhance K-storage performance. *Science China-Chemistry* **2017,** *60* (12), 1533-1539.
301. Liu, Y.; Tai, Z.; Zhang, J.; Pang, W. K.; Zhang, Q.; Feng, H.; Konstantinov, K.; Guo, Z.; Liu, H. K., Boosting potassium-ion batteries by few-layered composite anodes prepared via solution-triggered one-step shear exfoliation. *Nature Communications* **2018,** *9*.
302. Zhao, Y.; Zhu, J.; Ong, S. J. H.; Yao, Q.; Shi, X.; Hou, K.; Xu, Z. J.; Guan, L., High-Rate and Ultralong Cycle-Life Potassium Ion Batteries Enabled by In Situ Engineering of Yolk-Shell FeS2
@C Structure on Graphene Matrix. *Advanced Energy Materials* **2018,** *8* (36).
303. Yang, F.; Goo, H.; Hao, J.; Zhang, S.; Li, P.; Liu, Y.; Chen, J.; Guo, Z., Yolk-Shell Structured FeP@C Nanoboxes as Advanced Anode Materials for Rechargeable Lithium-/Potassium-Ion Batteries. *Adv. Funct. Mater.* **2019,** *29* (16).
304. Tan, Q.; Zhao, W.; Han, K.; Li, P.; Wang, W.; He, D.; Liu, Z.; Yu, Q.; Qin, M.; Qu,

X., The multi-yolk/shell structure of FeP@foam-like graphenic scaffolds: strong P–C bonds and electrolyte- and binder-optimization boost potassium storage. *Journal of Materials Chemistry A* **2019,** *7* (26), 15673-15682.

305. Zhao, X.; Gong, F.; Zhao, Y.; Huang, B.; Qian, D.; Wang, H.-E.; Zhang, W.; Yang, Z., Encapsulating NiS nanocrystal into nitrogen-doped carbon framework for high performance sodium/potassium-ion storage. *Chem. Eng. J.* **2020,** *392*.

306. Shen, Y.; Liu, J.; Li, X.; Wang, Q., Two-Dimensional T-NiSe2 as a Promising Anode Material for Potassium-Ion Batteries with Low Average Voltage, High Ionic Conductivity, and Superior Carrier Mobility. *Acs Applied Materials & Interfaces* **2019,** *11* (39), 35661-35666.

307. Chen, Q.; Ren, M.; Xu, H.; Liu, W.; Hei, J.; Su, L.; Wang, L., Cu2S@ N, S Dual-Doped Carbon Matrix Hybrid as Superior Anode Materials for Lithium/Sodium ion Batteries. *Chemelectrochem* **2018,** *5* (15), 2135-2141.

308. Li, J.; Yan, D.; Lu, T.; Qin, W.; Yao, Y.; Pan, L., Significantly Improved Sodium-Ion Storage Performance of CuS Nanosheets Anchored into Reduced Graphene Oxide with Ether-Based Electrolyte. *Acs Applied Materials & Interfaces* **2017,** *9* (3), 2309-2316.

309. Ren, Y.; Wei, H.; Yang, B.; Wang, J.; Ding, J., "Double-Sandwich-Like" CuS@reduced graphene oxide as an Anode in Lithium Ion Batteries with Enhanced Electrochemical Performance. *Electrochim. Acta* **2014,** *145*, 193-200.

310. Wang, Y.; Feng, X.; Xiong, Y.; Stoupin, S.; Huang, R.; Zhao, M.; Xu, M.; Zhang, P.; Zhao, J.; Abruna, H. D., An Innovative Lithium Ion Battery System Based on a Cu2S Anode Material. *Acs Applied Materials & Interfaces* **2020,** *12* (15), 17396-17405.

311. Peng, Q.; Zhang, S.; Yang, H.; Sheng, B.; Xu, R.; Wang, Q.; Yu, Y., Boosting Potassium Storage Performance of the Cu2S Anode via Morphology Engineering and Electrolyte Chemistry. *ACS nano* **2020**.

312. Cao, L.; Zhang, B.; Ou, X.; Wang, C.; Peng, C.; Zhang, J., Synergistical Coupling Interconnected ZnS/SnS2 Nanoboxes with Polypyrrole-Derived N/S Dual-Doped Carbon for Boosting High-Performance Sodium Storage. *Small* **2019,** *15* (9).

313. Su, D.; Kretschmer, K.; Wang, G., Improved Electrochemical Performance of Na-Ion Batteries in Ether-Based Electrolytes: A Case Study of ZnS Nanospheres. *Advanced Energy Materials* **2016,** *6* (2).

314. Lu, S.; Zhu, T.; Wu, H.; Wang, Y.; Li, J.; Abdelkaderkh, A.; Xi, K.; Wang, W.; Li, Y.; Ding, S.; Gao, G.; Kumarh, R. V., Construction of ultrafine ZnSe nanoparticles on/in amorphous carbon hollow nanospheres with high-power-density sodium storage. *Nano Energy* **2019,** *59*, 762-772.

315. Zeng, L.; Fang, Y.; Xu, L.; Zheng, C.; Yang, M.-Q.; He, J.; Xue, H.; Qian, Q.; Wei, M.; Chen, Q., Rational design of few-layer MoSe2 confined within ZnSe-C hollow porous spheres for high-performance lithium-ion and sodium-ion batteries. *Nanoscale* **2019,** *11* (14), 6766-6775.

316. Chu, J.; Wang, W.; Yu, Q.; Lao, C.-Y.; Zhang, L.; Xi, K.; Han, K.; Xing, L.; Song, L.; Wang, M.; Bao, Y., Open ZnSe/C nanocages: multi-hierarchy stress-buffer for boosting cycling stability in potassium-ion batteries. *Journal of Materials Chemistry A* **2020,** *8* (2), 779-788.

317. Tan, Q.; Li, P.; Han, K.; Liu, Z.; Li, Y.; Zhao, W.; He, D.; An, F.; Qin, M.; Qu, X., Chemically bubbled hollow FexO nanospheres anchored on 3D N-doped few-layer graphene architecture as a performance-enhanced anode material for potassium-ion batteries. *Journal of Materials Chemistry A* **2019,** *7* (2), 744-754.

318. Niu, X.; Zhang, Y.; Tan, L.; Yang, Z.; Yang, J.; Liu, T.; Zeng, L.; Zhu, Y.; Guo, L.,

Amorphous FeVO4 as a promising anode material for potassium-ion batteries. *Energy Storage Materials* **2019,** *22*, 160-167.

319. Liu, Y.; He, D.; Tan, Q.; Wan, Q.; Han, K.; Liu, Z.; Li, P.; An, F.; Qu, X., A synergetic strategy for an advanced electrode with Fe3O4 embedded in a 3D N-doped porous graphene framework and a strong adhesive binder for lithium/potassium ion batteries with an ultralong cycle lifespan. *Journal of Materials Chemistry A* **2019,** *7* (33), 19430-19441.

320. Deng, J.; Huang, X.; Gao, W.; Liu, H.; Xu, M.-W., 3D carbon framework-supported FeSe for high performance potassium ion batteries. *Sustainable Energy & Fuels* **2020**.

321. Jiang, H.; Huang, L.; Wei, Y.; Wang, B.; Wu, H.; Zhang, Y.; Liu, H.; Dou, S., Bio-Derived Hierarchical Multicore-Shell Fe2N-Nanoparticle-Impregnated N-Doped Carbon Nanofiber Bundles: A Host Material for Lithium-/Potassium-Ion Storage. *Nano-Micro Letters* **2019,** *11* (1).

322. Zhang, C.; Han, F.; Wang, F.; Liu, Q.; Zhou, D.; Zhang, F.; Xu, S.; Fan, C.; Li, X.; Liu, J., Improving compactness and reaction kinetics of MoS2@C anodes by introducing Fe9S10 core for superior volumetric sodium/potassium storage. *Energy Storage Materials* **2020,** *24*, 208-219.

323. Gao, H.; Zhou, T.; Zheng, Y.; Zhang, Q.; Liu, Y.; Chen, J.; Liu, H.; Guo, Z., CoS Quantum Dot Nanoclusters for High-Energy Potassium-Ion Batteries. *Adv. Funct. Mater.* **2017,** *27* (43).

324. Zhang, W.; Chen, J.; Liu, Y.; Liu, S.; Li, X.; Yang, K.; Li, L., Decoration of hollow nitrogen-doped carbon nanofibers with tapered rod-shaped NiCo2S4 as a 3D structural high-rate and long-lifespan self-supported anode material for potassium-ion batteries. *J. Alloys Compd.* **2020,** *823*.

325. Deng, Q.; Feng, S.; Hui, P.; Chen, H.; Tian, C.; Yang, R.; Xu, Y., Exploration of low-cost microporous Fe (III)-based organic framework as anode material for potassium-ion batteries. *J. Alloys Compd.* **2020**, 154714.

326. Li, C.; Wang, K.; Li, J.; Zhang, Q., Nanostructured potassium–organic framework as an effective anode for potassium-ion batteries with a long cycle life. *Nanoscale* **2020,** *12* (14), 7870-7874.

327. Wang, C.; Tang, W.; Yao, Z.; Cao, B.; Fan, C., Potassium perylene-tetracarboxylate with two-electron redox behaviors as a highly stable organic anode for K-ion batteries. *Chem. Commun.* **2019,** *55* (12), 1801-1804.

328. Liang, Y.; Luo, C.; Wang, F.; Hou, S.; Liou, S. C.; Qing, T.; Li, Q.; Zheng, J.; Cui, C.; Wang, C., An Organic Anode for High Temperature Potassium-Ion Batteries. *Advanced Energy Materials* **2019,** *9* (2), 1802986.

329. Lao, M.; Zhang, Y.; Luo, W.; Yan, Q.; Sun, W.; Dou, S. X., Alloy-Based Anode Materials toward Advanced Sodium-Ion Batteries. *Adv. Mater.* **2017,** *29* (48).

330. Li, Z.; Ding, J.; Mitlin, D., Tin and Tin Compounds for Sodium Ion Battery Anodes: Phase Transformations and Performance. *Acc. Chem. Res.* **2015,** *48* (6), 1657-1665.

331. Tan, H.; Chen, D.; Rui, X.; Yu, Y., Peering into Alloy Anodes for Sodium-Ion Batteries: Current Trends, Challenges, and Opportunities. *Adv. Funct. Mater.* **2019,** *29* (14).

332. Ying, H.; Han, W.-Q., Metallic Sn-Based Anode Materials: Application in High-Performance Lithium-Ion and Sodium-Ion Batteries. *Advanced Science* **2017,** *4* (11).

333. Min, X.; Sun, B.; Chen, S.; Fang, M.; Wu, X.; Liu, Y. g.; Abdelkader, A.; Huang, Z.; Liu, T.; Xi, K.; Kumar, R. V., A textile-based SnO2 ultra-flexible electrode for lithium-ion batteries. *Energy Storage Materials* **2019,** *16*, 597-606.

334. Ji, B.; Zhang, F.; Song, X.; Tang, Y., A Novel Potassium-Ion-Based Dual-Ion Battery. *Adv. Mater.* **2017,** *29* (19).

335. Sultana, I.; Ramireddy, T.; Rahman, M. M.; Chen, Y.; Glushenkov, A. M., Tin-based composite anodes for potassium-ion batteries. *Chem Commun (Camb)* **2016,** *52* (59), 9279-82.
336. Huang, K.; Xing, Z.; Wang, L.; Wu, X.; Zhao, W.; Qi, X.; Wang, H.; Ju, Z., Direct synthesis of 3D hierarchically porous carbon/Sn composites via in situ generated NaCl crystals as templates for potassium-ion batteries anode. *Journal of Materials Chemistry A* **2018,** *6* (2), 434-442.
337. Wang, H.; Xing, Z.; Hu, Z.; Zhang, Y.; Hu, Y.; Sun, Y.; Ju, Z.; Zhuang, Q., Sn-based submicron-particles encapsulated in porous reduced graphene oxide network: Advanced anodes for high-rate and long life potassium-ion batteries. *Applied Materials Today* **2019,** *15*, 58-66.
338. Li, D.; Sun, Q.; Zhang, Y.; Chen, L.; Wang, Z.; Liang, Z.; Si, P.; Ci, L., Surface-Confined SnS2@C@rGO as High-Performance Anode Materials for Sodium- and Potassium-Ion Batteries. *Chemsuschem* **2019,** *12* (12), 2689-2700.
339. Wang, Z.; Dong, K.; Wang, D.; Luo, S.; Liu, Y.; Wang, Q.; Zhang, Y.; Hao, A.; Shi, C.; Zhao, N., Ultrafine SnO2 nanoparticles encapsulated in 3D porous carbon as a, high-performance anode material for potassium-ion batteries. *J. Power Sources* **2019,** *441*.
340. Luo, S.; Wang, T.; Lu, H.; Xu, X.; Xue, G.; Xu, N.; Wang, Y.; Zhou, D., Ultrasmall SnO(2)nanocrystals embedded in porous carbon as potassium ion battery anodes with long-term cycling performance. *New J. Chem.* **2020,** *44* (27), 11678-11683.
341. Fang, L.; Xu, J.; Sun, S.; Lin, B.; Guo, Q.; Luo, D.; Xia, H., Few-Layered Tin Sulfide Nanosheets Supported on Reduced Graphene Oxide as a High-Performance Anode for Potassium-Ion Batteries. *Small* **2019,** *15* (10).
342. Li, D.; Sun, Q.; Zhang, Y.; Chen, L.; Wang, Z.; Liang, Z.; Si, P.; Ci, L., Surface-Confined SnS2 @C@rGO as High-Performance Anode Materials for Sodium- and Potassium-Ion Batteries. *ChemSusChem* **2019,** *12* (12), 2689-2700.
343. Zheng, J.; Yang, Y.; Fan, X.; Ji, G.; Ji, X.; Wang, H.; Hou, S.; Zachariah, M. R.; Wang, C., Extremely stable antimony-carbon composite anodes for potassium-ion batteries. *Energy & Environmental Science* **2019,** *12* (2), 615-623.
344. Liu, Q.; Fan, L.; Chen, S.; Su, S.; Ma, R.; Han, X.; Lu, B., Antimony-Graphite Composites for a High-Performance Potassium-Ion Battery. *Energy Technology* **2019,** *7* (10).
345. Han, Y.; Li, T.; Li, Y.; Tian, J.; Yi, Z.; Lin, N.; Qian, Y., Stabilizing antimony nanocrystals within ultrathin carbon nanosheets for high-performance K-ion storage. *Energy Storage Materials* **2019,** *20*, 46-54.
346. He, X.-D.; Liu, Z.-H.; Liao, J.-Y.; Ding, X.; Hu, Q.; Xiao, L.-N.; Wang, S.; Chen, C.-H., A three-dimensional macroporous antimony@carbon composite as a high-performance anode material for potassium-ion batteries. *Journal of Materials Chemistry A* **2019,** *7* (16), 9629-9637.
347. Luo, W.; Li, F.; Zhang, W.; Han, K.; Gaumet, J.-J.; Schaefer, H.-E.; Mai, L., Encapsulating segment-like antimony nanorod in hollow carbon tube as long-lifespan, high-rate anodes for rechargeable K-ion batteries. *Nano Research* **2019,** *12* (5), 1025-1031.
348. Tian, Y.; An, Y.; Xiong, S.; Feng, J.; Qian, Y., A general method for constructing robust, flexible and freestanding MXene@metal anodes for high-performance potassium-ion batteries. *Journal of Materials Chemistry A* **2019,** *7* (16), 9716-9725.
349. Cao, L.; Zhang, B.; Xia, H.; Wang, C.; Luo, B.; Fan, X.; Zhang, J.; Ou, X., Hierarchical chrysanthemum-like MoS2/Sb heterostructure encapsulated into N-doped graphene framework for superior potassium-ion storage. *Chem. Eng. J.* **2020,** *387*.
350. Zhang, Y.; Li, M.; Huang, F.; Li, Y.; Xu, Y.; Wang, F.; Yao, Q.; Zhou, H.; Deng, J.,

3D porous Sb-Co nanocomposites as advanced anodes for sodium-ion batteries and potassium-ion batteries. *Appl. Surf. Sci.* **2020,** *499*.

351. Xiong, P.; Wu, J.; Zhou, M.; Xu, Y., Bismuth-Antimony Alloy Nanoparticle@Porous Carbon Nanosheet Composite Anode for High-Performance Potassium-Ion Batteries. *Acs Nano* **2020,** *14* (1), 1018-1026.

352. Yi, Z.; Qian, Y.; Jiang, S.; Li, Y.; Lin, N.; Qian, Y., Self-wrinkled graphene as a mechanical buffer: A rational design to boost the K-ion storage performance of Sb2Se3 nanoparticles. *Chem. Eng. J.* **2020,** *379*.

353. Wang, J.; Wang, B.; Liu, Z.; Fan, L.; Zhang, Q.; Ding, H.; Wang, L.; Yang, H.; Yu, X.; Lu, B., Nature of Bimetallic Oxide Sb2MoO6/rGO Anode for High-Performance Potassium-Ion Batteries. *Advanced Science* **2019,** *6* (17).

354. Zhang, Q.; Mao, J.; Pang, W. K.; Zheng, T.; Sencadas, V.; Chen, Y.; Liu, Y.; Guo, Z., Boosting the Potassium Storage Performance of Alloy-Based Anode Materials via Electrolyte Salt Chemistry. *Advanced Energy Materials* **2018,** *8* (15).

355. Shen, C.; Cheng, T.; Liu, C.; Huang, L.; Cao, M.; Song, G.; Wang, D.; Lu, B.; Wang, J.; Qin, C.; Huang, X.; Peng, P.; Li, X.; Wu, Y., Bismuthene from sonoelectrochemistry as a superior anode for potassium-ion batteries. *Journal of Materials Chemistry A* **2020,** *8* (1), 453-460.

356. Zhao, Y.; Ren, X.; Xing, Z.; Zhu, D.; Tian, W.; Guan, C.; Yang, Y.; Qin, W.; Wang, J.; Zhang, L.; Huang, Y.; Wen, W.; Li, X.; Tai, R., In Situ Formation of Hierarchical Bismuth Nanodots/Graphene Nanoarchitectures for Ultrahigh-Rate and Durable Potassium-Ion Storage. *Small* **2020,** *16* (2).

357. Xiang, X.; Liu, D.; Zhu, X.; Fang, K.; Zhou, K.; Tang, H.; Xie, Z.; Li, J.; Zheng, H.; Qu, D., Evaporation-induced formation of hollow bismuth@N-doped carbon nanorods for enhanced electrochemical potassium storage. *Appl. Surf. Sci.* **2020,** *514*.

358. Li, H.; Zhao, C.; Yin, Y.; Zou, Y.; Xia, Y.; An, Q.; Jian, Z.; Chen, W., N-Doped carbon coated bismuth nanorods with a hollow structure as an anode for superior-performance potassium-ion batteries. *Nanoscale* **2020,** *12* (7), 4309-4313.

359. Gillard, C. H.; Jana, P. P.; Rawal, A.; Sharma, N., Electrochemical phase evolution of tetradymite-type Bi2Te3 in lithium, sodium and potassium ion half cells. *J. Alloys Compd.* **2020**, 155621.

360. Hu, J.; Xie, Y.; Zheng, J.; Lai, Y.; Zhang, Z., Unveiling nanoplates-assembled Bi2MoO6 microsphere as a novel anode material for high performance potassium-ion batteries. *Nano Research* **2020**.

361. Li, W.; Xu, Y.; Dong, Y.; Wu, Y.; Zhang, C.; Zhou, M.; Fu, Q.; Wu, M.; Lei, Y., Bismuth oxychloride nanoflake assemblies as a new anode for potassium ion batteries. *Chem. Commun.* **2019,** *55* (46), 6507-6510.

362. Wang, J.; Wang, B.; Lu, B., Nature of Novel 2D van der Waals Heterostructures for Superior Potassium Ion Batteries. *Advanced Energy Materials* **2020,** *10* (24).

363. Sultana, I.; Rahman, M. M.; Ramireddy, T.; Chen, Y.; Glushenkov, A. M., High capacity potassium-ion battery anodes based on black phosphorus. *Journal of Materials Chemistry A* **2017,** *5* (45), 23506-23512.

364. Wu, Y.; Hu, S.; Xu, R.; Wang, J.; Peng, Z.; Zhang, Q.; Yu, Y., Boosting Potassium-Ion Battery Performance by Encapsulating Red Phosphorus in Free-Standing Nitrogen-Doped Porous Hollow Carbon Nanofibers. *Nano Lett.* **2019,** *19* (2), 1351-1358.

365. Chang, W.-C.; Wu, J.-H.; Chen, K.-T.; Tuan, H.-Y., Red Phosphorus Potassium-Ion Battery Anodes. *Advanced Science* **2019,** *6* (9).
366. Fang, K.; Liu, D.; Xiang, X.; Zhu, X.; Tang, H.; Qu, D.; Xie, Z.; Li, J.; Qu, D., Air-stable red phosphorus anode for potassium/sodium-ion batteries enabled through dual-protection design. *Nano Energy* **2020,** *69*.
367. Li, D.; Zhang, Y.; Sun, Q.; Zhang, S.; Wang, Z.; Liang, Z.; Si, P.; Ci, L., Hierarchically porous carbon supported Sn4P3 as a superior anode material for potassium-ion batteries. *Energy Storage Materials* **2019,** *23*, 367-374.
368. Li, B.; Shang, S.; Zhao, J.; Itkis, D. M.; Jiao, X.; Zhang, C.; Liu, Z.-K.; Song, J., Metastable trigonal SnP: A promising anode material for potassium-ion battery. *Carbon* **2020**.
369. Verma, R.; Didwal, P. N.; Ki, H.-S.; Cao, G.; Park, C.-J., SnP3/Carbon Nanocomposite as an Anode Material for Potassium-Ion Batteries. *Acs Applied Materials & Interfaces* **2019,** *11* (30), 26976-26984.
370. Li, W.; Yan, B.; Fan, H.; Zhang, C.; Xu, H.; Cheng, X.; Li, Z.; Jia, G.; An, S.; Qiu, X., FeP/C Composites as an Anode Material for K-Ion Batteries. *Acs Applied Materials & Interfaces* **2019,** *11* (25), 22364-22370.
371. Yi, Z.; Liu, Y.; Li, Y.; Zhou, L.; Wang, Z.; Zhang, J.; Cheng, H.; Lu, Z., Flexible Membrane Consisting of MoP Ultrafine Nanoparticles Highly Distributed Inside N and P Codoped Carbon Nanofibers as High-Performance Anode for Potassium-Ion Batteries. *Small* **2020,** *16* (2).
372. Li, B.; He, Z.; Zhao, J.; Liu, W.; Feng, Y.; Song, J., Advanced Se3P4@C Anode with Exceptional Cycling Life for High Performance Potassium-Ion Batteries. *Small* **2020,** *16* (6).
373. Lei, K.; Wang, C.; Liu, L.; Luo, Y.; Mu, C.; Li, F.; Chen, J., A Porous Network of Bismuth Used as the Anode Material for High-Energy-Density Potassium-Ion Batteries. *Angew. Chem. Int. Ed. Engl.* **2018,** *57* (17), 4687-4691.
374. Huang, J.; Lin, X.; Tan, H.; Zhang, B., Bismuth Microparticles as Advanced Anodes for Potassium-Ion Battery. *Advanced Energy Materials* **2018,** *8* (19).